DokumentID	Version	Status	Reg nr	Sida
1395214	2.0	Godkänt		1 (93)
Författare Johan Öhman			Datum 2013-05-16	
Kvalitetssäkrad av			Kvalitetssäkrad datum	
Godkänd av Magnus Odén			Godkänd datum 2014-04-25	

TD08- SFR3 effect on the performance of the existing SFR1

Contents

1 TD description

1.1 Context and approach

The planned extension of SFR (SFR3) may not influence the performance measures of the existing facility (SFR1) negatively. Hence, the extension is not allowed to give rise to higher water fluxes through the waste packages in the existing facility, or, for example transport substances to the existing facility which will influence the existing SFR negatively. The uncertainty in results is addressed in a sensitivity analysis for a selection of alternative bedrock parameterisations

1.2 Objectives

The objective is to quantify how the planned SFR extension (Figure 1-1) affects the performance of the existing SFR1. The uncertainty in results is addressed in a sensitivity analysis for a selection of alternative bedrock parameterisations. The performance of the existing SFR1 and the planned extension (SFR3), version L1B, is evaluated in terms of the following measures:

1) Cross flow through disposal facilities
2) Interaction between disposal facilities (i.e., determined as the fraction of particles released in one disposal facility that pass another, downstream disposal facility)
3) Particle-tracking exit locations at bedrock surface

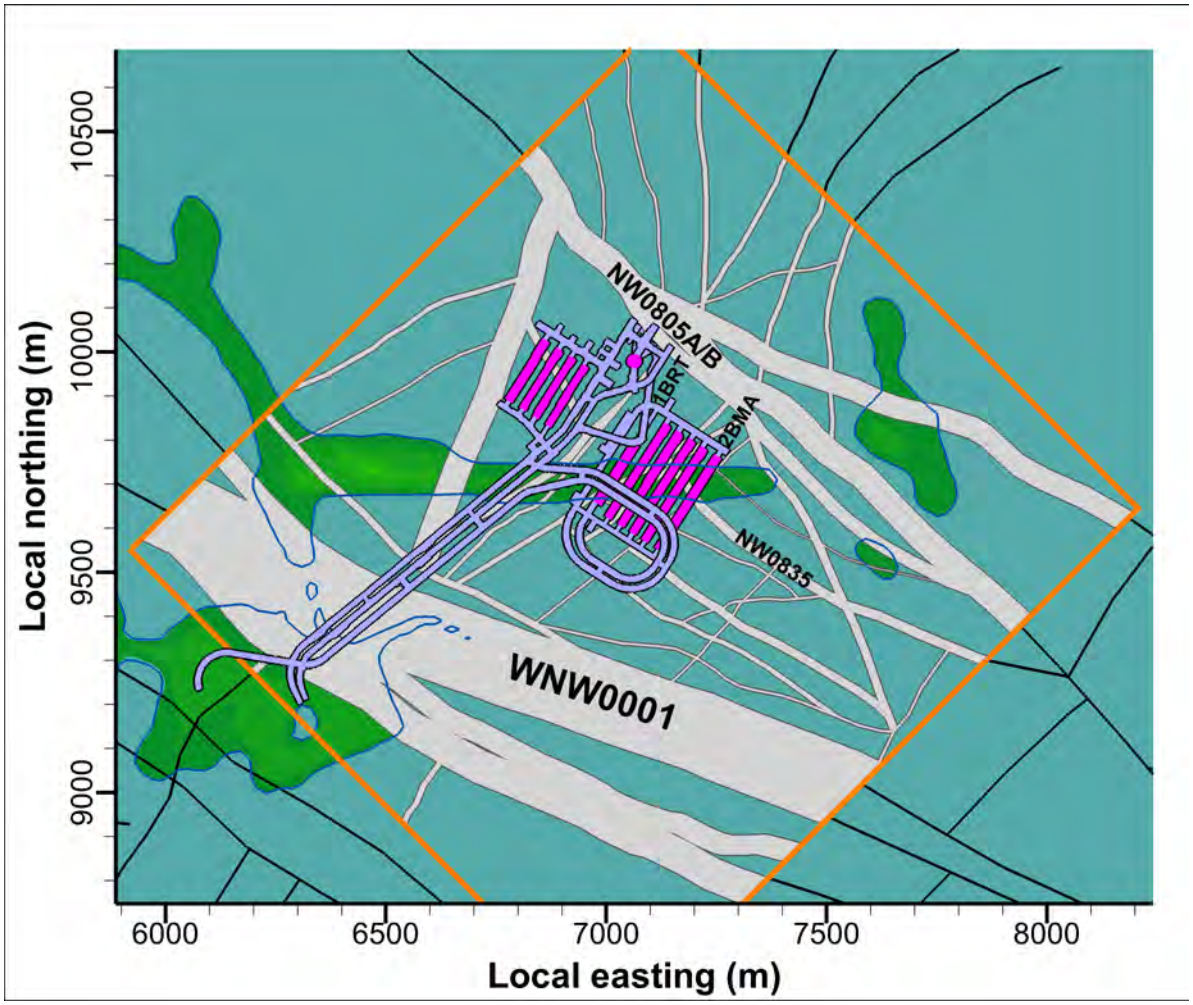

Figure 1-1. *Existing SFR1 and the planned extension, version L1B, in context of ground-surface intercepts of geologically modelled deformation zones (grey) and SFR Regional model domain (orange).*

1.3 Model cases

TD08 is divided into two subtasks, TD08a and TD08b (Table 1-1). TD08a focuses on the changing flow regime with future shoreline retreat, as well as, the influence of the planned extension on the existing SFR1. TD08b addresses the uncertainty in results arising from bedrock parameterisation by means of a sensitivity analysis.

Table 1-1. Varied model components in the sensitivity analysis

Variable	HCD	HRD	Time	Construction state
Refers to:	Deterministic structures Deformation zones Sheet joints SBA structures	Stochastic features DFN Unresolved PDZ	Shore-line retreat HSD dynamics (RLDM)	Alternative tunnel scenario, including technical barriers
TD08a cases	Base case	Stochastic realisation R85	Selected time slices: 2000 AD 2500 AD 3000 AD 3500 AD 5000 AD 9000 AD	SFR1 (only), versus coexistence of SFR1 **and** planned extension
TD08b cases	Base case Extended ZFM871 Heterogeneity (R01…R10)	Stochastic realisations R01…R20 + R85	Selected time slices: 3500 AD 9000 AD	Coexistence of SFR1 **and** planned extension

TD08a:

The task of TD08a is to study the effect that the planned extension has on the performance of the existing SFR1. The effect is evaluated by comparing performance measures for SFR1, *before* inclusion of the planned extension, L1B, versus its performance measures after inclusion of L1B (i.e., model setups No. 1 to 6 are compared pairwise against model setups No. 7 to 12 in Table 1-2). The effect is studied under the changing flow regime for six selected time slices (2000, 2500, 3000, 3500, 5000, and 9000 AD). A single bedrock case is studied (BASE_CASE1_DFN_R85).

TD08b:

The sensitivity analysis in TD08b consists of a simulation sequence for 62 bedrock parameterisations. Performance measures are evaluated for the flow regime at two selected time slices (3500 and 9000 AD) (i.e., $2 \times 62 = 124$ model setups). All simulations include both the existing SFR1 and the planned extension, L1B. The following bedrock parameterisation variants are adressed (Table 1-2):

1) One HCD parameterisation (BASE_CASE1) combined with 21 HRD realisations (R01 to R20 and R85)
2) One HCD parameterisation (EXT_ZFM871) combined with 21 HRD realisations (R01 to R20 and R85)
3) Ten heterogeneous HCD parameterisations (HETERO_R01 to R10) combined with 2 HRD realisations (R18 and R85)

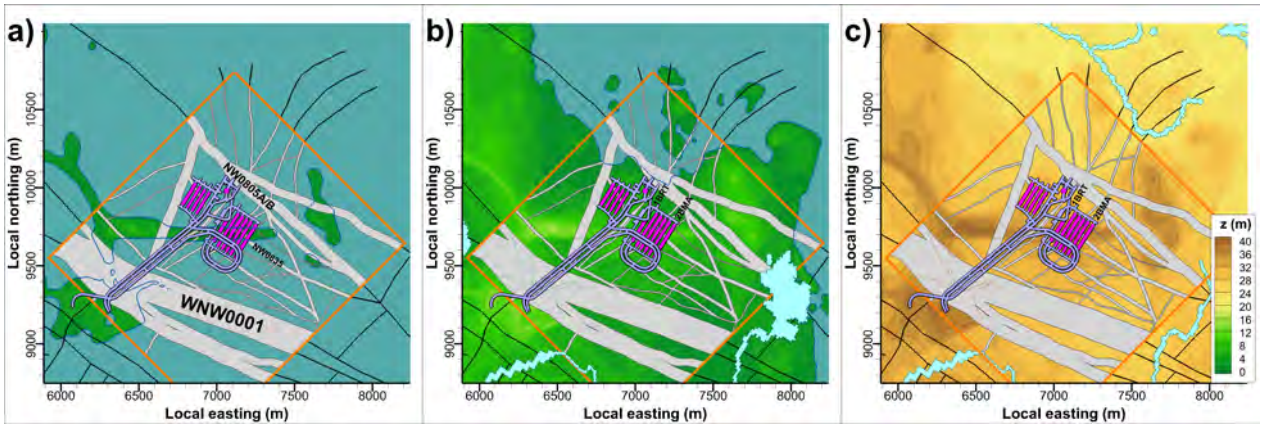

Figure 1-2. *Land lift and shoreline retreat over time; time slices a) 2000AD, b) 3500 AD, and c) 9000AD.*

Table 1-2. Model setups in the sensitivity analysis

No.	Time slice	HCD	HRD	Extension
Model setups in TD08a				
1	2000AD	BASE_CASE1	R85	Not included (**only** SFR1)
2	2500AD			
3	3000AD			
4	3500AD			
5	5000AD			
6	9000AD			
7	2000AD	BASE_CASE1	R85	Included (SFR1 **and** L1B)
8	2500AD			
9	3000AD			
10	3500AD			
11	5000AD			
12	9000AD			
Model setups in TD08b				
1…21	3500AD	BASE_CASE1	R01…R20, R85	Included (SFR1 **and** L1B)
22…42	9000AD			
43…63	3500AD	EXT_ZFM871		
64…84	9000AD			
85…94	3500AD	HETERO_R01…R10	R85	
95…104	9000AD			
105…114	3500AD		R18	
115…124	9000AD			

1.4 Modelling sequence

TD08 analyses model performance for a total of 136 different setups (Table 1-2). Even a single model setup, involves complex file management that must be processed in several steps (i.e., data preparation, parameterisation, execution, and post processing; Figure 1-3). There are (at least) three reasons to apply automatized data-file management in the modelling sequence:

- **minimisation of data-handling related errors**: automatizing ensures that: 1) all model setups are handled consistently (i.e., all model setups are treated the *same* way), and 2) appliance of input files is consistent with the specified <bedrock case>/<time slice> case (i.e., follows specifications in Table 1-1 and Table 1-2).
- **traceability:** automatizing provides traceable data management via the source codes, and also maintains a strict traceability between sequences by means of case-specific filenames for intermediate input and output (i.e., all I/O filenames are tagged by relevant specification to <bedrock case> and/or <time slice>). No output can be propagated until all required input data are available.
- **time efficiency**: automatizing allows: 1) parallel processing in different working directories and 2) continuous processing over weeks, day and night.

Consequently, data file management is automatized as far as possible. The modelling sequence is divided into four main sequences (Figure 1-3), which are handled by file-managing routines to maintain traceability between input and output:

a) **Data and grid preparation:** managed by a range of customized tools (see footnotes to Figure 1-3).
b) **ECPM upscaling:** described in Section 4.2.
c) **Final model setup and flow simulation:** described in Section 4.3.
d) **Post processing:** particle tracking (Section 4.4.2).

The file-managing routines are controlled by manually constructed input files, in which the list of bedrock cases (Table 1-2) and time slices (Table 1-1) are specified. Their purpose is to monitor and manage the parallel processing in different working directories, while maintaining strict traceability between input and output. The file managing codes typically operate in the following sequence:

1) Read the manually listed <bedrock case> and/or <time slice> from the input text file
2) Write and execute a DOS-command batch file (*.bat) that copies all required input files into the current working folder
3) Check that all necessary input files exist in the local working directory
4) Write the necessary DarcyTools input (i.e., construct the “cif.xml” file), but also specify information on the data set in either of two types of control files: [ECPM_setup.txt] and [DTS_setup.txt] (footnotes 16) and 17) in Figure 1-3).
5) Execute relevant DarcyTools module (FracGen, PropGen, or DTS). Within the DTS module, the file [DTS_setup.txt] is used to tag <bedrock case> and <time slice> to all output data filenames. It is also used, for example to prescribe the sea level for the specified <time slice>.
6) Write and execute a DOS-command batch file (*.bat) that creates a local folder into which all relevant output and input data are copied.
7) Steps 3-6 may be repeated, but at the end mark the current <bedrock case> / <time slice> as “DONE” and proceed to the next in sequence (return to Step 1)

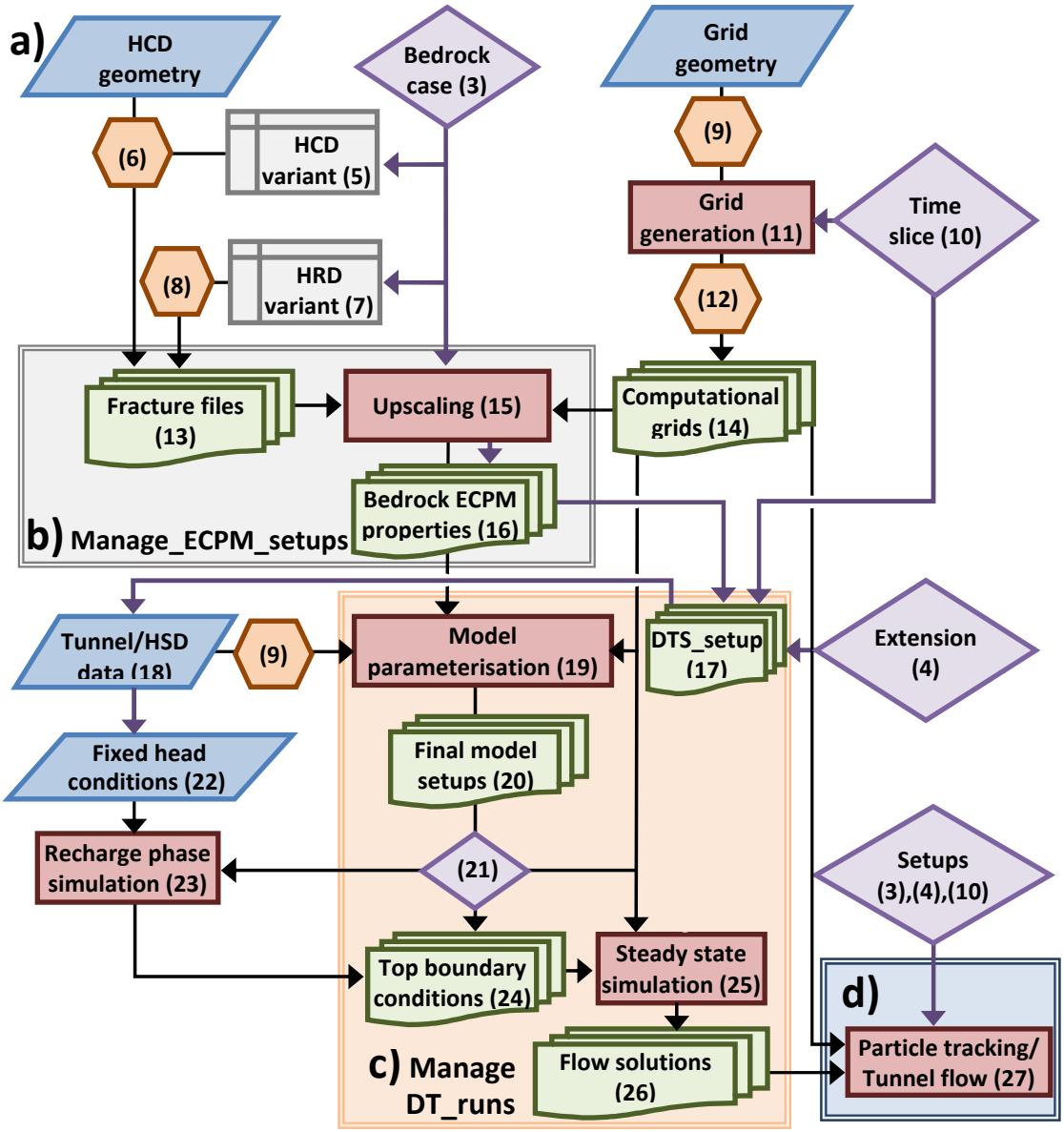

Figure 1-3. *Model execution structure consisting of four sequences; a) data and grid preparation, b) upscaling ECPM properties, c) model-setup finalisation and flow simulation, and d) post processing.*

1) **HCD geometry in the SFR Regional domain**; based on geological deformation-zone model /Curtis et al. 2011/, SFR_DZ_MASTER_v1.0 (SKBdoc 1244246), but includes extension of six lineaments (SFR DZ MASTER v1.0-hydro_extensions.xml). An alternative extension of ZFM871 geometry is also tested, referred to as "EXT_ZFM871" (Section 3.2.1). Used files: [`SFR DZ MASTER v1.0.DT` and `SFR HCD v1.0_Ext_ZFM871.DT`].
2) **Geometric data for grid discretisation**; Geometry of model domains, regolith layers, lakes, rivers, tunnels, and tunnel plugs are described in Chapter 2.
3) **Defined bedrock cases**; The TD08b sensitivity analysis involves 62 bedrock cases (Table 1-2; i.e., parameterisation variants). A <**Bedrock case**> consists of: a) a HCD parameterisation variant (<**HCD variant**>; Section 3.2.1) and b) a HRD variant (or realization, R**XX**; Section 3.2.2). Traceability and consistent management of the specified bedrock cases (i.e., file transfer between modelling sequences) is provided by two control files: [ECPM_setup.txt] (footnote 16) and [DTS_setup.txt] (footnote 17).

4) **Extension**; in **TD08a**, two situations are compared: 1) **only** SFR1 (<**Extension**> = "SFR1"), versus 2) SFR1 **and** planned extension L1B (<**Extension**> = "SFR2"). In **TD08b**, both facilities are included in all setups (i.e., <**Extension**> is always "SFR2").
5) **HCD variant**; the internal heterogeneity in HCD parameterisation and uncertainty in the extension of ZFM871 is addressed by HCD variants (Section 3.2.1). Five <**HCD variant**> are selected for analysis.
6) HCD parameterisation: A selection of 5 HCD-parameterisation variants is applied to deterministically modelled deformation zones inside SFR Regional domain. Sequence described in Table 3-3. Output is in DarcyTools "known-fracture" format: [R_Param_SFR_<**HCD variant**>], where <**HCD variant**> is specified in (3).
7) **HRD variants**; the heterogeneity in the rock mass outside deformation zones is addressed by HRD variants. Twenty-one stochastic combined realisations of DFN and Unresolved PDZs inside SFR Regional domain (R01 to R20, and R85) are studied in the sensitivity analysis (Table 3-5).
8) **File preparation**; Parameterisation, generation, and removal of isolated fractures follows the procedure described in Öhman et al. 2013 (summarized in Section 3.2.2). All files are converted into DarcyTools "known-fracture" format and rotated into the model coordinate system, as described in R-11-10. Used files: [R_SFR_DFN_connected_R**XX**_knwn] and [R_Unresolved_PDZ_R**XX**_knwn], for HRD variants **XX** = 01 to 20 and 85.
9) **File preparation**; All delivered geometry data, e.g., tunnel data (stl), topography and bedrock surface DEMs (xyz), lakes and rivers (GIS shape) are converted into DT "object"-format and rotated into the model coordinate system (details in Chapter 2).
10) **Time slices**; Model performance is evaluated at stages of shoreline retreat, defined as <**time slice**> in Table 1-1. In the modelling sequence, <**time slice**> controls: a) *cell marking* of inactive cells, topography, lakes, and rivers in grid generation (11), b) RLDM regolith layering in *HSD parameterisation* (19), and c) *fixed-head criteria* during recharge phase simulations (22). <**time slice**> is tagged in the control file [DTS_setup.txt] (17) to ensure consistent file management.
11) **Grid generation**; One grid per time slice is generated [xyz_<**time slice**>] by means of the DarcyTools module GridGen (Section 4.1). Notably, the discretisation is *static*, to facilitate time-independent compatibility in upscaled ECPM properties, while cell marking is *time dependent* to reflect the modelled dynamics in RLDM (shore line, DEM, lakes, and rivers). Grid generation commands are traceable via the standardised Compact Input File [TD08_cif_GGN_(all_time_slices).xml] and [TD08_GGN_<**time slice**>.log], where <**time slice**> is specified in (10).
12) **Grid modification**: Identified inconsistencies in the computational grid are edited via the DarcyTools module PropGen (Section 4.1).
13) **Fracture files**; The bedrock parameterisation in the flow model (HRD and HCD) is defined based on an underlying set of fracture files. These fracture files are prepared in the standard DarcyTools "known-fracture" format for the subsequent step of upscaling into ECPM properties (15). The principle for analysing the sensitivity to bedrock parameterisation is: 1) the uncertainty and heterogeneity *inside* the SFR Regional domain is addressed in terms of variants (Section 3.2), while 2) the bedrock parameterisation *outside* the SFR Regional domain is static (Section 3.3).
14) **Computational grids**; DarcyTools grids are generated, with *time-dependent* cell marking to reflect the landscape dynamics modelled in RLDM, but with *static* discretisation for time-independent compatibility with upscaled ECPM properties. Used files: [xyz_<**time slice**>], where <**time slice**> is specified in (10).
15) **Upscaling bedrock ECPM properties**; The ECPM properties for a given <**Bedrock case**>, (3), are upscaled from fracture files by means of the DarcyTools module FracGen (GEHYCO algorithm). Traceability between input (13) and output (16) is provided via automatized file-management (details in Section 4.2).

16) **Bedrock ECPM properties;** In DarcyTools, hydraulic fracture properties are approximated by those of a porous medium and referred to as Equivalent Continuous Porous Medium (ECPM) properties. Upscaled bedrock ECPM properties (conductivity, free fracture volume, and flow-wetted surface area), define the hydraulic domains HCD and HRD in the final model setup (19). File management and applied filename conventions for ECPM-upscaling input/output are described in Table 4-3. A control file is generated and stored along with data output files [ECPM_setup.txt], specifying <**HCD variant**> and <**HRD variant**>.
17) **DTS_setup.txt;** control file defining model setup, <**Bedrock case**> combined from [ECPM_setup.txt] (16), specified <**time slice**> in (10), and specified <**Extension**> in (4). Used to ensure traceability and consistency in file-management, between parameterisation (15) and final model output (27), and also to maintain name conventions for output files.
18) **HSD and tunnel data**; The final model setup (19) requires geometric and hydraulic data for the HSD and tunnels are described in Sections 2.2 and 2.3. control file [DTS_setup.txt] in (17) defines the grid and RLDM regolith layers for the specific <**time slice**>;
19) **Model parameterisation;** The final model setup for subsequent flow simulations, (23) and (25), is merged from three sub-domains: 1) the bedrock (HCD and HRD) is assigned ECPM properties (16), 2) HSD is parameterised based on RLDM regolith layering for <**time slice**> (Table 3-7), and 3) tunnel back-fill parameterisation (i.e., initially assuming intact tunnel plugs; Table 3-1). Minimum values are also applied for conductivity and porosity. Performed by means of the DarcyTools module PropGen (Section 4.3.1). <**time slice**> is specified in [DTS_setup.txt], (17).
20) **Final model parameterisation**; The final model parameterisation for a given <**Bedrock case**>, <**Extension**>, and <**time slice**>, (3), (4), and (10), defines all three hydraulic domains HCD, HRD, and HSD (also includes tunnel back-fill parameterisation). The grid parameterisation consists of the properties: permeability, porosity, and flow-wetted surface area, which are employed in flow simulations, (23) and (25), and post processing, (27). File management and applied filename conventions for input/output are described in Table 4-4.
21) **Simulation sequence selection**; in **TD08a**, the top boundary head condition is solved in a recharge phase (23). To reduce simulation time in **TD08b**, existing top boundary conditions of **TD08a** (24) are applied directly in steady state phase simulations (25).
22) **Fixed head conditions**; Rivers, lakes, and the seafloor are assigned fixed head based on RLDM data for the <**time slice**>, specified in control file [DTS_setup.txt], (17). A so-called basin-filled DEM for the specific <**time slice**> is used as a criterion for maximum head in top-layer grid cells; described in Section 4.3.2.
23) **Recharge phase simulation**; In **TD08a**, the top-boundary conditions for subsequent steady-state simulations, (25), are determined in this preceding simulation (Section 4.3.2). Head in the ground-surface layer is simulated by a principle of combining locally variable recharge and fixed-head conditions, (22). The solved top-boundary condition for each <**time slice**> is stored as a standard "DarcyTools restart file" (Table 4-6).
24) **Top boundary condition**; Input/output of the recharge-phase simulation are documented in Table 4-6. [rstslv_<**Extension**>_<**time slice**>] is used as a fixed-head boundary condition for the top layer of grid cells in subsequent steady state simulations (25). The boundary conditions solved in **TD08a** are assumed to be valid also for **TD08b** (i.e., independent of <**Bedrock case**>)
25) **Steady state simulation**; Based on the fixed-head condition in the model top boundary, the flow solution is progressed to better convergence (Section 4.3.3).
26) **Flow solutions**; Input/output of the steady-state simulation are documented in Table 4-7. The two key outputs are: [<**Bedrock case**>_<**Extension**>_<**time slice**>_Flow_solution.dat], used in post processing, (27). The complete model setups and results of **TD08a** are delivered to Comsol near-field simulations.

27) **Post processing**; Performance measures are extracted from the flow solutions by means of particle tracking (Section 4.4.2). Input/output of particle tracking is documented in Table 4-8, following the [DTS_setup.txt] convention, (17)

2 Geometric data

2.1 Model domains

2.1.1 Flow domain

The flow domain defines the outer perimeter of the model volume (i.e., the vertical sides of the model; Figure 2-1). The vertical sides of the model have no-flow boundary conditions in flow simulations, and therefore the flow domain is defined based on topographical water divides and sub-catchments. Areas that are currently below sea have been chosen with respect to: 1) modelled future topographical divides (Öhman 2010), 2) the deep Seafloor trench (the so-called Gräsörännan), and 3) general expectations of the regional future hydraulic gradient. The flow domain extends vertically from +100 m to -1,100 m elevation.

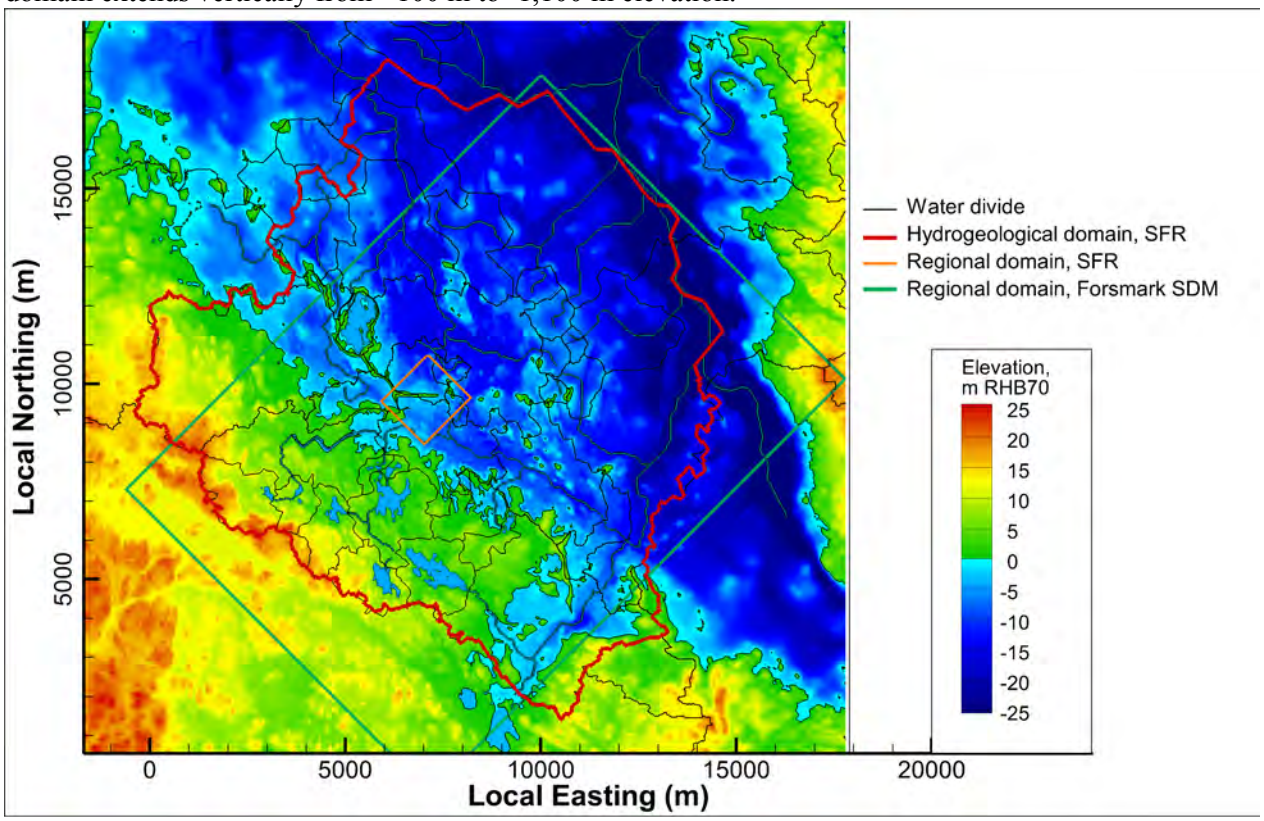

Figure 2-1. *The flow domain (red line) is the outer boundary in the model. The SFR Regional domain (orange line) is the boundary for bedrock parameterization variants studied in sensitivity analysis.*

The flow domain was defined during SDM-PSU, based on [SFR_ny_yta.dxf]. The domain was converted into an enclosed 3D CAD volume and converted into a DarcyTools object [WATERDIVIDE_z_1500m.dat] by means of the DarcyTools module OGN. The object is rotated into the local DarcyTools coordinate system [R_WATERDIVIDE_z_1500m.dat] by means of the Fortran code [Rotate_DT_objects.f90]. Pivot point in local coordinate system: [6400. 9200.], rotation angle: 32.58816946˚.
However, the modelled future topographical divides have been updated within the SR-PSU project, and the flow domain should be revised to conform to the updated topographical water-divide data (Figure 2-1). This update will be performed in Td10.

2.1.2 SFR Regional domain

The geoscientific execution programme (SKB 2008) defined two different model scales for site-descriptive modelling: a local scale and a regional scale. The local-scale model volume covers the near-field of the planned SFR extension, but is not being used in TD08. The regional-scale model volume, on the other hand, has a key role as a central geometric boundary for merging two types of bedrock parameterization: 1) developed within the SR-PSU/SDM-PSU project inside the SFR Regional domain, addressed by bedrock cases, with 2) developed in the SDM-Site/SR-Site Forsmark outside this domain. The SFR Regional domain also controls grid generation and defines the boundaries for DFN generation. The regional model volume extends from +100 m to -1,100 m elevation. The coordinates defining the horizontal extent of the model volumes are provided in Table 2-1.

Table 2-1. Coordinates defining model areas for SFR. RT90 (RAK) system

Regional model volume		Local model volume	
Easting (m)	Northing (m)	Easting (m)	Northing (m)
1631920.0000	6701550.0000	1632550.0000	6701880.0000
1633111.7827	6702741.1671	1633059.2484	6702388.9854
1634207.5150	6701644.8685	1633667.2031	6701780.7165
1633015.7324	6700453.7014	1633157.9547	6701271.7311

Based on the defined coordinates (Table 2-1), a DarcyTools object [SFR_modellområde_v01.dat] was constructed. The object is rotated into the local DarcyTools coordinate system [**R_**SFR_modellområde_v01.dat] by means of the Fortran code [Rotate_DT_objects.f90]. Pivot point in local coordinate system: [6400. 9200.], rotation angle: 32.58816946˚.

2.2 Tunnel geometry

Tunnel and tunnel-plug geometry is defined in CAD. The CAD data set contains disposal facilities, plugged tunnel sections, and back-filled tunnel sections for: 1) the existing SFR-1, and 2) the planned extension L1B.
These geometric tunnel data have two functions in grid generation: 1) to control local grid refinement, and 2) to define grid cells in different tunnel sections, by means of so-called "DarcyTools cell markers". In effect, the tunnel data can be said to have 4 central functions in the flow modelling:

1) **Local grid refinement**: tunnel cells have a maximum side length of 2 m,
2) **Parameterisation**: so-called "DarcyTools cell markers" are used to identify the different types of back-fill material in tunnel cells, which is used to set hydraulic properties (see Section 3.1; Table 3-1)
3) **Particle-release points:** defined as the entire volume of disposal facilities (pink volumes in Figure 2-3). Particle-release points are also identified via DarcyTools cell markers.
4) **Tunnel flow:** defined as net flow over tunnel walls. Likewise, DarcyTools cell markers are used to identify tunnel walls of disposal facilities.

Data processing for DarcyTools implementation

The implementation of tunnel geometry into the DarcyTools computational grid (Figure 2-3) requires processing of delivered data (Table 2-2):

1) all geometric tunnel data (original CAD format *.stl) are converted into the so-called DarcyTools-object format (changing file extension to *.dat). The file conversion is a standard procedure, and managed by the DarcyTools module OGN. Filename of DarcyTools objects are shortened, as DarcyTools has an upper limit of 32 characters in object names.
2) all geometric objects (*.dat) are translated and rotated into the local model coordinate system (adding the prefix "R_"*.dat).

3) Generated grids are inspected by means of 3D visualisation (i.e., Figure 2-3) and verified against CAD objects and the intentions in principle sketch (Figure 2-2).

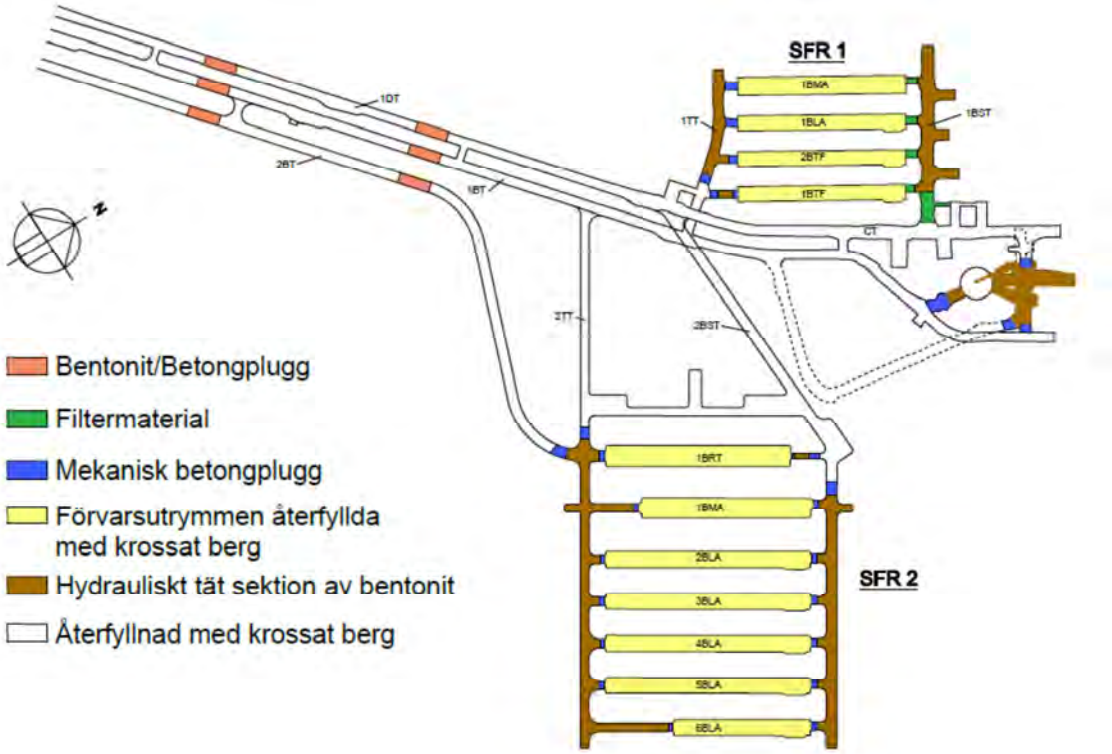

Figure 2-2. *Principle sketch over back-fill/plugging of tunnel sections (figur_6_REV5.pdf). Used to verify grid generation (Figure 2-3).*

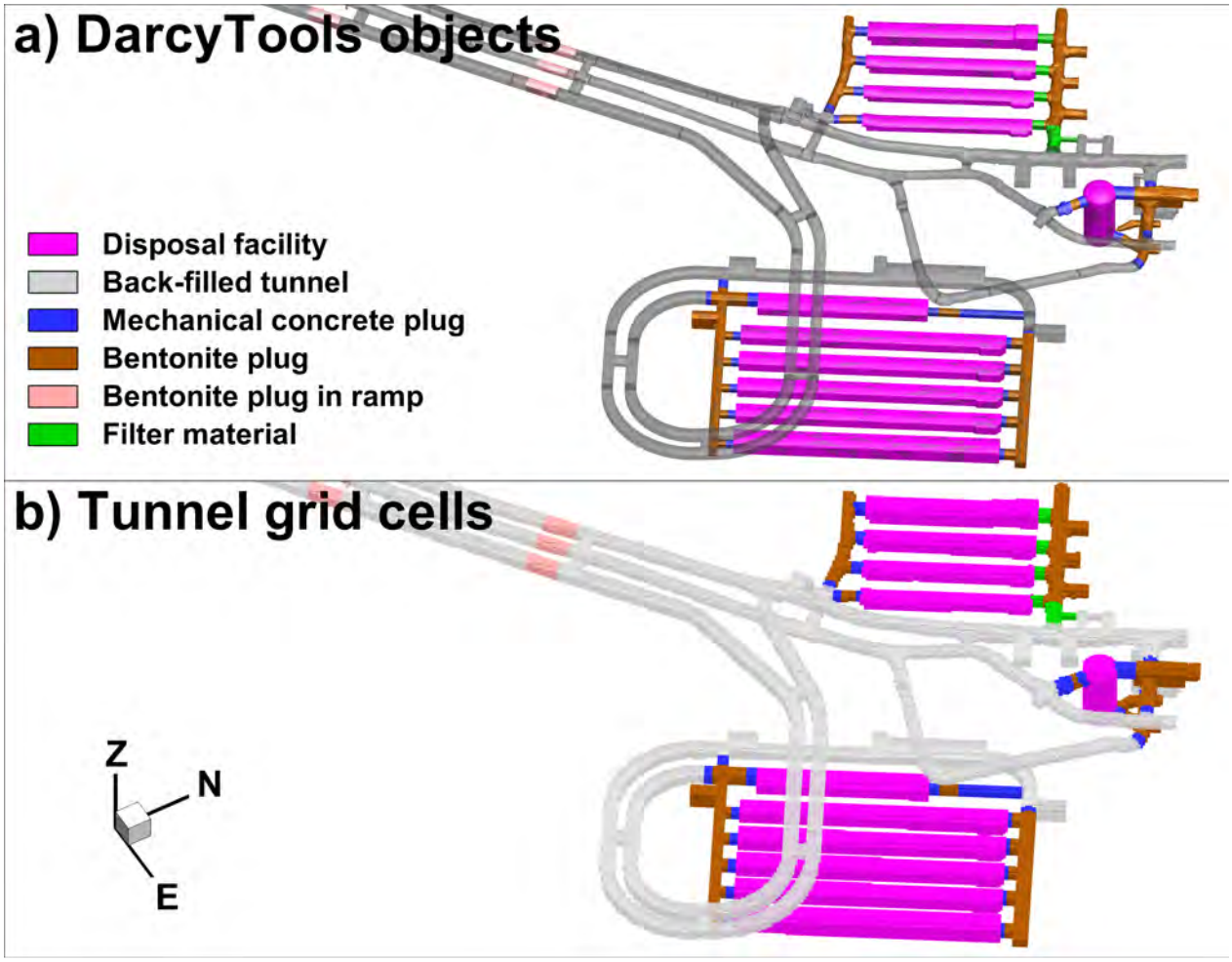

Figure 2-3. *Tunnel discretisation; a) geometric input data, and b) tunnel cells in the computational grid.*

Table 2-2. Used tunnel/tunnel plug geometry for tunnel discretisation

Source data (CAD format)	Rotated DarcyTools object
Disposal facilities	
1BTF to 1BMA	R_befSFR_forvaring_1BTF_M11.dat R_befSFR_forvaring_2BTF_M12.dat R_befSFR_forvaring_1BLA_M13.dat R_befSFR_forvaring_1BMA_M14.dat R_befSFR_silo_M15[1)]
2BLA.stl	[R_2BLA.dat]
3BLA.stl	[R_3BLA.dat]
4BLA.stl	[R_4BLA.dat]
5BLA.stl	[R_5BLA.dat]
3BMA.stl	[R_3BMA.dat]
1BRT_del1.stl	[R_1BRT_del1.dat]
Back-filled tunnel sections	
Entire, 16 to 21	R_entireSFR.dat[2)] R_ROD_M16.dat R_befSFR_GRON_M17.dat R_befSFR_BLA_M18.dat

	R_befSFR_VIT_NBT_M19.dat R_befSFR_VIT_SINGO_M20.dat R_ befSFR_ANSL_M21.dat
Plugged tunnel sections	
Mechanical concrete plugs	
	[R_all_blue.dat]
Bentonite plugs	
	[R_all_brown.dat]
Filter material	
	[R_all_green.dat]
Ramp bentonite plugs	
	[R_all_wskin.dat]

1) Note that no technical barriers are implemented for the silo.
2) [R_entireSFR.dat] covers the entire tunnel geometry of both SFR1 and L1B (i.e., including disposal facilities/back-fill/plugs).

2.3 RLDM data

2.3.1 Topography (DEM) and Regolith layers

Modelled regolith layer geometry is delivered from the dynamic landscape model, RLDM (GIS#12_09, Delivery12,13). Modelled regolith-layer data are defined in terms of upper-surface elevations and are delivered for the 6 selected time slices (Table 1-1). The regolith layers are: 1) Quaternary deposits, 2) filling material, and 3) peat (Table 2-3). It should be noted that, for simulating the time slice 2000AD, the static regolith model is an available alternative. However, due to conceptual model differences (Figure 2-4a), the dynamic landscape model, RLDM, is consistently used *for all time slices*. This is necessary to ensure consistency in comparisons of results between the 2000AD and other time slices (i.e., not model artefacts arising from conceptual differences). Owing to a "fixed-bedrock" model convention used (Section 2.3.5), the bedrock surface is modelled as *static* (i.e., envisaged as constant elevation over time). The bedrock surface can therefore be defined based on the original definition in the static regolith model.

Table 2-3. Regolith data files delivered from RLDM

Filenames[1)]	Description	Usage
pdem<time slice>.asc pdem<time slice>.xyz	Upper peat surface elevation (m). Peat starts to form -500 AD. This layer is therefore missing in earlier time steps.	HSD parameterisation Point data used for basin filling, defining lake/river objects, grid generation
lpgd<time slice>.asc	The upper surface of lacustrine accumulation of postglacial deposits, elevation (m). Lacustrine accumulation begins 1500 AD. This layer is therefore missing in earlier time steps.	HSD parameterisation
mpgd<time slice>.asc	The upper surface of marine accumulation of post glacial deposits, elevation (m). The same layer is used from 7000 AD to 55000 AD	HSD parameterisation
gkl<time slice>.asc	The upper surface of glacial clay, elevation (m). The same layer is used from 7000 AD to 55000 AD	HSD parameterisation
fill<time slice>.asc	The upper surface of filling, elevation (m). This layer is used for all time steps.	HSD parameterisation

glfl<time slice>.asc	The upper glaciofluvial-material surface elevation (m). Thickness is constant during all time steps.	HSD parameterisation
till<time slice>.asc	The upper till surface elevation (m). Thickness is constant during all time steps.	HSD parameterisation
bedr<time slice>.asc bedr<time slice>.xyz	The upper bedrock surface, level in the height system RH 70 (m). The level has been corrected for all layers from -8000 AD to 55000 AD using the Sea shoreline curve for the reference scenario.	HSD parameterisation Point data not used[2)]

1) Selected <time slice> are: 2000AD, 2500AD, 3000AD, 3500AD, 5000AD, and 9000AD. Extensions *.asc are in GIS raster format, while *.xyz is in point-data ASCII format.
2) Owing to the "fixed-bedrock" convention used, the bedrock surface is modelled as static. The bedrock surface is therefore defined by the original definition in the static regolith model [bedrock_up_v2_2000AD.xyz], GIS #12_08.

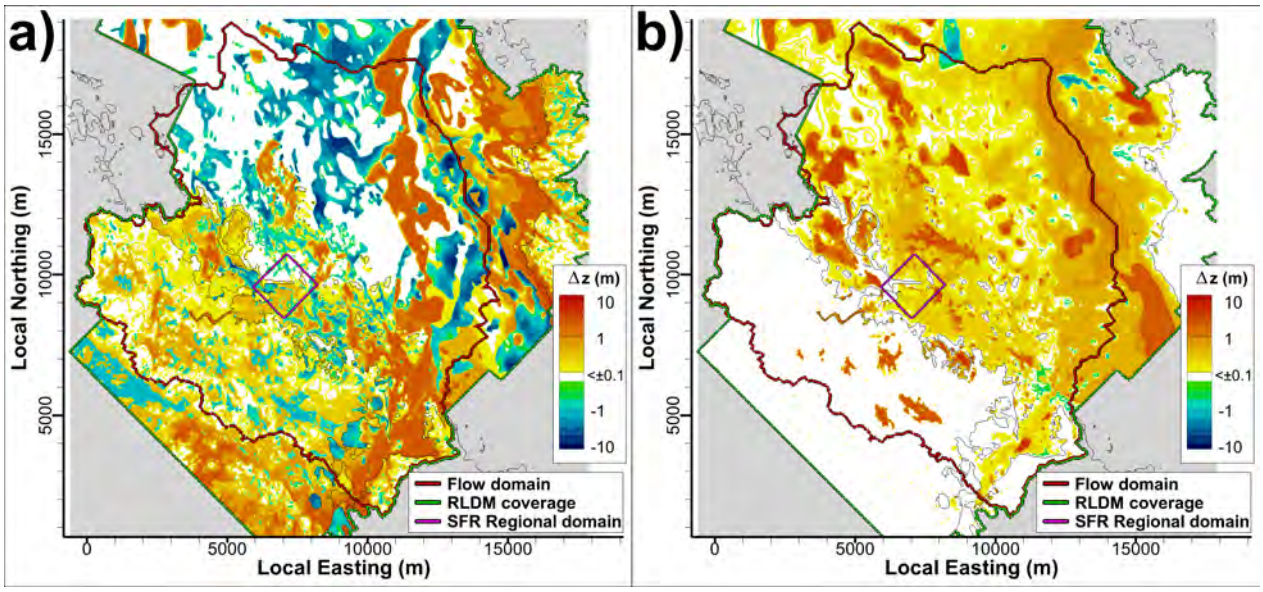

Figure 2-4. *Overview of regolith layers modelled in RLDM; a) topography discrepancy between RLDM (2000AD) and the static HSD model, and b) modelled change in topography between time slices 2000AD and 9000AD. Area outside RLDM coverage shaded in grey.*

The RLDM data have several different applications in modelling. The data are processed differently depending on application (see Section 2.3.2):

1) **Grid generation**: In the flow model, HSD is defined by grid cells between the bedrock surface (constant) and topography (varies over time, as modelled in RLDM). Grid generation requires pre-processing of geometric data into so-called "DarcyTools objects" (constructed from *.xyz files)
2) **HSD parameterisation**: raster data (*.asc files, after fixed-bedrock conversion) are used directly in the model parameterisation (Section 4.3.1)
3) **Maximum head at ground surface:** a so-called "basin-filled DEM" is used to define a criterion for maximum head in ground-surface cells, for a given time slice, in the so-called "Recharge-phase" simulations
4) **Prescribe river-bed head:** river cells are prescribed fixed head in flow simulations, which are interpolated from a constructed input data file [River_head.in]. This file is based on river trajectories, lake thresholds, sea level, and basin-filled DEMs.
5) **Visualisation**: visual confirmation of topography and surface hydrology objects, as well as, production of figures based on *.asc files converted into TecPlot *.plt format

Model areas outside RLDM coverage (grey-shaded parts of the Flow domain; Figure 2-4) are complemented by topography data from the static regolith model [DEM_xyz_batymetri_20120131.txt].

2.3.2 Processing RLDM data

The processing of RLDM data for input to the DarcyTools modelling is summarized in Table 2-4.

Conversion to fixed-bedrock format

Six different stages of shore-line retreat, resulting from the on-going land lift, are studied in TD08. The DarcyTools simulations employ the bedrock surface as a fix reference system for elevation (i.e., at land lift per 1970, m RHB 70). In this fixed-bedrock reference system, shore-line retreat is modelled by means of relative sea level displacement (SKBdocID1335997 - Shore level data Forsmark Global warming SR-PSU; Section 2.3.5).

However, all delivered regolith data (Table 2-3) account for the land lift (i.e., the bedrock surface elevation is not constant over time). The first step in processing RLDM data is therefore to encompass the delivered RLDM elevation data to the fixed-bedrock reference system, such that the bedrock elevation is constant over time. The elevation data are back-calculated by means of land-lift data [SKBdocID1335997 transferred into an ASCII input file FILES_TO_CONVERT.in] and Fortran code [Future_HSD_data_to_fixed_Bedrock_format.f90]. For traceability, the adjusted filenames, *.asc and *.xyz, are given the suffixes "*_Fixed_bedrock.asc" and "*_Fixed_bedrock.xyz" (Table 2-4).

Basin filling the uppermost RLDM layer (i.e., "DEM") to control surface head

Surface runoff is not modelled explicitly in DarcyTools. Consequently, excess ground-surface head may occur locally where net precipitation exceeds recharge (i.e., head locally exceeding topography). This model artefact is circumvented by using the uppermost RLDM layer (also referred to as "DEM") as the upper bound for ground-surface head. Note that areas modelled as submerged in RLDM (lakes, rivers, or below sea level) are treated separately (Sections 2.3.3, 2.3.4, and 2.3.5).

However, the landscape dynamics modelling (RLDM) only resolves surface water above a certain scale, and consequently, the DEM contains local depressions below the scale for deterministic RLDM modelling. Such depressions may be peat-filled or hold surface water, e.g., minor lakes, wet lands, or pools. Irrespectively of which, it can be argued that surface head in a local depression is not necessarily bounded by the DEM elevation, but instead by the topographical threshold of the basin. In other words, topography data must be processed in order to use as constraint for ground-surface head.

A so-called basin-fill approach is undertaken for this purpose. One basin-filled DEMs is constructed for each time slice [Filled_pdem<time slice>_Fixed_bedrock.asc], by filling local topographical depressions until reaching the surrounding geometric threshold. During this process, elevations in areas deterministically modelled as submerged are kept fixed (i.e., lakes, rivers, or below sea level). Thus, the final basin-filled DEMs slope towards: 1) the sea, 2) a lake with specified threshold (RLDM), or 3) a modelled river. The basin-fill is conducted in two steps (Table 2-4):

1) Automatized filling [Basin_fill_DEMs.f90], millimetre by millimetre, of topographical basins above sea level for a given <time slice> (Figure 2-5). To avoid unmotivated filling along the seafloor, basins below sea level are not included.
2) The basin-filled DEMs are exported into GIS raster format, by means of the Fortran code [Create_Upper_DEM_ASC.f90]

The basin filled DEM is used as a criterion for maximum local groundwater level (i.e., the maximum head in a local depression is determined by the *geometric* threshold of the

surrounding DEM elevations). Although the basin-fill is a substantial improvement for constraining surface head in flow simulations, it does *not guarantee* absence of local depressions, due to inexact matching between RLDM and the DarcyTools grid. The inexact matching is due to: 1) discretisation differences (e.g., the DarcyTools grid has variable refinement) and 2) coordinate-system differences (e.g., the DarcyTools grid has a rotated coordinate system). To minimise the discrepancy related to coordinate system rotation, the SFR near-field (approximately covering the area of particle exit locations) is also basin-filled in the rotated coordinate system.

Constructing DarcyTools objects to implement HSD in grid generation

In the standard DarcyTools procedure, the model top boundary is defined by removal of grid cells above topography (i.e., as defined by a DEM DarcyTools object). SR-PSU addresses several stages of shore-line retreat (time slices), during which the topography alters due to landscape dynamics. The altering topography is honoured by using time-specific computational grids [xyz_<**time slice**>], where the model top boundary is defined by [R_Filled_pdem<**time slice**>_Fixed_bedrock.dat]. For time efficiency, a *cell inactivation* method is used, where:

1) cells are *permanently* deleted, if located above the maximum DEM elevation, determined over the time period 2000 to 9000AD, [R_MAX_Filled_DEM_2000AD_to_9000AD(onlyRLDM).dat].
2) cells are *inactivated* in the time-specific grid, if located above the DEM for the particular <**time slice**>, determined by [R_Filled_pdem<**time slice**>_Fixed_bedrock.dat]

The benefit of this method is that the discretisation of all time-specific grids is identical, which allows re-using the same upscaled ECPM properties for any time slice (i.e., ECPM upscaling is a time-consuming step that is only valid for a specific grid discretisation). The top boundary is defined as the uppermost layer of active cells in the grid (i.e., immediately below a permanently deleted cell or a temporarily inactivated cell). The regolith is defined as above computational cells above the bedrock surface [R_bedrock_up_v2_2000AD.dat]. This particular file is the original data source for bedrock surface (GIS #12_08; [bedrock_up_v2_2000AD.xyz]), defined in the static regolith model. Due to the "fixed-bedrock" reference convention, all bedrock surface data are identical (apart from negligible round-off errors).

Table 2-4. RLDM data processing in 3 steps

Purpose [input]	**Execution code [output]**
1. Conform to DarcyTools elevation reference system	
Convert regolith layer elevations (Table 2-3) into fixed-bedrock format. [*.asc], [*.xyz]	Future_HSD_data_to_fixed_Bedrock_format.f90 (adds suffix *"**_Fixed_bedrock**") [*_Fixed_bedrock.asc], [*_Fixed_bedrock.xyz]
2. Basin fill uppermost regolith layer (i.e., "DEM")	
Fill local topographical basins above sea level [pdem*_Fixed_bedrock.xyz]	Basin_fill_DEMs.f90 (adds prefix "**Filled_**"*) [Filled_pdem*_Fixed_bedrock.xyz] [Filled_pdem*_Fixed_bedrock.plt]
File-format conversion to GIS raster format. [Filled_pdem*_Fixed_bedrock.xyz]	Create_Upper_DEM_ASC.f90 (extension *".**asc**") [Filled_pdem*_Fixed_bedrock.asc]
Complementary filled DEM in particle-tracking area. Basin-filling in rotated coordinate system [Filled_pdem*_Fixed_bedrock.asc]	Basin_fill_ROTATED_DEM.f90 [Filled_ROTATED_LOCAL_DEM_*.dat] [Filled_ROTATED_DEM_*.plt]
3. DarcyTools objects in grid generation	
Construct DarcyTools object defining topography and bedrock surface [Filled_pdem*_Fixed_bedrock.xyz] [bedrock_up_v2_2000AD.xyz]	DEM_to_DT_object.f (extensions *".**dat**", *".**plt**") [Filled_pdem*_Fixed_bedrock.dat], [Filled_pdem*_Fixed_bedrock.plt] [bedrock_up_v2_2000AD.dat], [bedrock_up_v2_2000AD.plt]

Construct a universal DarcyTools object, defining maximum RLDM topography 2000AD to 9000AD [Filled_pdem*_Fixed_bedrock.xyz] Rotate DarcyTools objects into local model coordinate system [Filled_pdem*_Fixed_bedrock.dat], [bedrock_up_v2_2000AD.dat], [MAX_Filled_DEM_2000AD_to_9000AD(onlyRLDM).dat]	DEM_Maximum_Z.f (extensions *“.**dat**”, *“.**plt**”) [MAX_Filled_DEM_2000AD_to_9000AD(onlyRLDM).dat] [MAX_DEM.plt] Rotate_DT_objects.f90 (adds prefix “**R_**”*) [R_Filled_pdem*_Fixed_bedrock.dat], [R_bedrock_up_v2_2000AD.dat], [R_MAX_Filled_DEM_2000AD_to_9000AD(onlyRLDM).dat]

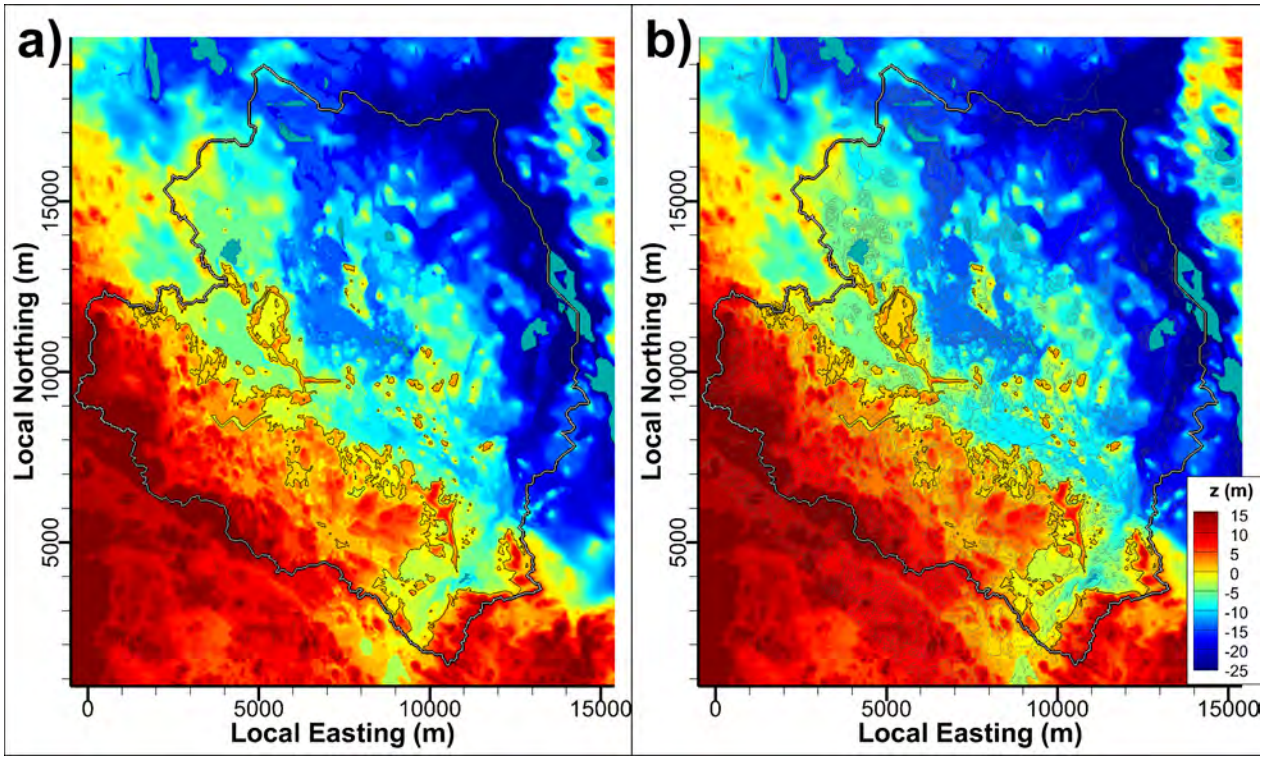

Figure 2-5. *Example of automatized filling of basins above sea level; a) original DEM 9000AD and b) basin-filled DEM 9000AD. Lakes shown as blue areas.*

2.3.3 Lakes

Lakes are used as prescribed head-boundary conditions in the flow model. More precisely, “Lake cells” are defined and refined in the computational grid by means of so-called “DarcyTools objects”. Lake cells are identified via a unique DarcyTools cell marker, which is translated into a prescribed-head value in the subsequent flow simulations (Table 2-5). The prescribed-head values (Table 2-5) are taken from the modelled lake thresholds in RLDM. The number of lakes, as well as the spatial extent of individual lakes, varies over time. Lake data are also used as fix points in defining prescribed head along riverbeds (Section 2.3.4).
Geometry of RLDM lakes and rivers are delivered in GIS vector format for all 6 time slices.

Transferring RLDM lake geometry into “DarcyTools object”-format

Implementation of geometric data in the DarcyTools grid generation requires that data are converted into the so-called “DarcyTools object” file format. Therefore, time-specific DarcyTools objects representing lakes at a given time slice are constructed, in the following 4 steps:

1. RLDM lake vector shapes (lakes_<**time slice**>.shp) and RLDM topography point data (pdem<**time slice**>_Fixed_bedrock.xyz) are joined in ArcGIS. Topographical points (x,y,z) falling inside, and on the border of, a lake vector object are exported as a text file, under the name [Lake_<Lake ID>_<**time slice**>.txt] . All lakes for a given

<**time slice**> is stored in a separate working directory, which also includes a directory list [List_of_LAKES.txt], containing the filenames and threshold data for all lakes.

2. Lake data [Lake_<Lake ID>_<**time slice**>.txt] are transformed into watertight 3D CAD volumes [Lake_<Lake ID>_<**time slice**>.**stl**], enclosing each lake water volume. The conversion is made by the code [Make_Lakes.F90], which extrudes the volume between the bottom and the surface of a lake. The extrusion is facilitated by duplicating a unit CAD cuboid [Box_Template.txt], which locally is vertically bounded by the bottom (i.e., local RLDM topography) and the surface (i.e., the specified threshold) of a lake. The CAD objects are also translated from their original RT90 coordinate system by [-1626000., -6692000.].
3. By means of the DarcyTools module OGN, CAD volumes [Lake_<Lake ID>_<**time slice**>.stl] are then converted into so-called "DarcyTools objects" [Lake_<Lake ID>_<**time slice**>.**dat**] and Tecplot output [Lake<Lake ID>.plt]. The conversion is a standard DarcyTools procedure. The TecPlot output facilitates 3D visualisation and verification against topographical depressions in the RLDM DEMs.
4. Finally, lake objects [Lake_<Lake ID>_<**time slice**>.dat] are rotated into the local DarcyTools coordinate system [**R_**Lake_<Lake ID>_<**time slice**>.dat] by means of the Fortran code [Rotate_DT_objects.f90]. Pivot point in local coordinate system: [6400. 9200.], rotation angle: 32.58816946°.

These time-specific, individual lake objects [R_Lake_<Lake ID>_<**time slice**>.dat] are only used to define lake cells in the computational grid. Grid refinement of lake is controlled by a joined, time-independent DarcyTools object [R_MAX_EXTENSION_ALL_LAKES.dat], which confines the maximal extension of all lakes (horizontally and vertically) for all time slices. This object is constructed parallel to the preparation of time-specific, individual lake objects, described above. The purpose of time-independent grid refinement (i.e., refining) is time efficiency, as ECPM conversion becomes compatible with all grids (motivated in Section 2.3.2).

Table 2-5. Prescribed head for lake cells, identified by DarcyTools cell markers

Lake ID	Lake threshold (m, elevation)	DarcyTools marker, for <time slice>					
		2000AD	2500AD	3000AD	3500AD	5000AD	9000AD
107	-6.24				158	189	214
108	-15.23					188	
110	-6.05				157		
114	-33.49						215
116	-14.24					187	216
117	-5.72				156	186	
118	-5.13			136	155	185	
120	-2.6		123	135	154	184	
121	-10.42					183	
123	-10.91					182	
124	0.48	103	122	134	153		
125	0.4	104					
126	-12.24					181	
129	5.82	105	121	133	152		
132	3.66	106	120	132	151		
134	-1.35		119	131	150	180	217
136	0.42	107	118	130	149	179	
142	1.82	108	117	129	148		

144	0.41	109	116	128	147		
146	-13.87					178	218
148	0.56	110	115	127	146	177	
149	5.32	111	114	126	145	176	
150	-8.22				144	175	219
151	-16.83						220
152	-15.41					174	221
153	-8.29				143	173	
154	-15.36					172	222
155	-6.6				142	171	
156	-6.06				141	170	223
157	-13.99					169	
159	-11.84					168	
160	-7.09				140	167	
163	-16.19					166	224
164	-20.19						225
165	-18.62						226
166	-16.2					165	227
167	-16.99						228
170	-10.14					164	229
173	-10.53					163	230
175	-10.06					162	
176	-4.95			125	139	161	
177	-8.73					160	
178	-7.59				138		
179*)	-1.67*)	112	113	124	137	159	
180	-20.34						231
184	-24.24						232

3) *) Lake 179 is the Biotest lake. It is inactivated at 2000 AD.

2.3.4 Rivers

Rivers are also treated as prescribed head-boundary conditions in the flow model. Unlike the lakes, the riverbed head varies along the trajectory of a modelled river, which requires a somewhat different modelling procedure (i.e., the cell-marking principle cannot be applied analogously). Similar to implementation of lakes (Section 2.3.3), so-called "DarcyTools objects" are used to define "river cells" in the computational grid (Table 2-6). In the flow simulations, any cell marked as a river (i.e., all river cells are assigned the same marker = 102) is prescribed a head value that is linearly interpolated between the nearest two points in an input text file [River_head.in] (Table 2-6). Riverbed head is not provided in RLDM data, but is estimated according to principles described below.

Transferring RLDM river data to DarcyTools

DarcyTools objects representing rivers at different time slices are constructed, in 4 steps:

1. RLDM river data are prepared for DarcyTools modelling by combining river data (GIS vector format) with topography data (GIS raster format). To facilitate this joint analysis, the river nodes are exported into a text file (vattendrag_SDEADM.UMEU_FM_GEO_10171.txt;). This river-node list is organised in such a way that the corresponding element list of river-segments is straightforward to construct manually [Connectivity_list.dat]. The modelled river geometry in RLDM is "stationary" (rivers do not meander or vanish over time). Therefore, the nodal data,

exported at "maximal river extension" (i.e., a late stage of shoreline retreat, t > 9000 AD), represent the river geometry at any given <**time slice**>, provided the nodes below sea level are inactivated in the subsequent flow simulations.

2. Two corrections are made to [Connectivity_list.dat]: 1) junctions between river branches are forced to occur at the nearest common river node, and 2) river starting locations (i.e., origin point of tributaries) are harmonized with topography data (i.e., a few river nodes that are inconsistent with raster topography data are removed).
3. The local riverbed head is interpolated for each <**time slice**> and stored in a condensed input file for flow simulations [River_head.in] (see Table 2-6). In this interpolation, three types of river nodes are treated as deterministic, fixed values:
    a. the starting point of river tributaries (taken as local topography elevation),
    b. river nodes inside lakes (i.e., any node falling inside [Lake_<Lake ID>_<**time slice**>.txt] is assigned head equal to lake threshold, Table 2-5),
    c. river segments below sea level are temporarily set equal to sea level, but are later inactivated in the subsequent flow simulations.

    Remaining river nodes are treated as flexible points and are interpolated by iterations [Interpolate_River_Head.f90], until:

    a. head variability along the riverbed is smoothened out, such that the river gradient is directed towards the sea, and
    b. difference between river head and local RLDM topography is minimized (node topography elevation extracted from [pdem<**time slice**>_Fixed_bedrock.xyz]).
4. For the grid generation, watertight 3D CAD volumes [Filled_Streams_<**time slice**>_z25.**stl**] are constructed based on the node list and the element list. This conversion is made by the code [Make_Rivers.F90], which extrudes a 5 m wide channel, extending from below the local estimated riverbed head (H(x,y) -1 m) to a fixed elevation of 25 m (note that any part extending above ground surface is eliminated in the grid generation). The CAD objects are also translated from their original RT90 coordinate system by [-1626000., -6692000.].
5. Next, the DarcyTools module OGN, is used to convert the CAD volumes [Filled_Streams_<**time slice**>_z25.stl] into so-called "DarcyTools objects" [Filled_Streams_<**time slice**>_z25.**dat**] and Tecplot output [Filled_Streams_<**time slice**>_z25.**plt**]. This conversion is a standard DarcyTools procedure. The TecPlot output facilitates 3D visualisation and verification against RLDM topography.
6. Finally, the river objects [Filled_Streams_<**time slice**>_z25.dat] are rotated into the local DarcyTools coordinate system [**R_**Filled_Streams_<**time slice**>_z25.dat] by means of the Fortran code [Rotate_DT_objects.f90]. Pivot point in local coordinate system: [6400. 9200.], rotation angle: 32.58816946˚.

Table 2-6. Input data files used to prescribe head in rivers

Input file	Description
R_Filled_Streams_<**time slice**>_z25.dat	Geometric DarcyTools object used in grid generation to define river cells above sea level at <**time slice**>. All river cells are given the cell marker 102.
River_head.in	Input text file used to prescribe fixed head along riverbeds in flow simulations. Local riverbed head is estimated for 4,821 points (x,y,H) along river trajectories. (x,y) are in local rotated model coordinates. H is available in 6 columns, one for each <**time slice**>. The prescribed head for a riverbed cell is linearly interpolated between the two nearest points.

2.3.5 Relative sea level displacement in fixed-bedrock reference

One of the main objectives of SR-PSU is to study effects of shoreline retreat resulting from the on-going land lift. For practical reasons, the DarcyTools simulations employ the bedrock surface as a fix reference for elevation (i.e., land lift per 1970 AD, expressed in m, RHB 70). In this fixed-bedrock reference system, shore-line retreat is modelled by means of relative sea level displacement (Table 2-7). The relative shore level data are taken from the Global warming climate case (SKBdocID1335997 - Shore level data Forsmark Global warming SR-PSU).

Table 2-7. Relative sea level at selected time slices.

Year AD	Relative sea level*), m
2000	-0.17
2500	-3.08
3000	-5.92
3500	-8.69
5000	-16.60
7000	-26.16
9000	-34.62

*) Land lift is expressed as a relative sea level displacement to the bedrock surface, since 1970AD (reproduced from SKBdocID1335997).

3 Parameterisation and numerical implementation

3.1 Tunnel back-fill

Intact tunnel plugs are assumed in TD08 (Table 3-1). During the execution of TD08, no geometric data were available for differentiating the technical barriers of the silo. Therefore, the technical barriers of the silo are not resolved in TD08, and instead the silo is assigned a homogeneous conductivity of 10^{-6} m/s. This conductivity is very high in comparison to specifications in SKBdocID 1341293 (i.e., on the order 10^{-12} to 10^{-9} m/s).
As stated earlier, particle tracking performance measures only address bedrock, and therefore porosity and fws are set to 0.0 in tunnel back-fill, which provides zero contribution in transit time and F-quotient.

Table 3-1. Tunnel back-fill parameterisation (see Figure 3-1)

Facility	Mk	Tunnel	Conductivity (m/s)	Description (SKBdocID 1341293)
SFR-1	11	1BTF	10^{-5}	Förvarsutrymmen återfyllda med krossat berg
	12	2BTF		
	13	1BLA		
	14	1BMA		
	15[1)]	Silo	10^{-6}	[Assumed value. Specifications in SKBdocID 1341293 not applied, as geometric data for differentiating the technical barriers are not available.]
	16-21	Ramp	10^{-5}	Återfyllnad med krossat berg
Extension	22	2BLA	10^{-5}	Förvarsutrymmen återfyllda med krossat berg
	23	3BLA		
	24	4BLA		
	25	5BLA		
	26	2BMA		
	27	1BRT		

	28	Ramp	10^{-5}	Återfyllnad med krossat berg
Intact plugs	30	Blue	10^{-6}	Mekanisk betongplugg
	31	Brown	10^{-10}	Hydrauliskt tät sektion av bentonit
	32	Green	10^{-6}	Filtermaterial
	33	Pink	$5 \cdot 10^{-10}$	Bentonit/betongplugg (ramp)

1) Technical barriers of the silo are not resolved. A homogeneous parameterization K = 10^{-6} m/s is applied, which is very high compared to specifications in SKBdocID 1341293.

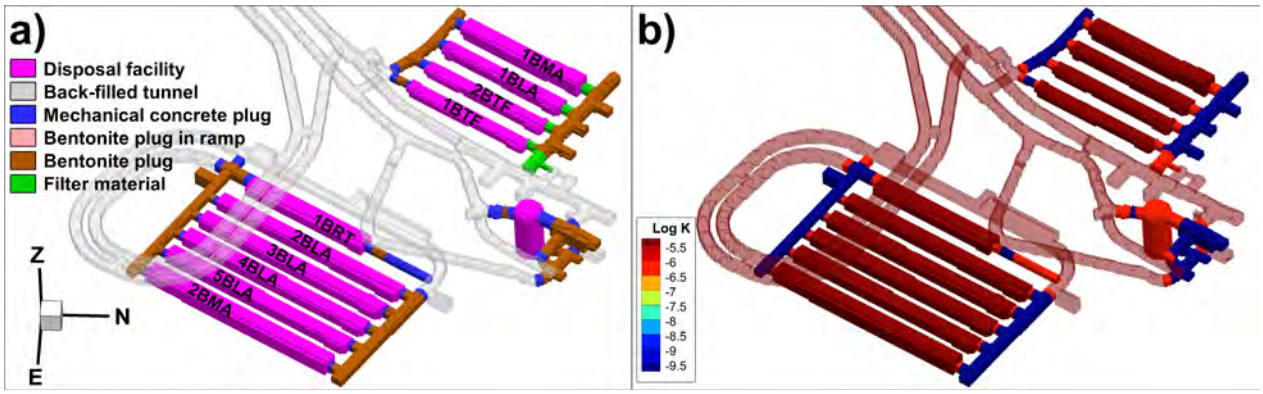

Figure 3-1. *Tunnel conductivity parameterisation; a) back-filling material, and b) parameterised conductivity. Note that the technical barriers of the silo are not implemented.*

3.2 Bedrock parameterisation inside the SFR Regional domain

The performance of the groundwater flow model is subject to *heterogeneity* and *conceptual uncertainty* in the bedrock parameterization. In the groundwater flow model, the bedrock is conceptually divided into two hydraulic domains: HRD and HCD. The combined effect of uncertainty/heterogeneity in bedrock parameterisation is studied by means of a sensitivity analysis of bedrock cases (Table 1-2). Here, a "bedrock case" refers to a combination of parameterization variants of the two hydraulic domains. "HRD variants" are coupled stochastic realisations of discrete fracture networks (DFN) and Unresolved PDZs (as defined in Öhman et al. 2013). "HCD variants" are based on deterministic structural geometry, but with stochastic transmissivity parameterisation to reflect local heterogeneity. To address the uncertainty in the extension of ZFM871, the modelled ZFM871 geometry in /Holmén and Stigsson 2001/ is included as one model variant (referred to as EXT_ZFM871 in Table 1-2).
The variants of bedrock parameterisation are only implemented inside the SFR Regional domain (Figure 2-1). Outside the SFR Regional domain, all bedrock properties outside are kept fixed in the sensitivity analysis.

SBA structures

No variants of SBA structures are addressed in the sensitivity analysis. Similarly to earlier TDs, all simulations include a fixed SBA variant, in which all 8 structures are included (SBA1 to SBA8). Used file is: [R_Parameterized_SFR_SBA1_to_SBA8], based on parameterisation in Appendix B and H in Öhman et al. 2012.

3.2.1 HCD variants

Inside the SFR Regional domain, model sensitivity to HCD parameterisation is analysed by comparing both homogeneous and heterogeneous parameterisation variants in (Table 1-2). The deformation-zone geometry is defined by the geological model v.1.0 /Curtis et al. 2011/. To avoid artificial boundary effects, five HCDs are extended outside the SFR Regional domain according to lineament data.
The following HCD parameterisations are numerically implemented as bedrock variants in TD08 (see Table 1-2):

1) BASE_CASE1 (homogeneous transmissivity with depth trend, according to Appendix 6, SKB 2013)
2) EXT_ZFM871 (identical to BASE_CASE1, but with extended geometry of ZFM871)
3) HETERO_RXX (non-conditioned parameterisation, realisation XX = 01 to 10)

The implementation sequence is presented in Table 3-3.

Borehole-conditioned base case (BASE_CASE1)

A deformation-zone base case parameterisation has been defined in SDM-PSU (Appendix 6, SKB 2013), referred to as BASE_CASE1. In this base case, deformation zones are parameterised by homogeneous transmissivity with depth trend, defined by ground-surface transmissivity, T_0, and the depth interval over which transmissivity is reduced by an order of magnitude, k = 232.5 m (as described in Öhman et al. 2013). Following the methodology applied in SDM-Site Forsmark /Follin 2008/, the depth-trend is implemented as a step function, binned over 100 m-intervals (e.g., Figure 3-2). The reason for this is to reduce artefacts related to the resolution of the HCD-geometry triangulation. Note that a consequence of this step function is that the HCD parameterisation at tunnel intersections in SFR1 and L1B, respectively, are taken from different depth-interval bins. More precisely, the tunnel intersections in SFR1, at $z \approx$ - 80 m, are assigned $T_{eff}(z = 0$ m elevation), while the L1B intersections, at $z \approx$ - 130 m, are assigned $T_{eff}(z = -100$ m elevation).
Moreover, the BASE_CASE1 and EXT_ZFM871 are locally conditioned by available data (Figure 3-2). The zone ZFMNNW1209 (Zone 6), which intersects 4 facilities in SFR1, is locally conditioned by early observations in tunnel inflow and reported grouting requirements (Öhman et al. 2013). It is noteworthy that its intercept with 1BLA is conditioned by one order of magnitude higher transmissivity than $T_{eff}(z)$ (Appendix A-2 in Öhman et al. 2013). Other deformation zones, for example those intersecting L1B, are locally conditioned by available borehole data. Of particular relevance for the L1B disposal-facility cross flow, is that observed transmissivity contrasts, between deep and shallow data, cause uncertainty in the parameterisation of ZFMWNW0835 and ZFMENE3115 (Figure 3-2a). These zones are locally conditioned by borehole data in BASE_CASE1 and EXT_ZFM871, which implies a significant local transmissivity reduction at L1B intercepts, as compared to their effective parameterisation (Figure 3-2b).

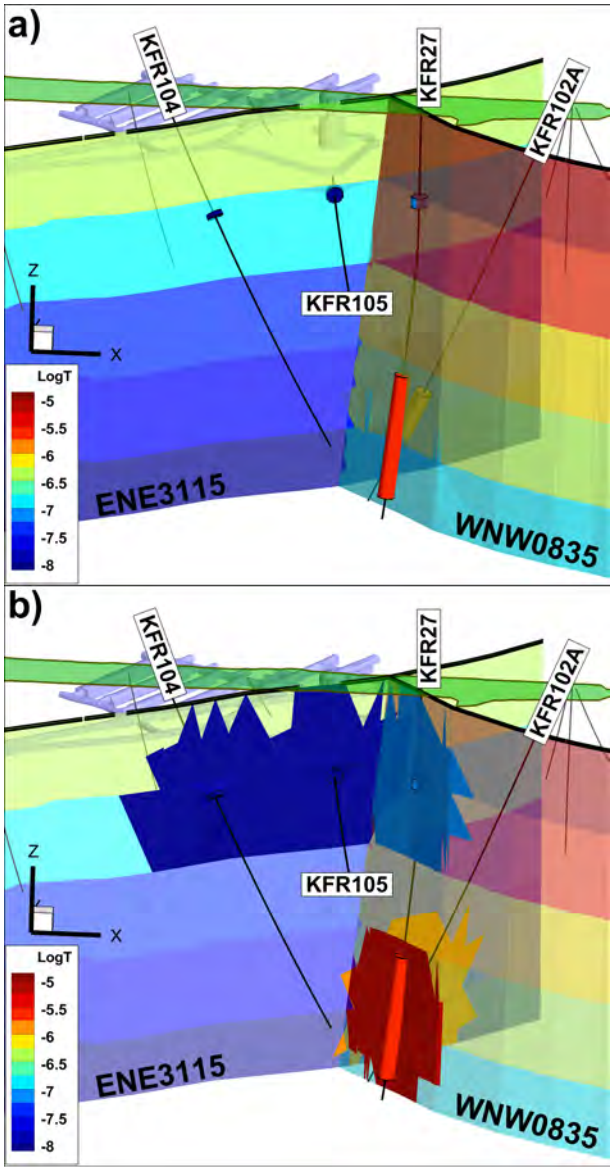

Figure 3-2. *Borehole conditioning of two zones with particular significance for disposal-facility flow; a) borehole data and homogeneous parameterisation with depth trend, b) borehole-conditioned [BASE_CASE1].*

Extended geometry of ZFM871 (EXT_ZFM871)

Owing to uncertainty in the geometric extension of ZFM871, the TD08b sensitivity analysis includes a HCD variant with extended geometry of ZFM871. Note that, in all other aspects except geometric definition of ZFM871, this HCD variant is identical to BASE_CASE1.
The gently dipping ZFM871 (former zone H2) is characterised as highly heterogeneous and, locally, highly transmissive. Owing to its location, just below the existing SFR-1, ZFM871 is speculated as a potential key structure in downstream particle transport. In the geological SFR model v. 1.0 /Curtis et al., 2011/, ZFM871 was terminated against 5 steeply dipping structures (Figure 3-3a). These terminations are highly uncertain, as they were based on modelling principles, generally made due to *lack of data* (lacking borehole coverage), rather than based on evidence of termination. With the exception of the recent site investigations southeast of ZFMENE3115, the data coverage is poor beyond the 5 steeply dipping zones. Geological data from the recent site investigations provide no support for extending ZFM871 southeast of ZFMENE3115. On the other hand, hydrogeological data analysis (Öhman et al. 2012and Öhman et al. 2013) suggests that the hydraulic connection, or influence, of ZFM871 extends:

1) southeast of ZFMENE3115,

2) northeast of ZFMNW0805A/B,
3) northwest of ZFMNNE0869 (although not outcropping).

It is also noteworthy that an additional structure with similar hydrogeological characteristics has been deterministically modelled, SBA6, which has similar geometry as a hypothetical extension of ZFM871 southeast of ZFMENE3115.

Several alternative extensions of this central structure have been suggested in earlier SFR models. In TD08b, the impact of the uncertainty in ZFM871 extension is tested by including a variant with extended geometry, as modelled by /Holmén and Stigsson 2001/ and /Odén 2009/. This variant is referred to as "EXT_ZFM871" (geometry of ZFM871 defined in Table 3-2). Apart from the extended geometry of ZFM871, the parameterisation of variant is *identical* to BASE_CASE1 (i.e., homogeneous transmissivity with depth trend, according to Appendix 6, SKB 2013). Note that two corner points are defined above ground surface (Table 3-2). This implies that in the extended ZFM871 case, its north-western side is assumed to outcrop below seafloor sediments (Figure 3-3b).

Table 3-2. Corner points of assumed geometry in the extended ZFM871 case[1)]

Easting (m)	Northing (m)	Elevation (m)
1631635	6701612	33.1
1632547	6700700	-318.8
1633997	6702149	-292.6
1633085	6703061	65.2

1) Geometric definition in /Holmén and Stigsson 2001/ and /Odén 2009/

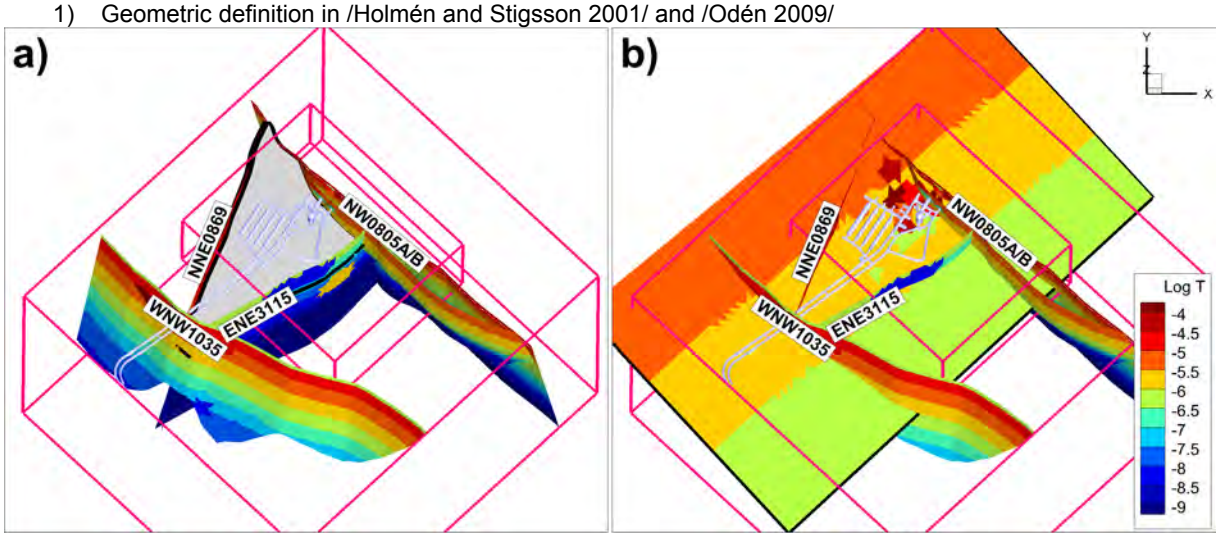

Figure 3-3. *Alternative geometries tested for ZFM871 in TD08b, in context of terminating structures; a) BASE_CASE1 (grey), following the geological model by /Curtis et al. 2011/, and b) EXT_ZFM871, as modelled by /Holmén and Stigsson 2001/ and /Odén 2009/.*

Heterogeneous transmissivity parameterisation (HETERO_RXX)

Local heterogeneity in transmissivity parameterisation is implemented by superimposing a lognormal-distributed random component onto the effective HCD transmissivity. This random component follows $N(0,\sigma_{HCD})$, where σ_{HCD} is the standard deviation of logarithmic transmissivity of an individual HCD, or a group of HCDs (tabulated in Appendix 6, SKB 2013). The random component has a zero expectation value, and therefore the expectation value of the Base case is preserved (including the "binned" depth trend). Extreme values, outside 95%

variability, are rejected and re-sampled. It should be noted that an error has been detected in retrospect, which includes values outside the 95% interval (Section 5.2.3) in TD08.
The HCD geometry is exported from RVS, via RVSinfo.bat, which produces highly irregular triangulation (some triangles are very small, or have high aspect ratio). A selection of HCDs has refined triangulation to allow studying certain issues in Öhman et al. 2013 (e.g., HSD choking in NBB/SBB, borehole conditioning in ZFM871, tunnel conditioning of ZFMNNW1209). Consequently, care must be taken so as to reduce the impact of triangulation in the heterogeneity pattern.

Furthermore, hydrogeological data analysis indicates horizontal anisotropy in the shallow bedrock at SFR, which motivates an anisotropic correlation in heterogeneous HCD transmissivity. To achieve this, HCD heterogeneity is implemented via a regularly meshed random field, which is "draped" onto the HCD geometry (Figure 3-4a). In other words, the random field, which controls σ_{HCD} (-), is aligned parallel with the HCD geometry (in a coordinate system defined by the strike and dip of the HCD; Figure 3-4). To accommodate anisotropic correlation, the bin sizes of the random field are asymmetric, to correspond to a 50 m correlation length in the vertical direction and 100 m in the horizontal direction. The following procedure was taken to implement heterogeneous HCD parameterisation:

1) Based on the centre point of each triangular element of the HCD geometry, the entire HCD geometry can be mapped onto the regularly binned random field. To implement anisotropic correlation, bins are asymmetric (100 m along strike and 50 m along dip; Figure 3-4a).
2) Each triangular HCD element is assigned the value from its mapped random-field bin (Figure 3-4b). Retained random values [0.025 to 0.0975] correspond to 95% of the cumulative normal distribution of N(0,1). Given the parameterised standard deviation of the deformation zone, σ_{HCD} (Appendix 6, SKB 2013) the cumulative percentiles can be translated to the random component following a logarithmic transmissivity distribution, $\log T \sim N(0, \sigma_{HCD})$, where the parameterised standard deviation of the deformation zone, σ_{HCD} is tabulated Appendix 6, SKB 2013. The translation of cumulative percentiles is made via a tabulated inverse cumulative normal distribution [Norm_dist.dat] (Table 3-3).
3) The logarithmic transmissivity of each triangular HCD element, log T(z), is finally calculated by superimposing the random component onto the parameterised effective HCD transmissivity, which is defined as a step function over 100 m intervals (Figure 3-4c): $\log T(z) = \log T_{eff}(z = 0m) + \log(10^{z/k}) + N(0, \sigma_{HCD})$, where T_{eff} is tabulated for z = 0 m in Appendix 6, TR-11-04, *z* is the element-centre elevation, and *k* is the assumed depth interval over which transmissivity decreases one order of magnitude (232.5 m).

This principle is demonstrated for ZFMNW0805B (Figure 3-4). The applied transmissivity parameterisation is the result of: 1) a binned heterogeneity field and 2) expectancy value defined over depth-trend intervals, which are superimposed onto an irregular HCD geometry triangulation (Figure 3-4d). For the three gently dipping zones (ZFM871, ZFMB1, ZFMA2), the "dip" direction is very different from vertical; hence they are correlated 100 m in both directions – along strike and along dip.

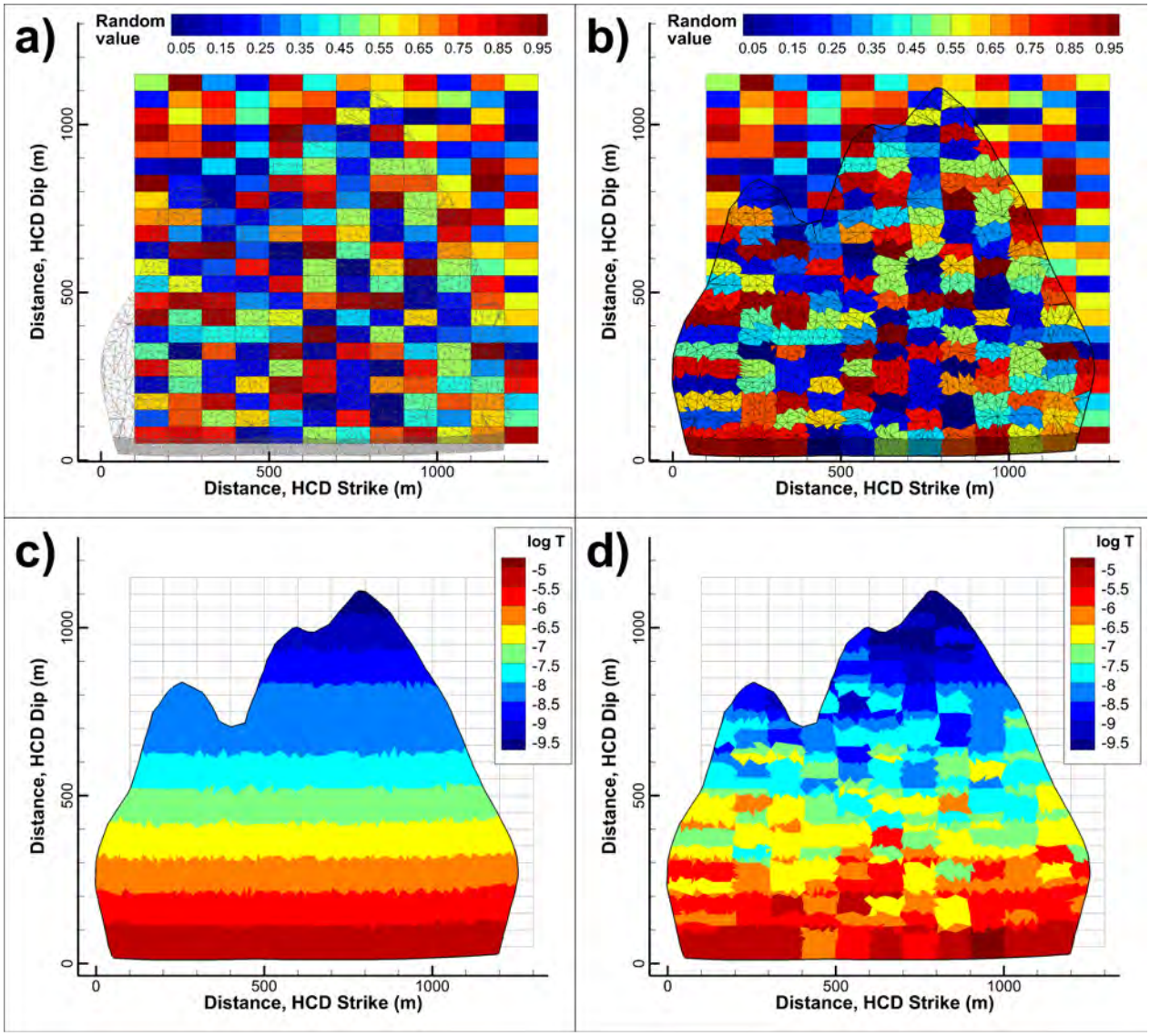

Figure 3-4. *Principle of heterogeneous HCD parameterisation (note that the zone is upside-down, as "distance along dip" is positive along y-axis); a) random field draped onto geometry of ZFMNW0805B, b) random values mapped onto triangular HCD elements, c) effective transmissivity with assumed depth trend (Appendix 6 in TR-11-04), and d) final parameterisation superimposing the random transmissivity component.*

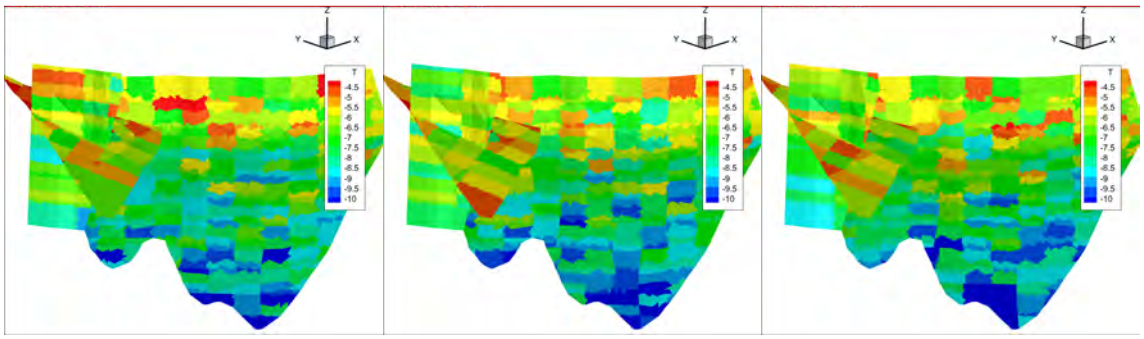

Figure 3-5. *Example of parameterised HCD heterogeneity (R01, R02, and R03). Only deformation zones ZFMNNW1209 (zone 6), ZFM871 (zone H2), and ZFMNW0805b (zone 8) are included in this figure. Applied correlation lengths are 100 m horizontally (along strike) and 50 m vertically (along dip). Gently dipping zones (ZFM871, ZFMB1, ZFMA2) are correlated 100x100m, as dip does not reflect vertical.*

Table 3-3. Implementation of selected HCD variants

Purpose [input]	Execution [output]
1. Define structural geometry data	
Triangulate surfaces of 6 extended HCDs [SFR DZ MASTER v1.0-hydro_extensions.xml]	RVS_info.bat [LINEAMENT_EXTENSIONS.DT]
Combine extended HCDs with geological model v.1.0 /Curtis et al. 2011/ [SKBdoc 1244246 SFR_DZ_MASTER_v1.0.xml] [LINEAMENT_EXTENSIONS.DT]	RVS_info.bat Manual merging in text editor [SFR DZ MASTER v1.0.DT]
Replace the modelled ZFM871 extension in [SFR DZ MASTER v1.0.DT] by triangulated area defined by (Table 3-2)	Manual merging in text editor [SFR HCD v1.0_Ext_ZFM871.DT]
2. Parameterise HCD variants	
Generate HCD variants in DarcyTools "known-fracture" format, by combining: 1. structural geometry [SFR DZ MASTER v1.0.DT] or [SFR HCD v1.0_Ext_ZFM871.DT] 2. hydraulic data [DZ_data.dat][1)] 3. conditional data [Conditional_DZ_data.dat][2)] 4. tabulated inverse cumulative normal distribution [Norm_dist.dat]	[Assign_SFR_HCDs 120116.f], or [Assign_SFR_HCDs_Ext_ZFM871.f], or [Assign_SFR_HCDs heterogeneity.f] (Export fracture file with prefix "**Param_SFR_**"*) [Param_SFR_<HCD variant>] [Param_SFR_<HCD variant>.plt]
3. Rotation	
Rotate DarcyTools known-fracture files into local model coordinate system [Param_SFR_<HCD variant>]	Rotate_DT_objects.f90 (adds prefix "**R_**"*) [R_Param_SFR_<HCD variant>]

1) ASCII input file with HCD parameterisation according to Appendix 6, SKB2013
2) ASCII input file with borehole-conditioning points, Table A-2 in Öhman et al. 2013

3.2.2 HRD realisations (coupled DFN and Unresolved PDZ realisations)

The HRD represents the rock mass domain outside deterministic deformation zones and consists of stochastic realisations of connected discrete fracture networks (DFN) and Unresolved PDZs (conceptually modelled as connected to deformation zones of the Southern and Northern boundary belts; Öhman et al. 2012). The connectivity of the DFN/Unresolved PDZs is combined in the stochastic realisations (i.e., the connected fracture network of RXX, is coupled to the stochastic realisation RXX of Unresolved PDZs). As part of TD05, two realisations, R18 and R85, were identified as "optimistic" and "pessimistic" for SFR1 (Figure 3-6). These are assumed to be representative for the range of HRD heterogeneity, and they are therefore both combined with the heterogeneous HCD parameterisations, HETERO_R01…R10 (see Table 1-2), to evaluate the "maximum model sensitivity" to bedrock parameterisation. To isolate model sensitivity to HRD heterogeneity, 21 DFN realisations (R01 to R20 and R85) are combined with the two homogeneous HCD parameterisations, BASE_CASE1 and EXT_ZFM871 (Table 1-2).

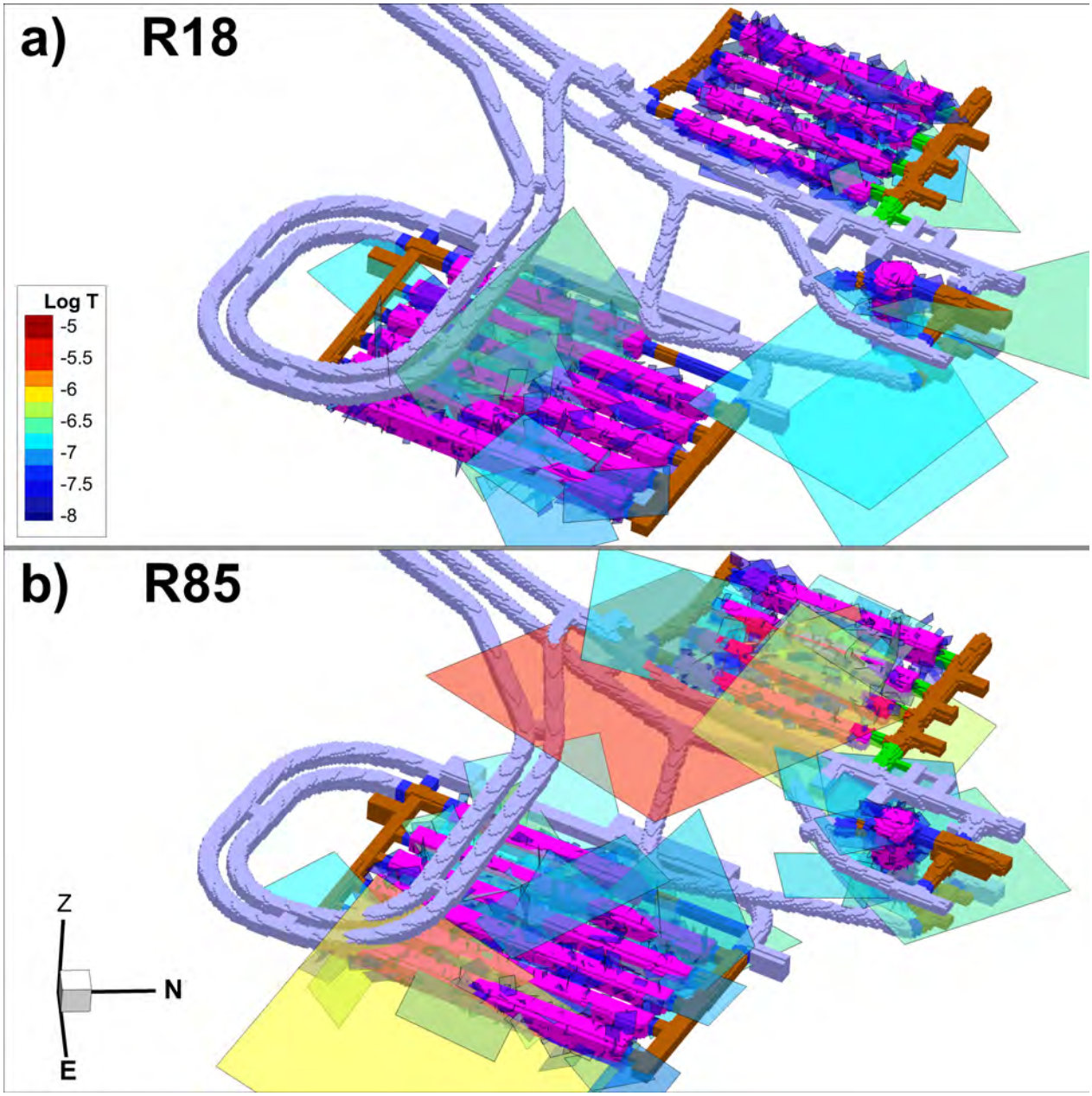

Figure 3-6. *Fractures intersecting disposal facilities (pink-shaded); a) in "optimistic" realisation R18 and b) "pessimistic" realisation R85.*

The DFN generation is described in Öhmnan et al. 2013 ("connectivity analysis" size-distribution alternative); it can be summarized as follows:

1) In the first step, DFNs are generated in a region that exceeds the SFR Regional domain. This is done by means of the DarcyTools module FracGen, for which the DFN model parameterisation (Appendix 5 in SKB 2013) is specified in a Compact Input Command file, cif.xml.
2) In a second step, fractures centres outside the SFR Regional domain are removed (performed by the code [Exclude_Frax_outside_SFR_Reg_dom.f]).
3) Isolated fractures are removed (i.e., fractures that are not part of the globally connected, flowing fracture network). Global connectivity is determined by means of the DarcyTools module FracGen and a Compact Input Command file, cif.xml, specifying the connectivity bounds (Table 3-4). Note that tunnel geometry is part of the

connectivity analysis, and L1B is **always** included in the connectivity analysis, even for TD08a model setups where L1B is not included in the flow model.

4) The DFN realisations are converted into the DarcyTools "known-fracture format" [SFR_DFN_connected_R**XX**_knwn] by means of [Sample_DFN.F90].
5) Finally, the DFNs are rotated into the local DarcyTools coordinate system [**R**_SFR_DFN_connected_R**XX**_knwn] by means of the Fortran code [Rotate_DT_objects.f90]. Pivot point in local coordinate system: [6400. 9200.], rotation angle: 32.58816946˚.

Table 3-4. Deterministic geometries defining bounds in the isolated-fracture removal

Files	Description
Parameterized_SFR_HCD	Deformation-zone geomtery (Section 3.2.1). Note that the alternative extension of ZFM871 is **not** included in the connectivity analysis.
Parameterized_SFR_SBA1_to_SBA8	Deterministic SBA-structure geometry
SERCO_DFN_WITH_HOLE	Deterministic DFN outside the SFR Regional domain. Truncated version, excluding fractures located more than 300 m outside SFR Regional domain (Table 3-6).
Unresolved_PDZ_R**XX**_knwn	Corresponding Unresolved PDZ realisation (**XX** = 18 and 85).
EXISTING_SFR_knwnf	Tunnel geometry of the existing SFR1 in "known-fracture format".
ENTIRE_L1_z117_knwnf	Tunnel geometry of the extension in "known-fracture format", constructed from TecPlot files by means of [Convert_TEC_to_knwnf.f]. Note that this file is **always** included in the connectivity analysis, even for TD08a model setups where L1B is not included.

Table 3-5. HRD realisations (Discrete fracture network + Unresolved PDZs)

Realisation	Files	Description
R18	R_SFR_DFN_connected_R18_knwn R_Unresolved_PDZ_R18_knwn	Optimistic realisation for existing SFR1, used earlier (few large fractures connecting disposal facilities in existing SFR1)
R85	R_SFR_DFN_connected_R85_knwn R_Unresolved_PDZ_R85_knwn	Pessimistic realisation for existing SFR1, used earlier (large fractures connecting disposal facilities in existing SFR1)
RXX	R_SFR_DFN_connected_RXX_knwn R_Unresolved_PDZ_RXX_knwn	Arbitrary realisations, XX = 01 to 20 (note that R18 is identified as "optimistic")

3.3 Bedrock outside SFR Regional domain

The sensitivity analysis of the bedrock parameterisation variants are confined to the SFR Regional domain (Figure 2-1). The bedrock description outside the SFR Regional domain is taken from SR-Site/SDM-Site Forsmark and kept constant (i.e., defined by data in Table 3-6). Note that the filename tags "WITH_HOLE" and "med_hål_i_mitten" denote removal of fractures/HCD geometry inside the SFR Regional domain (explained in Öhman et al. 2013); this is necessary to avoid artificial overlaps at the SFR Regional domain. Similarly, truncations of the SDM-Site sheet joints inside the SFR Regional domain are described in Öhman et al. 2013. The HRD outside the SFR Regional domain is parameterised based on a single DFN realisation, originally delivered from SR-Site [SRS-FFM01-06_v4_alterFinal_nocpm_r1_sets1-65_all_96.asc] (Table 3-6). Within the SDM-PSU/SR-PSU project, the coverage of this DFN realisation has been expanded, by a duplication procedure described in Öhman et al. 2013, to conform to the flow domain (Figure 2-1). It should be noted that this DFN realisation have no fracture centres above z = 0 m elevation, which causes an artificially low hydraulic conductivity in bedrock above c. z = -10 m elevation, with implications to bedrock recharge in the elevated

parts of the Forsmark inland. To compensate this, a minimum bedrock conductivity of $3 \cdot 10^{-8}$ m/s is assigned above z = -10 m elevation (see Table 3-7).
The fracture files representing the bedrock outside the SFR Regional domain are specified in Table 3-6. It should be noted that all fracture files used in the model are rotated into the DarcyTools coordinate system, which tags the prefix "R_" to all filenames with rotated data.

Table 3-6. Fracture files used outside SFR Regional domain

Filename[1)]	Description	Source
PFM_zoner_med_hål_i_mitten	Parameterized HCD, outside SFR Regional domain Exclusion of HCD geometry inside SFR Regional domain (+ entire ZFM871) described in Section 3.3.2 in Öhman 2010. Converted from "dt" into "known-fracture format".	861006_DZ_PFM_REG_v22
EXTENDED_SERCO_DFN_WITH_HOLE	Stochastic DFN outside SFR Regional domain in "known-fracture format". Original file from SDM-Site Forsmark, expanded to cover the SFR flow domain (Figure 3-7).	SRS-FFM01-06_v4_alterFinal_nocpm_r1_65_all_96.asc
PLU_sheet_joints_truncated	Hydraulic deterministic structures (HCD), converted from ifz into "known-fracture format", and locally reduced transmissivity near SFR ramp, as described in Section 3.4.1 in Öhman et al. 2013.	081006_sheet_joints_v5.ifz
Parameterized_SFR_BRIDGES	Used to fill in geometric discontinuities when merging SFR HCDs with those in SDM-Site Forsmark. Parameterised and converted from xml into "known-fracture format" via RVSinfo.	SKBdoc 1282650 – SFR DZ MASTER v1.0-bridges.xml

1) All fracture files are rotated into the local model coordinate system. The prefix "R_" is added to all rotated files, denoting the rotated coordinate system.

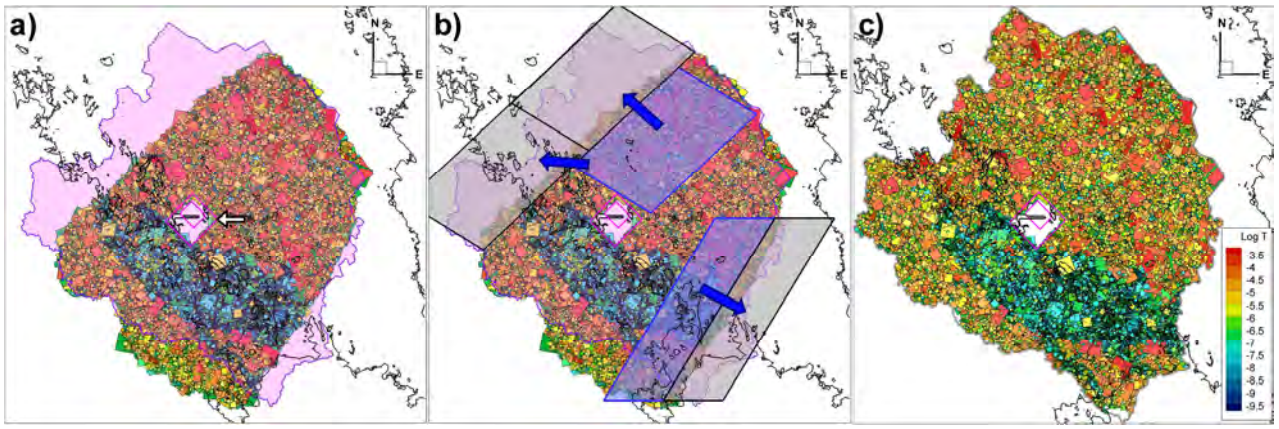

Figure 3-7. *DFN representation outside the SFR Regional domain; a) the SDM-Site Forsmark model domain does not fully cover the SFR flow domain (pink shade), b) representative DFN subareas (blue shade) are duplicated into the uncovered areas (grey shade), and c) merged DFN representation.*

3.4 HSD parameterisation

HSD conductivity of RLDM regolith layers are based on Table 2-3 in Bosson et al. 2010. Porosity is assumed equal to specific yield (Table 3-7). However, particle-tracking performance

measures address only bedrock properties and therefore porosity and fws are nullified in the particle tracking to eliminate the risk of contribution to accumulated transit time or F-quotient.

Table 3-7. HSD hydraulic conductivity of regolith layers

Regolith layer	K_h (m/s)	K_v (m/s)	Porosity[3] (-)	Layer definition (Table 2-3)
Peat[1]	3.00E-7	3.00E-7	0.2	From <lpgd> to <Filled_pdem[1]>
Lacustrine accumulation of postglacial deposits	1.50E-8	1.50E-8	0.05	From <mpgd> to <lpgd>
Marine accumulation of post glacial deposits	1.50E-8	1.50E-8	0.03	From <gkl> to <mpgd>
Glacial clay	1.50E-8	1.50E-8	0.03	From <fill> to <gkl>
Filling	1.50E-4	1.50E-4	0.2	From <glfl> to <fill>
Glaciofluvial material	1.50E-4	1.50E-4	0.2	From <till> to <glfl>
Till	7.50E-6	7.50E-7	0.05	From <bedr> to <till>
Upper bedrock[2]	≥3.0E-8	≥3.0E-8	≥1.0E-5	Thin soil coverage (soil depth < 4.0 m) and elevated bedrock (z>-10 m)

1) Note that the upper surface of peat refers to the basin-filled DEM (Section 2.3.2), which implies that local basins are assumed to be peat-filled, or at least filled with a relatively high-conductive material.
2) A minimum bedrock conductivity of $3 \cdot 10^{-8}$ m/s is assigned in two cases: 1) at thin soil coverage (soil depth < 4 m), and above an elevation of -10 m (this is to compensate that DFN coverage above z = 0 m, is unavailable outside the SFR Regional domain, Section 3.3).
3) HSD porosity set equal to 0.0 in particle tracking to avoid unintentional contribution to performance measures of the bedrock.

As an overview for the SFR near-field, the modelled HSD is visualised in the area where particle-tracking exit points occur (Figure 3-8). The following should be noted in this visualisation:

1) The SFR Regional model domain (orange lines) and land above sea level, 2000 AD are included for spatial reference of the areal extent visualised (c.f. Figure 2-1).
2) Lakes and rivers are not included in the figure (c.f. Figure 2-1).
3) The visualisation employs the "fixed-bedrock" elevation reference, where the bedrock elevation is envisaged as static over time (Section 2.3.5).
4) The filling material of the constructed SFR pier is not visualised.
5) The "filled peat layer" (Figure 3-8e and f) includes two components: 1) peat, as modelled in RLDM, and 2) additional basin-filling of local depressions (performed exclusively in DarcyTools modelling to circumvent model artefacts in modelled groundwater table; Section 2.3.2).

Till is modelled as static (i.e., constant thickness and elevation over time) with wide-spread areal coverage and thicknesses typically ranging from a few meters to 10 m (Figure 3-8b). The till layer is covered by three low-conductive layers (Glacial clay and Lacustrine/Marine accumulated postglacial deposits; Table 3-7). The modelled total thickness of these three layers in RLDM has a patchy appearance in (i.e., accumulation in sheltered topographical basins and partial coverage in areas exposed to wave erosion; Figure 3-8c and d). The change over time is small for these low-conductive layers; the most notable effects are found north of the SFR pier (Figure 3-8d). Basin-filled areas are potential wetlands (i.e., local depressions where the groundwater level is locally allowed to exceed ground surface); these areas are assigned the same properties as peat (Table 3-7).

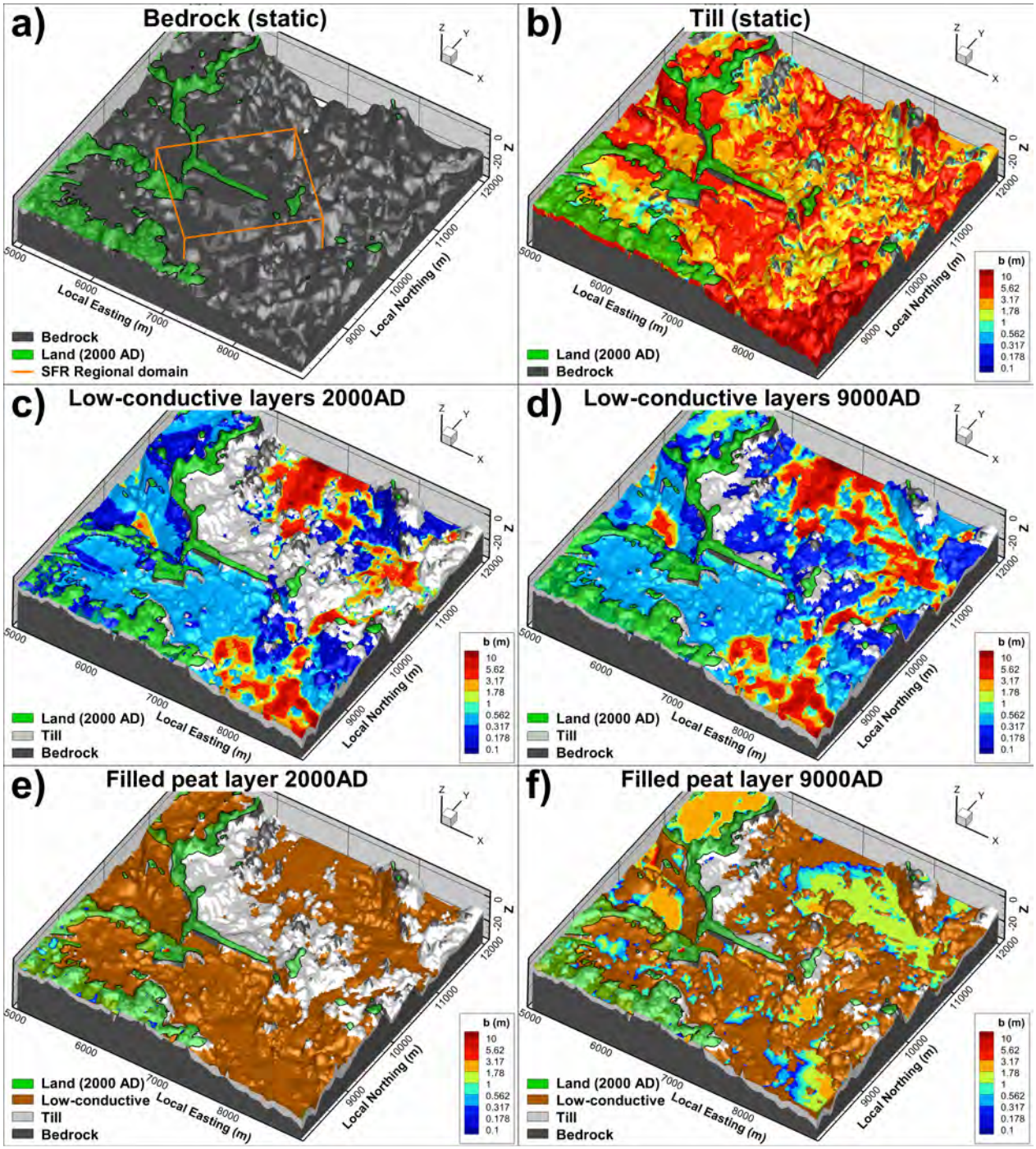

Figure 3-8. *Regolith layers in the SFR near-field, as modelled in RLDM; a) static bedrock surface (dark grey), SFR Regional domain (orange), and land above current sea level (green), b) static till layer thickness (contoured), c) and d) total thickness of low-conductive layers (K = $1.5 \cdot 10^{-8}$ m/s; Table 3-7) of two time slices, and e) and f) modelled peat thickness (i.e., including filling of local basins).*

4 Simulation sequence

4.1 Grid generation

Computational grids are generated by means of the DarcyTools module GridGen. The grids are unstructured, which allows the flexibility of local refinement (e.g., near ground surface and

tunnel geometry). The discretization is carried out via a sequence of commands specified in the standardised Compact Input File on xml-format, [cif.xml] /Svensson 2010/. A discretisation command consists of a geometric reference (i.e., DarcyTools objects in Chapter 2) and either: 1) a specification on local maximum cell side length (Table 4-1), and/or 2) classification of grid subdomains by means of a cell marker ID (Table 4-1). Cell-marker IDs have a key role in subsequent modelling; for example they are used in property assignment, boundary conditions, and particle release points.

Cell-inactivation principle

In the standard DarcyTools approach, the model top boundary is defined by removal of grid cells above topography (i.e., as defined by a DEM). SR-PSU addresses six stages of shore-line retreat (time slices), for which topography alteration is modelled in the dynamic landscape model, RLDM. This time aspect makes the standard "cell-removal approach" very inefficient. The reason is that upscaled ECPM properties (Section 4.2) are valid for a unique grid discretisation, only, which would imply that ECPM conversion must be repeated for each time slice (time consuming and complex file management). Instead, a so-called *cell-inactivation* method is employed, to mimic this topography alteration via cell makers in a *static* grid discretisation. The benefit of the static discretisation is that full compatibility is maintained between grids and ECPM properties. In principle, only time-invariant geometries are used in discretisation, while both time-variant and static geometries are used in classification of cell markers (e.g., Mk 999 = cell inactivation).

Table 4-1. Grid generation

Input files	**Description**
[TD08_cif_GGN_(all_time_slices).xml]	Compact Input File in xml-format, specifying the sequence of discretization commands (i.e., commands specify local grid refinement via geometry of DarcyTools objects)
Geometry data	Prepared in so-called DarcyTools-object format (Section 2). Complete list of input geometry used is traceable via the Compact Input File, and log files.
Output files	**Description**
[xyz_<**time slice**>]	Computational grid used in flow simulations. Six grids are generated with identical discretisation, but different cell classification to reflect the landscape dynamics modelled in RLDM. The identical discretisation implies time-independency in compatibility with upscaled ECPM properties.
[TD08_GGN_<**time slice**>.plt]	Tecplot output, visualising discretisation and cell marking in tunnels and flow-domain cross sections.
[TD08_GGN_<**time slice**>.log]	Log file, per default generated by GridGen

Grid discretisation, in summary[1]		**Max. cell side length**[2] **(m)**	
Domain, defined by [geometric object]	**Delimitation**	**ΔL_H**	**ΔL_Z**
Flow domain [R_WATERDIVIDE_z_1500m.dat]	Outside SFR Regional domain	128	
-1,100 m ≤ z ≤ [R_MAX_Filled_DEM_2000AD_to_9000AD(onlyRLDM).dat]			
SFR Regional domain	z ≥ -180 m	8	
Inside [R_SFR_modellområde_v01.dat]	-400 ≤ z < -180 m	16	
	-1,100 ≤ z < -400 m	64	
HSD	Outside SFR Regional domain	32	1
Above [R_bedrock_up_v2_2000AD.dat]	Inside SFR Regional domain	8	0.5
All tunnel sections of SFR1 and L1B (including disposal facilities and tunnel plugs) [R_entireSFR.dat]		2	
Volume enclosing particle-exit locations[4]	z ≥ -60 m	16	
	-200 ≤ z < -60 m	32	
Volume enclosing Sheet-joints[4]			16

Domain	**Delimitation**	**Cell marker ID**

Bedrock	HCD and HRD	Outside SFR Regional domain	1
		Inside SFR Regional domain	10
RLDM objects	Cell inactivation	Above [R_Filled_pdem<time slice>_Fixed_bedrock.dat]	999
	HSD	Above [R_bedrock_up_v2_2000AD.dat]	100
	Ground surface	[R_Filled_pdem<time slice>_Fixed_bedrock.dat]	101
	Rivers	[R_Filled_Streams_<time slice>_z25.dat]	102
	Lakes	[R_Lake_<Lake ID>_<time slice>.dat]	Table 2-5
Back-filled tunnel sections[3]			
SFR1		[R_ROD_M16.dat]	16
		[R_befSFR_GRON_M17.dat]	17
		[R_befSFR_BLA_M18.dat]	18
		[R_befSFR_VIT_NBT_M19.dat]	19
		[R_befSFR_VIT_SINGO_M20.dat]	20
		[R_ befSFR_ANSL_M21.dat]	21
L1B		Remaining [R_entireSFR.dat] (i.e., not covered by Mk = 11 to 27)	28
Facilities			
SFR1	1BTF	[R_befSFR_forvaring_1BTF_M11.dat]	11
	2BTF	[R_befSFR_forvaring_2BTF_M12.dat]	12
	1BLA	[R_befSFR_forvaring_1BLA_M13.dat]	13
	1BMA	[R_befSFR_forvaring_1BMA_M14.dat]	14
	Silo[5]	[R_befSFR_silo_M15]	15
L1B	2BLA	[R_2BLA.dat]	22
	3BLA	[R_3BLA.dat]	23
	4BLA	[R_4BLA.dat]	24
	5BLA	[R_5BLA.dat]	25
	2BMA	[R_3BMA.dat]	26
	1BRT	[R_1BRT_del1.dat]	27
Plugs[6]			
Mechanical concrete plugs		[R_all_blue.dat]	30
Bentonite plugs		[R_all_brown.dat]	31
Filter-material plugs (Table 2-2)		[R_all_green.dat]	32
Bentonite plugs in ramp		[R_all_wskin.dat]	33

1) This summary only presents an overview of grid discretisation. Full details are traceable via [TD08_cif_GGN_(all_time_slices).xml] and [TD08_GGN_<**time slice**>.log].
2) Refinement expressed in terms of maximum side lengths of cells, in the horizontal and/or vertical direction, ΔL_H and ΔL_z, respectively.
3) Remaining tunnel sections, i.e., not defined as plugged or a disposal facility.
4) Approximate refinement volumes for particle-exit locations and sheet joints specified directly in Compact Input File (i.e., not based on formal CAD geometry). Details in [TD08_cif_GGN_(all_time_slices).xml].
5) No differentiation between Silo storage volume and technical barriers (Section 3.1).

In a secondary step, any HSD cells on top of: a) an inactivated cell, b) a lake cell, or c) a river cell, are inactivated by means of the DarcyTools module PropGen.

4.2 ECPM upscaling

DarcyTools employs a Continuum Porous-Medium (CPM) representation /Svensson et al. 2010/, in which the hydraulic properties of a flowing fracture network are approximated by those of a porous medium. DarcyTools allows transferring fracture-network characteristics onto its computational grid by means of geometric upscaling. The upscaled properties are referred to as Equivalent Continuous Porous Medium (ECPM) properties. As the ECPM approach is based on an underlying stochastic DFN model, the resulting ECPM properties are also stochastic. Geometric up-scaling does not always ensure *hydraulic* consistency between the complex heterogeneity of the underlying flowing fracture network and the approximated ECPM. Thus, "Equivalent" implies a fine resolution of the computational grid in order to be valid.

DarcyTools employs a *staggered* grid arrangement with ECPM properties which are derived from geometric fracture-network upscaling over local control volumes /Svensson et al. 2010/. This staggered grid involves *scalar* properties, defined at cell centres (e.g., porosity and flow-wetted surface area), and so-called *tensor* properties, stored at cell walls (e.g., conductivity). In other words, scalar and tensor ECPM properties do not represent identical control volumes, but are offset by half a grid cell.
A consequence of the staggered grid arrangement is that each step in the cell-jump particle tracking approach involves *one* cross-cell flow, but *two* grid-cell porosities and fws-values (Section 4.4.2). The ECPM conversion relies on several approximations:

- all fractures inside a cell-wall control volume contribute to advection
- the advection takes place over their full fracture surface area
- porosity of fractures below the fracture-size truncation is negligible.

ECPM Porosity

In SR-PSU, the performance measures from DarcyTools simulations are only calculated for the bedrock; therefore both porosity and fws are nullified in tunnel backfill and in overlying sediments. Kinematic porosity is a critical parameter for determining particle transport time, but unfortunately the parameter is difficult to measure in field. Therefore, four different variants of porosity parameterisation are tested in TD08 (Table 4-2). Based on consideration of results (Section 5.5), a project decision was taken that variant 1 (Upscaled ECPM porosity) with a minimum porosity of 10^{-5}, will be used in formal deliveries for SR-PSU.

Table 4-2. Porosity parameterisation variants

Variant		Description
1	Upscaled ECPM porosity	ECPM porosity, upscaled from transport apertures in the underlying fracture network, Eq. (4-1), by means of the DarcyTools algorithm GEHYCO. Note that porosity contribution of fractures below size criterion is not included.
2	Empirical relation of equivalent transport apertures	Direct application of Eq. (4-2), assuming that an empirical relation for *equivalent apertures*, compiled from cross-hole tracer tests (Hjerne et al. 2010) can be *directly* applied as *ECPM* properties in the numerical grid.
3	Constant, n = 0.0001	A global (constant) value of n = 0.0001 (typical value along particle trajectories, as obtained through GEHYCO upscaling of Eq. (4-1); Figure 4-1)
4	Constant, n = 0.005	A global (constant) value of n = 0.005 (used in earlier SFR performance measures (Holmén and Stigsson 2001) and SAR-08)

Kinematic porosity can be calculated in the numerical flow model, by means of the GEHYCO algorithm (Svensson et al. 2010), which upscales ECPM porosity based on transport apertures of fracture networks. Äspö Task Force 6c results (Dershowitz et al. 2003), has suggested a fracture transport aperture correlated to transmissivity, according to

$$e_t = 0.46\sqrt{T}. \qquad (4\text{-}1)$$

which was also used as a starting point for model calibration in SDM-Site Forsmark (Follin 2008).

Hjerne et al. (2010) compiled 74 field tracer tests, conducted at different sites and at various scales, and fitted an empirical relation between transport aperture and transmissivity of *equivalent fractures*

$$e_t = 0.327\, T^{0.306}. \qquad (4\text{-}2)$$

In other words, the relation in Eq. (4-2) reflects *equivalent properties* for assumed, idealized, single-fracture geometry*;* in reality the compiled tracer tests are expected to cover a wide range of complex fracture-network geometry configurations. There is a conceptual analogy between the equivalent properties in Eq. (4-2) and the ECPM properties in the DarcyTools grid. It is therefore tempting to consider Eq. (4-2), as an alternative representation of equivalent porosity over different scales. However, at least two systematic biases should be noted in empirical relation Eq. (4-2): 1) tracer tests are never performed in non-conducting borehole sections, and 2) non-recovered tracer tests are excluded (more detailed discussion in Ch. 7 of Hjerne et al. (2010).

Porosity along preferential flow paths

The general porosity of the SFR Regional domain, as resulting from GEHYCO, is typically in the range 10^{-4} to 10^{-5} (blue bars in Figure 4-1). However, particle trajectories do not represent average bedrock, but preferential flow paths of minimum resistance, i.e., along conductive features. Thus, the porosity along particle trajectories is considerably higher than it is in the average bedrock (red bars in Figure 4-1). Based on these results, a constant porosity of 10^{-4} is tested as variant 3 in Table 4-2. Nevertheless, the porosity along trajectories is still low compared to field observations (Hjerne et al. 2010).

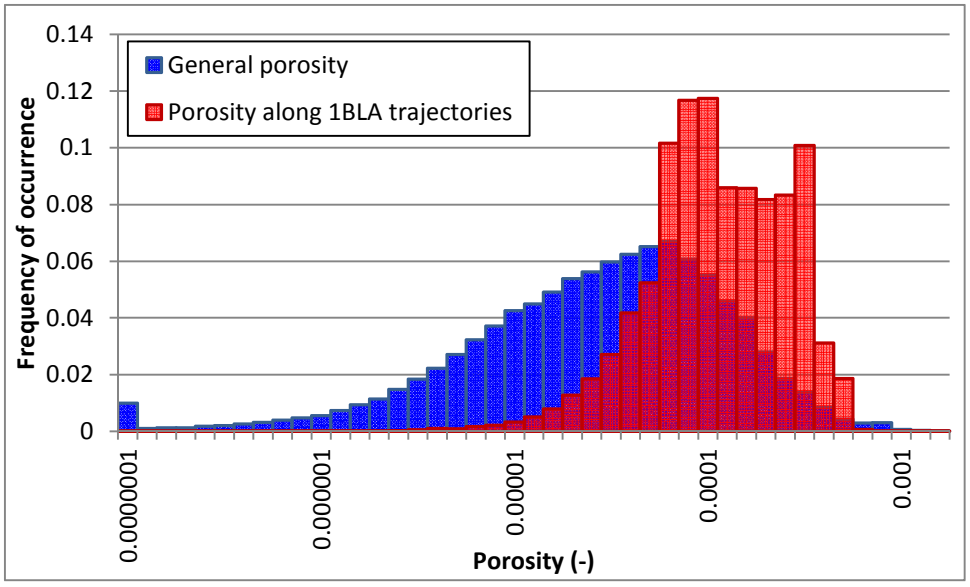

Figure 4-1. *Example of porosity distributions from case EXT_ZFM871_DFN_R18; a general sample (300,000 random cells; blue) compared to porosity along preferential flow paths (500,000 cells along trajectories from 1BLA; red).*

File management

The ECPM conversion is executed by Golder [TD08_ECPM_conversion_READ_ME.txt], and the results are uploaded to the Project place. ECPM properties are the result of: 1) a given set of input fracture files and 2) a given grid discretisation, and therefore the results are only valid for a specific grid discretisation. The six stages of landscape dynamics, as modelled in RLDM, are represented by six grids with "time-dependent" cell marking (Section 4.1). However, the *discretisation* is identical in all grids and therefore ECPM properties are generic for all grids. ECPM upscaling is featured by the DarcyTools module FracGen (GEHYCO algorithm) /Svensson et al. 2010/, for which all input data are specified in a standardised Compact Input File, on xml-format [cif.xml]. The file management is automatized. ECPM upscaling is managed by means of [Manage_ECPM_setups.f90] in 6 steps:

1) Identify a <**Bedrock case**> from the manual input file [List_of_model_setups_for_ECPM.txt]
2) Ensure existence of all required input files (Table 4-3),
3) write the Compact Input File for FracGen, i.e., a temporary cif.xml specifying input files for the given <**Bedrock case**>,
4) execute FracGen with the temporary cif.xml,
5) write control file [`ECPM_setup.txt`],
6) write and execute [`Store_data.bat`], which creates the folder [<**Bedrock case** >] in which ECPM-property files are stored (Table 4-3).

Table 4-3. ECPM conversion [DarcyTools module FracGen] 1)

Input files	**Description**
List_of_model_setups_for_ECPM.txt	List of bedrock cases (Table 1-2) and layouts.
Cif.xml	Compact Input File in xml-format, which is the default input file for the DarcyTools module FracGen, specifying involved indata for ECPM upscaling (fracture files and computational grid). The input file is automatically generated by [Manage_ECPM_setups.f90] and is not stored.
[xyz]	Computational grid. A single grid can be used in ECPM uspscaling, as *discretisation* is static in all grids. Note that [xyz_<**time slice**>] refers to time-dependent marked grids (i.e., lakes, rivers, and HSD-layering), which does not affect upscaling.
One HRD variant in Table 3-5	Stochastic realisation of bedrock outside deterministic deformation zones, inside the SFR Regional domain
One HCD variant (Section 3.2.1)	Parameterisation variant of deterministic deformation zones inside the SFR Regional domain
R_Parameterized_SFR_SBA1_to_SBA8	Deterministic representation of SBA structures, inside the SFR Regional domain
All fracture files in Table 3-6	Static bedrock parameterisation outside the SFR Regional domain
Output files	
[ECPM_setup.txt]	Control file specifying <**Bedrock case**>
[<**Bedrock case** >_condx.dat]	Cell-wall ECPM conductivity in x-direction (rotated coordinate system)
[<**Bedrock case** >_condy.dat]	Cell-wall ECPM conductivity in y-direction (rotated coordinate system)
[<**Bedrock case** >_condz.dat]	Cell-wall ECPM conductivity in z-direction
[<**Bedrock case** >_frevol.dat]	Cell ECPM free volume (i.e., intersectional volume sum of fracture aperture, Eq. (4-1), used to calculate bedrock porposity)
[<**Bedrock case** >_fws.dat]	Cell ECPM flow-wetted surface area (i.e., intersectional sum of fracture area)

1) Manual procedures described in [TD08_ECPM_conversion_READ_ME.txt]. <Bedrock case> = <HCD variant>"_DFN_RXX" (see Table 1-2).

4.3 Flow simulations

DarcyTools is primarily a modelling tool for site-scale groundwater flow in deep rock. As such, surface runoff can typically not be resolved in detail. Consequently, a model artefact of local excess head may occur at ground surface, if net precipitation exceeds local recharge (i.e., local excess head defined as exceeding topography). Two methods are commonly applied to circumvent this model artefact:

1) Prescribed-head boundary condition at the model top boundary (e.g., assume H = $z_{topography}$)
2) Free-groundwater table (inbuilt DarcyTools algorithm)
3)

Both approaches have their merits and drawbacks. The prescribed-head approach is a numerically convenient approach, as it is determined from topography alone. However, it *assumes* that saturated conditions apply without consideration to locally varying hydrogeological conditions, and therefore it is not very realistic in areas that can be expected to be unsaturated (e.g., local topographical peaks and glaciofluvial deposits). This approach is particularly inappropriate in SR-PSU, as the model representation of SFR pier may have a significant impact on model performance. The standardised free-groundwater algorithm, on the other hand, is based on a combination of topographical data and a rudimentary depiction of hydraulic properties in the uppermost 20 m of the soil/bedrock (i.e., not data based). The result is a smooth groundwater table and a realistic representation of unsaturated areas. The drawbacks are: 1) the method allows excess head, 2) the parameterisation is not expected to be generic (calibrated for the current shoreline, and for a specific lake/river data set), and 3) a generalization of the uppermost 20 m is inappropriate for the shallow location of SFR. Instead, a hybrid approach is suggested, where the two boundary-condition types "flux" and "fixed head" are mixed in a preceding "Recharge phase" to simulate realistic head for the model top boundary (allowing unsaturated areas, but not excess head). The top-boundary head is then applied as a fixed-head boundary condition in subsequent steady state simulations, in order to establish a high-convergent flow solution. The flow simulations are managed in three steps:

1) Final setup of the model parameterisation (Section 4.3.1)
2) Solve a realistic top-boundary condition in a so-called "Recharge phase" (Section 4.3.2)
3) Apply the top-boundary condition in a so-called "Steady-state phase" (Section 4.3.3) to obtain a high-convergent flow solution

Manage flow simulations

The Recharge-phase simulations in TD08a are "executed manually" (i.e., conventional DarcyTools approach, under manual supervision of convergence, see [TD08_DTS_Recharge_READ_ME.txt]). The subsequent steady-state simulations, in TD08a and TD08b, are automatized[1] in 6 steps:

1) Identify a <**Bedrock case**> from the manual input file [List_of_model_setups_for_DTS.txt]
2) Retrieve and ensure the existence of required input files (Table 4-4)
3) Loop steps 4 to 6 for hard-coded selection of <**time slice**>
4) Write the control file [DTS_setup.txt], which is used in subsequent model parameterisation, flow simulations, and particle tracking
5) Write a Compact Input Files for the steady state flow simulation (cif.xml)
6) Write and execute [`Run_DarcyTools.bat`], which:

a. Creates a local folder [RUN_<**time slice**>] in the working folder [<**Bedrock case**>],
b. Finalises the model parameterisation[2]
c. Applies the top-boundary condition from TD08a for a given <**time slice**> to solve the flow field[3]
d. Renames output/input to tag <**Bedrock case**>, <**time slice**> and <**Extension**>
e. Moves simulation input/output files into the local run folder [RUN_<**time slice**>].

[1] Two virtually identical codes are used, [Manage_TD08a.f90] and [Td8b_Manage_DT_runs.f90], for the execution.
[2] PropGen compiled from two virtually identical codes [prpgen_TD08a_Final.f] and [prpgen_TD08b_FINAL.f]
[3] DTS compiled from Fortran Input File [fif - TD08_final.f]

4.3.1 Finalise model setup

The final model setup (i.e., property assignment in the computational grid) is performed by means of the DarcyTools module PropGen (Svensson et al. 2010), as compiled from customized source code variants. PropGen has the following key functions:

1) Finalise the hydraulic-domain parameterisation. Input data on bedrock ECPM conductivity (HRD and HCD in Table 4-3) and HSD conductivity (Table 3-7) are merged and converted into permeability (i.e., the operational unit in DarcyTools). Any bedrock conductivity below 10^{-10} m/s are re-set to a minimum value of $3 \cdot 10^{-11}$ m/s. Cells marked as 999 are inactivated, by setting cell-wall conductivities $K_{inactive} = 10^{-20}$ m/s.
2) Identify tunnel and tunnel-plug cells, based on cell markers (Table 3-1), and implement as permeability (i.e., over-writing "bedrock values"),
3) Calculate cell porosity, *n*, for variant 1 in Table 4-2, defined as sum of intersectional fracture volume per cell volume (i.e., fracture volume is based on fracture area and transport aperture in Eq. (4-1). A minimum porosity of 10^{-5} [-] is applied.
4) Output is also exported in TecPlot format for visual verifications (e.g., Figure 3-1).

Numerical implementation inactive cells

The modelling procedure employs a *cell inactivation method*, to be able to represent topographical changes between different time slices with a single grid. Grid cells above the basin filled DEM for a given time slice are defined by setting the DarcyTools cell marker to 999. Two measures are taken to isolate these cells from taking part in the flow solution: 1) an extremely low conductivity value is assigned to all cell walls, $K_{inactive} = 10^{-20}$ m/s, and 2) an arbitrary fixed-head boundary condition is prescribed to the cells, i.e., H = 0.0 m. In effect, the cells marked 999 are isolated from the flow solution. The benefit is that the cells are not permanently deleted, but can be re-activated for modelling a different time slice. Special care must be taken to inactivated cells in recharge calculations.

Numerical implementation of HSD conductivity

Soil cells are identified by two DarcyTools cell markers: 1) mk = 100, representing general soil, defined as cells above bedrock surface, and 2) mk = 101, representing the uppermost, contiguous cell-layer intersected by the DEM of the current time slice. The HSD parameterisation is facilitated by a separate subroutine "HSD"[2], which can be summarized in 4 steps:

1) Use DarcyTools cell markers to identify grid cells classified as HSD
2) Match the DarcyTools grid cell, by coordinate, to relevant raster point(s) in RLDM (Table 2-3)
    a) DarcyTools cells below the RLDM resolution are matched to the *nearest* RLDM point
    b) DarcyTools cells exceeding RLDM resolution are matched to *an array* of RLDM points
    c) Matching cells by coordinate requires back-rotation and translation into the RT90 coordinate system.
3) Calculate an effective HSD conductivity for the cell, based on the fractional intersection thicknesses, b_i, between the cell-wall control volume and the layer *i*, which has hydraulic conductivities K_{hi} and K_{vi} (Table 3-7).
    a) Effective horizontal conductivity is calculated as *arithmetic* mean of all $b_i \times K_{hi}$
    b) Effective vertical conductivity is calculated as *harmonic* mean of all $b_i \times K_{vi}$
4) Defaults are applied at inconsistencies between the DarcyTools grid and the RLDM data (i.e., for cells where $\Sigma b_i = 0$ m)
    a) *Outcrops* are set to $K = 10^{-7}$ m/s, for cell markers = 101 where RLDM thickness = 0 m.

b) *Till* is assumed, for cells located outside the horizontal coverage of RLDM
c) The *uppermost* or *lowest* RLDM layer with non-zero thickness is assumed, respectively, if the grid and RLDM layer elevations should mismatch vertically.

Table 4-4. Final model setup [prpgen_TD08_Final.f][1)]

Input files	Description
[DTS_setup.txt]	Defines <**Bedrock case**>, <**time slice**>, and <**Extension**>
[xyz_<**time slice**>]	Computational grid (i.e., time-dependent marking of lakes, rivers, and HSD-layering; Table 4-1)
[<**Bedrock case**>_condx.dat] [<**Bedrock case**>_condy.dat] [<**Bedrock case**>_condz.dat]	Cell-wall ECPM bedrock conductivity in x, y, and z-directions (Table 4-3)
[<**Bedrock case**>_frevol.dat]	Cell ECPM free volume (Table 4-3; i.e., intersectional volume sum of fracture aperture, Eq. (4-1)
[Filled_pdem<time slice>_Fixed_bedrock.asc]	Upper surface of basin-filled DEM, z (m, elevation; fixed-bedrock format)
[lpgd<time slice>_Fixed_bedrock.asc]	Upper surface of lacustrine accumulation of postglacial deposits, z (m, elevation; fixed-bedrock reference)
[mpgd<time slice>_Fixed_bedrock.asc]	Upper surface of marine accumulation of post glacial deposits, z (m, elevation; fixed-bedrock reference)
[gkl<time slice>_Fixed_bedrock.asc]	Upper surface of glacial clay, z (m, elevation; fixed-bedrock reference)
[fill<time slice>_Fixed_bedrock.asc]	Upper surface of filling, z (m, elevation; fixed-bedrock reference)
[glfl<time slice>_Fixed_bedrock.asc]	Upper surface of glaciofluvial-material, z (m, elevation; fixed-bedrock reference)
[till<time slice>_Fixed_bedrock.asc]	Upper surface of till, z (m, elevation; fixed-bedrock reference)
[bedr<time slice>_Fixed_bedrock.asc]	Static bedrock surface, z (m, elevation; fixed-bedrock reference)
Table 3-7	HSD conductivity parameterisation (hard coded in separate subroutine)
Table 3-1	Tunnel back-fill parameterisation (hard coded in separate subroutine). Identification via cell markers.
Output files	
[<**Bedrock case**>_PERMX_<**Extension**>_<**time slice**>] [<**Bedrock case**>_PERMY_<**Extension**>_<**time slice**>] [<**Bedrock case**>_PERMZ_<**Extension**>_<**time slice**>]	Cell-wall ECPM permeability in x, y, and z-directions
[<**Bedrock case**>_PORO_<**Extension**>_<**time slice**>]	Cell ECPM porosity
[<**Bedrock case**>_ECPM_K.plt]	Tecplot output for visualisation. Contains conductivity of tunnel-walls (e.g., Figure 5-10) and flow-domain cross sections.

1) More precisely, two variants are used: [prpgen_TD08a_Final.f] and [prpgen_TD08b_FINAL.f]. <Bedrock case> = <HCD variant>"_DFN_RXX" (see Table 1-2). <time slice> defined in Table 1-1. <Extension> = "SFR1" for only SFR1 and "SFR2" for coexisting SFR1 and L1B.

4.3.2 Determining top-boundary condition in a recharge phase

The top boundary is defined as the uppermost layer of *active cells* in the grid (i.e., the cell layer immediately below, either permanently deleted, or temporarily inactivated cells, at a given time slice). The purpose of this initial "recharge phase" is to establish a realistic top-boundary condition for the subsequent steady-state simulations (i.e., head condition for surface-layer

cells). The recharge phase is simulated for all six time slices (Table 1-1) in TD08a (i.e., **only** for <Bedrock case> = BASE_CASE1_DFN_R85). The ground-surface head solutions of TD08a are then *assumed* to be realistic boundary conditions for all bedrock cases in TD08b. As such, the recharge phase has two primary targets:

1) constrain unrealistic excess head, i.e., ground-surface head cannot exceed topography, except in local depressions. Basin-filled DEMs (Section 2.3.2) are applied to allow excess head in local depressions.
2) allow unsaturation, for example, in local topographical peaks. Two such examples with particular significance for the local flow field in SR-PSU are: 1) the SFR pier and 2) islets east of the SFR pier.

The determination of head in the model top boundary is primarily based on the following four key components:

1) Fixed head in pre-defined surface-water areas in RLDM (Section 2.3; Table 4-5)
2) Spatially variable recharge, locally ranging from 0 to full net precipitation, P-PET = 160 mm/yr,
3) Maximum-head criterion in surface-layer cells, determined by local topography, and
4) Local HSD conductivity.

Table 4-5. Fixed head in pre-defined surface-water areas

Surface-water	Identification	Prescribed head, H (m, elevation)
1. Seafloor	Uppermost cell layer below relative sea level (Table 2-7)	$z_{sea\ level}$ (Table 2-7)
2. Lakes	cell markers (Table 2-5)	$z_{lake\ threshold}$ (Table 2-5)
3. Rivers	cell marker Mk = 102	[River_head.in][1)]

1) The input file [River_head.in] contains river-trajectory nodes (x,y) and estimated riverbed head for each time slice (Section 2.3.4). Prescribed head for river cells are interpolated based on the nearest two river-trajectory nodes.

Maximum-head criterion in surface-layer cells

Excess head in ground-surface cells is defined as head exceeding the local topography. As discussed in Section 2.3.2, the DEMs modelled in RLDM [pdem<time slice>.asc] contain local depressions that are below the scale for defining lakes. These depressions may hold surface water, e.g., minor lakes, wet lands, pools, or be peat-filled. Irrespectively of which, it can be argued that the head criterion should not relate to the local elevation in depressions, but by the geometric *threshold* surrounding depression. Therefore, the "excess head" in top-boundary cells is defined as H - z_{DEM} (m, elevation in fixed-bedrock reference), where z_{DEM} refers to the local basin-filled DEM elevation (Section 2.3.2).
The elevation of ground-surface cells, z_{DEM}, is determined from two files (Table 2-4):

1) [Filled_pdem<time slice>_Fixed_bedrock.asc], which covers most of the flow domain area (Figure 2-4). Mapping grid cells onto the RLDM raster data requires a step of back-rotating and translating cell coordinates into the RT90 coordinate system. This mapping between RLDM and DarcyTools is inexact due to combined effect of: 1) discretisation differences and 2) coordinate-system rotation.
2) [Filled_ROTATED_LOCAL_DEM_<time slice>.dat], which covers the approximate area of particle exit locations. This DEM has been basin-filled in the *rotated coordinate system*, to improve the mapping between DarcyTools cells and the RLDM grid.

Although the basin-fill is a substantial improvement, the inexact mapping implies that a complete absence of local depressions cannot be guaranteed in groundwater flow simulations. Ground-surface head oscillates between iterations, due to: 1) step-wise adjustments in local recharge, and 2) resulting non-stationary flow solution. Therefore, an "excess-head tolerance"

was introduced, which declines as a function of iterations (Figure 4-2). After c. 30 iterations, this tolerance levels out to a constant 0.25 m, which is judged to reflect the combined errors from: 1) RLDM modelling and 2) the inexact mapping between DarcyTools and RLDM. For ground-surface cells exceeding the tolerance, the boundary-condition type is switched from "flux" to "fixed head", where $H = z_{DEM}$ (m, elevation). The resulting ground-surface head after 100 iterations are used to specify fixed head in the subsequent steady-state phase (Section 4.3.3).

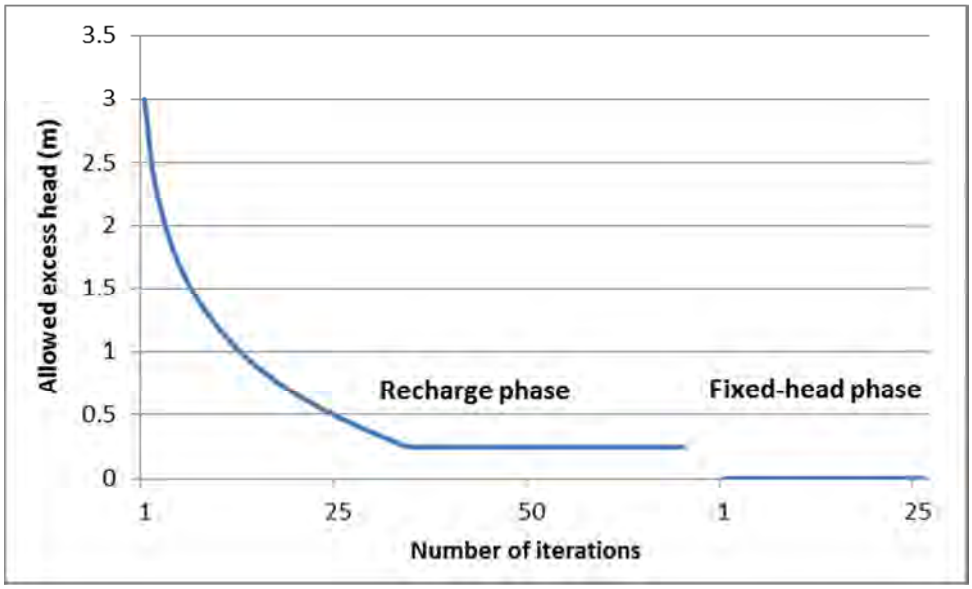

Figure 4-2. *Tolerance in simulated excess head of ground-surface cells in the recharge phase.*

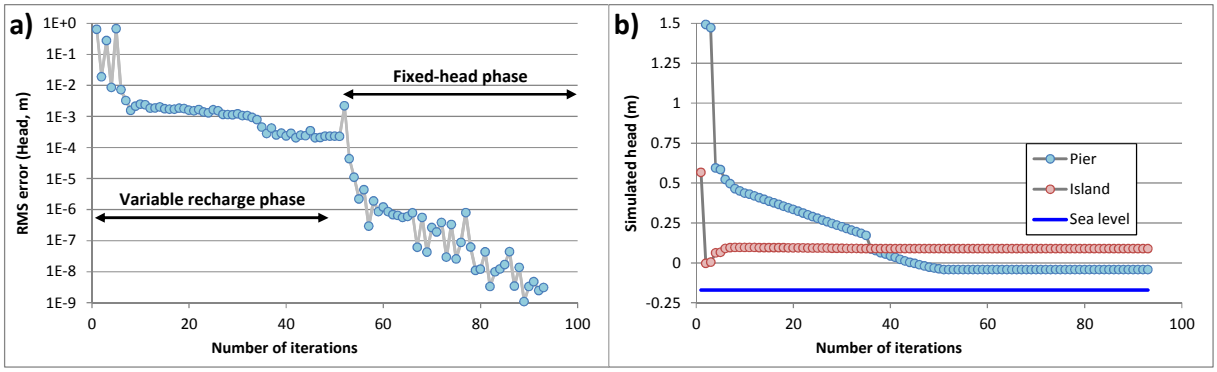

Figure 4-3. *Example of the two simulation phases for 2000AD; a) convergence expressed in root-mean-square error in simulated head, and b) simulated head in two elevated areas in the SFR-near field, with particular relevance for the simulated flow field and particle trajectories.*

Conceptualisation of local recharge

The flow domain has a generally flat topography (Figure 2-1), particularly in areas that are currently below sea. Therefore, large areas are expected to be saturated with large runoff components (i.e., in addition to the pre-defined open-water types in Table 4-5). Surface runoff is controlled by surface-hydrology components below the resolution scale of the DarcyTools model setup (e.g., small brooks and overland flow); in other words, geometric details with high hydraulic contrasts, that cannot be realistically represented in a model that primarily targets bedrock and future conditions. Consequently, neglecting the runoff component leads to local excess head where net precipitation exceeds recharge (i.e., local excess head defined as exceeding basin-filled topography). Excess head is an unrealistic model artefact, which implies

a risk of exaggerating local gradients and flow, as well as, distorting the particle-tracking exit locations. Two means are therefore taken to deplete artificial excess head in surface-layer cells:

1) Local recharge is envisaged as [net precipitation - runoff]. In cells with excess head, the local recharge is reduced sequentially by iterations, from a maximum of P-PET = 160 mm/yr to a minimum of 0.0 mm/yr. The reduction is done on a cell-specific basis.
2) Excess head larger than the tolerance (Figure 4-2) changes the boundary condition of the individual cell from "flux type" to "fixed-head type".

Input/output of the "Recharge-phase "simulation

The recharge phase is simulated under conditions compiled from a Fortran Input File (Fif.f) [fif - RECHARGE_TD08]. The recharge phase is simulated for all six time slices (Table 1-1) of TD08a (i.e., <**Bedrock case**> = BASE_CASE1_DFN_R85). The ground-surface head solution is then *assumed* to be a valid boundary condition for all bedrock cases in TD08b. The input/output of the Recharge phase is described in (Table 4-6).

Table 4-6. "Recharge-phase" simulation (TD08a), input/output[1)]

Input files	Description
[DTS_setup.txt]	Manually constructed, defining <**Bedrock case**>, <**time slice**> and <**Extension**>
[TD08_DTS_Recharge_cif.xml]	Template for manually constructed standard Compact Input File.
[xyz_<**time slice**>]	Computational grid (Table 4-1)
[PERMX_<**Extension**>_<**time slice**>] [PERMY_<**Extension**>_<**time slice**>] [PERMZ_<**Extension**>_<**time slice**>]	Cell-wall ECPM permeability in x,y, and z-direction. Note that TD08a includes only <**Bedrock case**> = BASE_CASE1_DFN_R85; this is not tagged in the input file name (c.f., Table 4-4).
[Filled_pdem<time slice>_Fixed_bedrock.asc]	Surface of basin-filled DEM, z (m, elevation; fixed-bedrock format). Defines maximum-head criterion for ground-surface cells.
[Filled_ROTATED_LOCAL_DEM_<time slice>.dat]	Local DEM surface covering SFR Regional domain, z (m, elevation; fixed-bedrock format). Basin-filled in the rotated coordinate system. Defines maximum-head criterion for ground-surface cells.
[River_head.in]	Fixed-head condition along riverbeds (Table 2-6)
Output files	
[rstslv_<**Extension**>_<**time slice**>]	Flow solution (standardised DarcyTools restart file). The head solution in ground-surface cells is propagated as a top-boundary condition for the "Steady-state phase" in TD08b (Section 4.3.3).

1) Manual procedures described in [TD08_DTS_Recharge_READ_ME.txt]. <Bedrock case> = <HCD variant>"_DFN_RXX" (see Table 1-2). <time slice> defined in Table 1-1. <Extension> = "SFR1" for only SFR1 and "SFR2" for coexisting SFR1 and L1B.

4.3.3 Applying top-boundary condition in Steady-state phase

Time-specific head solutions in the grid top layer, resulting from the TD08a Recharge phase (Section 4.3.2), are applied as top-boundary conditions in steady-state simulations. The steady-state simulations are both performed for TD08a, to improve convergence in the flow solutions, but also in the TD08b sensitivity analysis (i.e., assuming that the top-boundary conditions are realistic for *all* bedrock cases). The Fortran Input File [fif - TD08_final.f] is used. The input/output of the "Steady-state" phase is described in (Table 4-7).

Table 4-7. "Steady-state" phase simulation, input/output[1)]

Input files	Description
[DTS_setup.txt]	Automatically generated, defining

	<Bedrock case>, <time slice> and <Extension>
[cif.xml]	Automatically generated for specified <Bedrock case>, <time slice> and <Extension>. Temporary standard Compact Input File. Not stored.
[xyz_<time slice>]	Computational grid (Table 4-1)
[<Bedrock case>_PERMX_<Extension>_<time slice>] [<Bedrock case>_PERMY_<Extension>_<time slice>] [<Bedrock case>_PERMZ_<Extension>_<time slice>]	Cell-wall ECPM permeability in x,y, and z-directions (Table 4-4)
[rstslv_<Extension>_<time slice>]	Flow solution from the TD08a "Recharge phase" (Table 4-6), defining a fixed-head condition for the top boundary (standard DarcyTools restart file).
Output files (TD08a)	
[<Bedrock case>_<Extension>_<time slice>_ hist<1-8>]	History files, logging convergence statistics, appended from the Recharge phase (Table 4-6).
[<Bedrock case>_<Extension>_<time slice>_ rstslv]	Final steady-state solution (DarcyTools restart file). Not used.
[<Bedrock case>_<Extension>_<time slice>_Flow_solution.dat]	Final steady-state solution, accessable for Post processing (Section 4.4.2). Contains cell-wall Darcy velocity and cell-centre pressure.
[<Bedrock case>_<Extension>_<time slice>_ Tunnel_flows.dat]	Disposal-facility cross-flows, ASCII text
[<Bedrock case>_<Extension>_<time slice>_ Tunnel_walls.plt]	Tecplot output for visualisation (containing conductivity, head, and cross-flow for all tunnel walls)
[<Bedrock case>_<Extension>_<time slice>_DTS.plt]	Tecplot output for visualisation (containing conductivity, head, cell markers, and Darcy flux for vertical and horizontal flow-domain cross sections)
[GWT_Steady_state<time slice>.dat]	Tecplot output for visualising simulated ground-surface head
Output files (TD08b)	
[<Bedrock case>_<time slice>_hist<1-8>]	History files, logging convergence statistics, appended from the Recharge phase (Table 4-6).
[<Bedrock case>_<time slice>_rstslv]	Final steady-state solution (DarcyTools restart file). Not used.
[<Bedrock case>_Flow_solution_<Extension>_<time slice>.dat]	Final steady-state solution, accessable for Post processing (Section 4.4.2). Contains cell-wall Darcy velocity and cell-centre pressure.
[<Bedrock case>_Tunnel_flows_<Extension>_<time slice>.dat]	Disposal-facility cross-flows, ASCII text
[<Bedrock case>_ Tunnel_walls_<Extension>_<time slice>.plt]	Tecplot output for visualisation (containing conductivity, head, and cross-flow for all tunnel walls)
[<Bedrock case>_<time slice>_DTS_output.plt]	Tecplot output for visualisation (containing conductivity, head, cell markers, and Darcy flux for vertical and horizontal flow-domain cross sections)

1) <Bedrock case> = <HCD variant>"_DFN_RXX" (see Table 1-2). <time slice> defined in Table 1-1. <Extension> = "SFR1" for only SFR1 and "SFR2" for coexisting SFR1 and L1B.

4.4 Performance measures

The primary performance measures in TD08 are:

1) Cross flow in disposal facilities (Section 4.4.1)

2) Disposal facility interactions, defined as the fraction of particle trajectories from one disposal facility that passes through a downstream disposal facility. The interactions are determined by means of particle tracking (Section 4.4.2)
3) Bedrock retention properties along particle trajectories, defined as from the tunnel wall to the bedrock surface. Retention properties are determined as cumulative measures during particle tracking (Section 4.4.2)

Post-processing of flow solutions is conducted by means of the DarcyTools module PropGen, as compiled from a customized Fortran code. The post-processing is executed in batches, in which the traceability between input and output data is automatized.

4.4.1 Disposal-facility cross flow

The cross flow over disposal facilities (see objectives in Section 1.2) is calculated as the last step of flow solutions. All files [<**Bedrock case**>_Tunnel_flows_<**Extension**>_<**time slice**>.dat] (Table 4-7) are joined into a single file and analysed. Cross flow refers to the total flow over a predefined cross-sectional area in the computational grid. For flow calculation over disposal facilities, this area is identified as cell-walls between tunnel cells (identified by cell marker Mk = i) and surrounding, arbitrary grid cells (cell marker Mk = $j \neq i$, where j may refer to several cell markers). Two flow components are determined over the ij-interface:

1) total inflow to tunnel i, ΣQ_{ij+}
2) total outflow from tunnel i, ΣQ_{ij-}

For the closed volume of a tunnel, i, without sink or source terms, mass balance holds that, $\Sigma Q_{ij+} = |\Sigma Q_{ij-}|$.

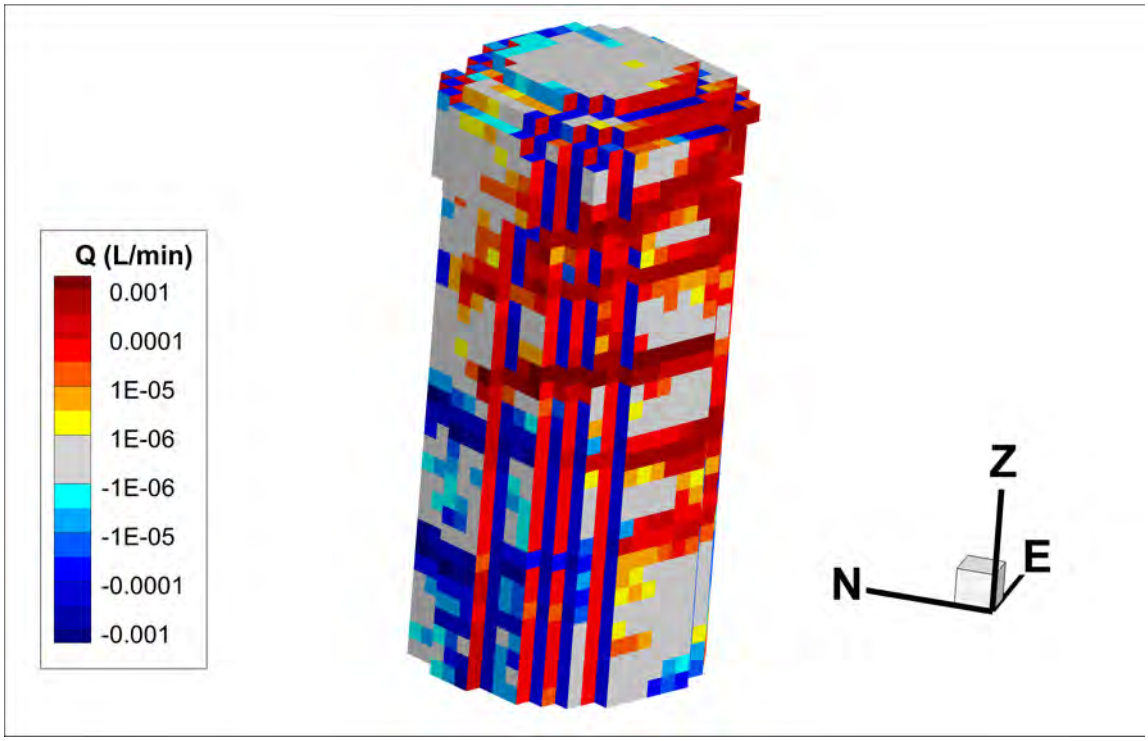

Figure 4-4. *Flow components, Q_{ij}^{wall}, of discretised flow across Silo walls, as defined over x/y/z-cell walls.*

Method 1. Net flow, on cell basis

Evaluation of tunnel flow is complicated by discretisation artefacts, if the grid is not geometricly aligned with the local flow field (e.g., discussions in Odén 2009). Highly conductive tunnels, such as addressed in SR-PSU, tend to re-direct the local flow parallel to the

tunnel wall. If the tunnel is not aligned with the computational grid, flow paths along the tunnel wall tend to be double-counted as a repeated pattern of inward/outward directed local flow (e.g., the blue-red striped vertical pattern in Figure 4-4). SR-PSU and SDM-PSU therefore employ a rotated coordinate system, aligned with the tunnel geometry of the existing SFR to reduce the exaggeration in tunnel cross flow. Even in the rotated grid system, some artefacts remain at curved surfaces, such as tunnel ceilings and the silo walls.

A simple approach to reduce discretisation artefacts is used in TD08, based on the summation of cell-net flow components (Note that more sophisticated methods are suggested in Td10). In a first step, cell net flow, $Q_{ij}^{cell,\ net}$, is calculated for all tunnel cells located along the tunnel wall,

$$Q_{ij}^{cell,net} = \sum_{n} Q_{ij}^{wall},\ i \neq j, \qquad (4\text{-}3)$$

where Q_{ij}^{wall} is a cell-wall flow between the tunnel cell (Mk = i) and n ambient grid cells (Mk = j $\neq i$). The total cross flow over tunnel i is then calculated as: 1) either the sum of *positive* cell-net flows, ΣQ_{ij+}, or 2) the sum of *negative* cell-net flows, ΣQ_{ij-}, for all cells with marker Mk = i. The benefit of this approach is that "corner flow" in cells with more than one flow components of opposite direction over the ij interface to some extent balance out in the net calculation (i.e., not included in the summation, ΣQ_{ij}).

4.4.2 Particle tracking

DarcyTools facilitates two inbuilt particle-tracking methods: 1) stream-line routing and 2) the so-called cell-jump method (Svensson et al. 2010). Unfortunately, the inbuilt particle-tracking methods are not very feasible due to the extensive demands of SR-PSU (involving multiple model setups and large numbers of particles released). Instead, particle tracking is performed as a post process applied to a steady-state flow field (i.e., outside the DarcyTools flow solver). There are reasons for using a stand alone post process:

1) Rapid execution time (processing steady-state solutions reduces particle tracking to a geometric problem, circumventing the computational demanding (and time consuming!) iterative time-stepping within the DarcyTools solver. The post-processor algorithm also allows simultaneous processing in parallel working folders)
2) Flexibility: the code can easily be adapted to meet the various needs within the SR-PSU project (customize definition of performance measures, target specific issues, etc.)
3) File management: Output can be customized to meet the particular demands within the SR-PSU project (e.g., apply file-naming conventions, condense output to reduce file sizes, export in defined delivery structures, user-specified Tecplot output, etc.)

In principle, the used algorithm is very similar to the so-called "DarcyTools to MARFA interface" used in SR-Site Forsmark. It is based on the cell-jump method, where particles (i.e., discretisation of water volumes) traverse the computational grid on a cell-to-cell basis, according to inter-nodal flow between cells. The method assumes complete mixing of water in all cells, which implies a stochastic component in the routing of particle trajectories. Four different porosity parameterisation variants are tested (Table 4-2; all variants traceable in the last version [P_track_random_TD08a_FINAL_DELIVERY.f]). For the formal SR-PSU deliveries, Variant 1 (Upscaled ECPM porosity), with a minimum value of 10^{-5}, is applied.

Particle-tracking principles and performance measures

A particle trajectory represents the advective flow path of a discretised water volume through the bedrock. The purpose of particle tracking is to quantify cumulative bedrock retention properties along an ensemble of trajectories. The evaluation targets only the retention properties

in bedrock, and therefore no properties of tunnel-backfill or HSD are included in the performance measures.
Particles are released uniformly within disposal facilities (identification via cell markers, Table 4-8). However, the "release point" is defined as the tunnel-wall passage (i.e., or put in other words, the bedrock entry point). Particle trajectories are terminated at the bedrock surface, where the "exit point" is defined by the cell wall between a bedrock cell and a HSD cell.
The probability, P_{ij}, of navigating from cell i to cell j is assumed to be proportional to the flow in that direction, Q_{ij}, where a *sign-criterion* applies to Q_{ij}, depending on the *direction* of particle tracking:

$$P_{ij} = \frac{Q_{ij}}{\sum Q_{ij}}. \qquad (4\text{-}4)$$

Particle tracking can be performed in two directions: in *forward* tracking, only outward-directed flows are included in Eq. (4-4), whereas in *backward* tracking only includes inward-directed flows.
Path length, L (m), is calculated as the cumulative length between the centre points of passed cell walls. The travel time, t_{ij}, taken to move from the centre of cell i to the centre of cell j is assumed to be:

$$t_{ij} = \frac{n_i V_i + n_j V_j}{2Q_{ij}}, \qquad (4\text{-}5)$$

, where n is porosity and V is cell volume (i.e., the product nV is the cell volumetric water content). The factor 2 in the denominator reflects that only *half* of the cell volumetric water contents, $n_i V_i$ and $n_j V_j$, are involved in the inter-nodal flow Q_{ij}. Note that $n_i = n_j$ in porosity parameterisations 2 to 4 in Table 4-2.

The F-quotient, F_{ij}, for the step from cell centre i to cell centre j is assumed to be:

$$F_{ij} = a_w t = \frac{fws_i + fws_j}{2Q_{ij}}, \qquad (4\text{-}6)$$

, where a_w is flow-wetted surface area per volume of water and *fws* is the flow-wetted surface areas in cells i and j, respectively (based on Svensson et al. 2010 and MARFA interface). Calculated performance measures only reflect the bedrock; therefore both porosity and *fws* are nullified in tunnel backfill and in overlying sediments.

The input and output data files are summarized in Table 4-8. The output follows a standardised convention
[<**Bedrock case**>_<**Extension**>_<**time slice**>_<**Release location**>_<**File type**>.dat]. In addition so-called disposal-facility *interactions*,
[<**Bedrock case**>_<**Extension**>_<**time slice**>_Cross-List.dat], are joined into a separate output file [Assembled_Cross-lists.dat] (ASCII format). Disposal-facility interactions are statistics on the fraction of released particles from one disposal facility that crosses one or more adjacent disposal facilities.

Table 4-8. Particle tracking[1)]

Input files	Description
[DTS_setup.txt]	Defines <**Bedrock case**>, <**time slice**>, and <**Extension**>
[xyz_<**time slice**>]	Computational grid (from Table 4-1)
[<**Bedrock case**>_fws.dat]	ECPM flow-wetted surface area (cell property from Table 4-3)
[<**Bedrock case**>_PORO_<**Extension**>_<**time slice**>]	ECPM porosity (cell property from Table 4-4)
[<**Bedrock case**>_<**Extension**>_<**time slice**>_Flow_solution.dat]	Final steady-state solution, containing cell-wall Darcy velocities and cell-centre pressures

(result from Table 4-7).

Source code used	
P_track_random_TD08a_FINAL_DELIVERY.f	Allows all 4 porosity variants (Table 4-2). Variant 1 (Upscaled ECPM porosity), with a minimum value of 10^{-5}, is selected for formal deliveries within SR-PSU.

Output files: <**Bedrock case**>_<**Extension**>_<**time slice**>_<**Release location**>_<**File type**>.dat

<Release location>	**Markers**		**Tunnels**	**No. particles**
All_SFR1_D_	11-15	SFR1	All 5 disposal facilities	1,000,000
SFR-1_1BTF_(11)	11	SFR1	1BTF	100,000
SFR-1_2BTF_(12)	12	SFR1	2BTF	100,000
SFR-1_1BLA_(13)	13	SFR1	1BLA	100,000
SFR-1_1BMA_(14)	14	SFR1	1BMA	100,000
SFR-1_Silo_(15)	15	SFR1	Silo1	100,000
All_SFR2_D_	22-27	L1B	All 6 disposal facilities	1,000,000
SFR-2_2BLA_(22)	22	L1B	2BLA	100,000
SFR-2_3BLA_(23)	23	L1B	3BLA	100,000
SFR-2_4BLA_(24)	24	L1B	4BLA	100,000
SFR-2_5BLA_(25)	25	L1B	5BLA	100,000
SFR-2_3BMA_(26)	26	L1B	2BMA	100,000
SFR-2_1BRT_(27)	27	L1B	1BRT_del1	100,000

<**File type**>.dat

Exit_loc	Exit locations, or recharge locations, at the bedrock surface depending on direction of particle tracking.
Discharge	2-D histogram of exit locations used for visualisation in TecPlot format, resolving number of particles per m^2 and mean travel time.
Recharge	2-D histogram of recharge locations used for visualisation in TecPlot format, resolving number of particles per m^2 and mean travel time.
FORWARD_Paths	3-D trajectories from forward particle tracking (max 3000 exported). Used to visualise user-specified performance measures in TecPlot.
BACKWD_Paths	3-D trajectories from backward particle tracking (max 3000 exported). Used to visualise user-specified performance measures in TecPlot.

1) <Bedrock case> = <HCD variant>"_DFN_RXX" (see Table 1-2). <**time slice**> defined in Table 1-1.

5 Results

5.1 Demonstration of simulated top-boundary conditions (TD08a)

This section demonstrates the top-boundary conditions determined the preceding "Recharge phase" simulations (Section 4.3.2). The top-boundary conditions determined in TD08a (bedrock case: BASE_CASE1_DFN_R85) are applied in the sensitivity analysis for all bedrock cases in TD08b. Therefore, the TD08a results are presented as: 1) a three-dimensional example for 9000 AD (Figure 5-1), and 2) a more comprehensive analysis of all time slices (Figure 5-2 to Figure 5-5).

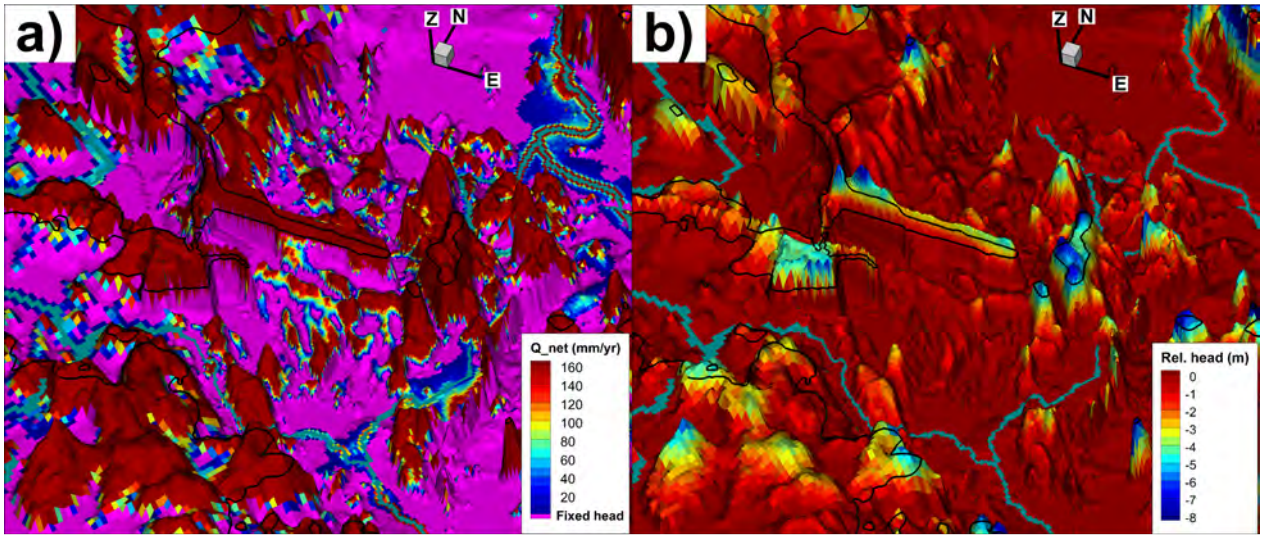

Figure 5-1. *Simulation results of TD08a at 9000 AD; a) local recharge/fixed-head and b) relative ground-surface head. Pre-defined surface water shown as blue-grey surfaces. Vertical exaggeration: 50. The 2000 AD coast line is included for spatial reference (black line).*

Topography and shoreline retreat

The shoreline retreat in the SFR near-field is shown for the six selected time slices (Figure 5-2). Note that all elevations are expressed in the so-called fixed-bedrock reference system, where the sea level is envisaged as declining, relatively to a static bedrock surface (Section 2.3.5). Pre-defined surface water areas in RLDM (lakes and rivers) are shown as blue-grey surfaces. Head is monitored below two topographical peaks (one in the pier and the other in an islet, east of the pier; grey points in Figure 5-2).
In the 3000 AD time slice, a gap in "topography above sea level" exists along the verge of Lake 118, just west of the SFR pier. In other words, the "white areas" west of the SFR pier indicate top-layer cells below prevailing sea level (-5.92 m elevation; Table 2-7), which is inconsistent with the modelled lake level (-5.13 m elevation; Table 2-5). This inconsistency arises from model artefacts in the RLDM . Furthermore, this artificial depression has not been basin-filled, as basins below sea level are not included in the numerical algorithm applied (Section 2.3.2). The reason for excluding basins below sea level is to avoid unmotivated filling of the seafloor (i.e., seafloor filling would in effect be parameterised as artificial peat layers below sea; Table 3-7). This inconsistency is corrected in TD11, where particular emphasis is paid to lake verges and identified basins *below* sea level, but with geometric thresholds *above* sea level, are manually filled.

Local recharge and fixed head

Simulated local recharge and cells switched to "fixed-head" conditions are shown in Figure 5-3. The fixed-head conditions (i.e., pink areas) occur where the simulated head in ground-surface cells has exceeded the tolerance (Figure 4-2). Typically, the fixed-head conditions tend to occur: 1) along the coast line, and 2) in areas of lower elevation with flat topography (i.e., in several cases basin-filled areas). Recharge conditions occur at local topographical peaks (Figure 5-1). The spatial pattern in results can be described as "patchy" and of "binary character". In other words, a distinct separation into: 1) recharge areas, with *maximum* net precipitation of 160 mm per year (dark red), and 2) discharge subareas, where the boundary condition is switched to fixed head (pink). This suggests that the recharge-phase simulations applied in TD08 is not fully mature, and that a more gradual appearance could be obtained if the modelling approach is refined.

It is noted that fixed-head conditions occur at the base of the SFR pier (Figure 5-1). The model representation of the constructed SFR pier is complicated by simultaneous contrasts in topography and in hydraulic conductivity (Table 3-7). Owing to its location above SFR, the constructed pier may have a significant impact on the local flow field, at least during later stages of shoreline retreat. Therefore, the details in model representation of the SFR pier are given more attention in forthcoming SR-PSU Tasks (TD10 and TD11).

Relative ground-surface head

The outcome of the applied "recharge-phase concept" is demonstrated in terms of simulated "relative head" in the top boundary (Figure 5-4).This relative head is expressed as ground-surface head relative to local ground surface, H - z_{DEM} (m, elevation in fixed-bedrock reference), where z_{DEM} refers to the local basin-filled DEM elevation (Section 2.3.2). In other words, this measure demonstrates the difference between the *applied boundary condition* (i.e., simulated outcome) versus the simpler boundary condition assuming H = z_{DEM} (discussed in Section 4.3). *Less strictly speaking*, the absolute value of this relative head can be envisaged as an approximate measure of groundwater depth (i.e., this analogy requires that the vertical hydraulic gradients are negligible). This relative head is equal to zero where the boundary condition is set to fixed head (i.e., pink areas in Figure 5-3). The relative head is considerably lower at local topographical peaks (i.e., can be envisaged as deep groundwater table; e.g., Figure 5-1).

Top-boundary head

Ground-surface head has a somewhat "smoothened" appearance in comparison to topography (e.g., islets east of the pier; c.f. Figure 5-2 and Figure 5-5). At 2000 AD, the head inside the pier is close to sea level, with local higher head associated to thin soil coverage. With the retreating shoreline, the head inside the pier is on par with, or slightly above, the head in *local peaks* of surrounding natural sediments. This is not very realistic, as owing to its high hydraulic conductivity, the groundwater level inside the pier is expected to be drained to the *topographical low points* of surrounding sediments. This model artefact is caused by the combination of steep topography and high contrast in hydraulic conductivity that occurs along the sides of the pier.This combination causes discharge through the sides of the pier and relative heads exceeding the tolerance (Figure 4-2). Consequently, the sides of the pier are assigned fixed head (i.e., pink-shaded in Figure 5-1). The details in model representation of the SFR pier are given more attention in forthcoming SR-PSU Tasks (TD10 and TD11).

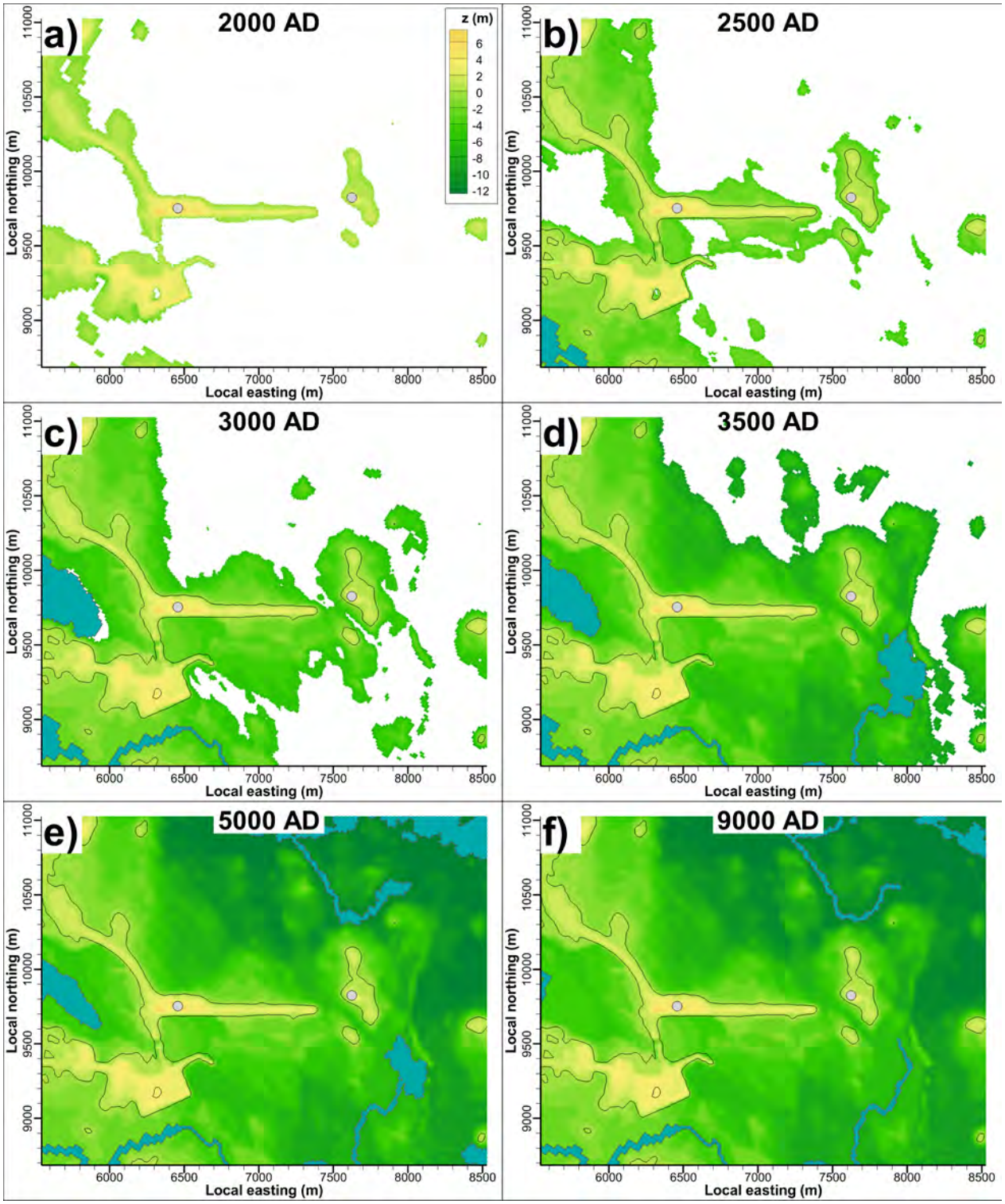

Figure 5-2. *Elevation of ground-surface cells above the retreating sea level, expressed in the so-called fixed-bedrock elevation reference (Section 2.3.5). Pre-defined surface water shown as blue-grey surfaces. Head is monitored below topographical peaks in the pier and in an islet east of the pier (grey points).*

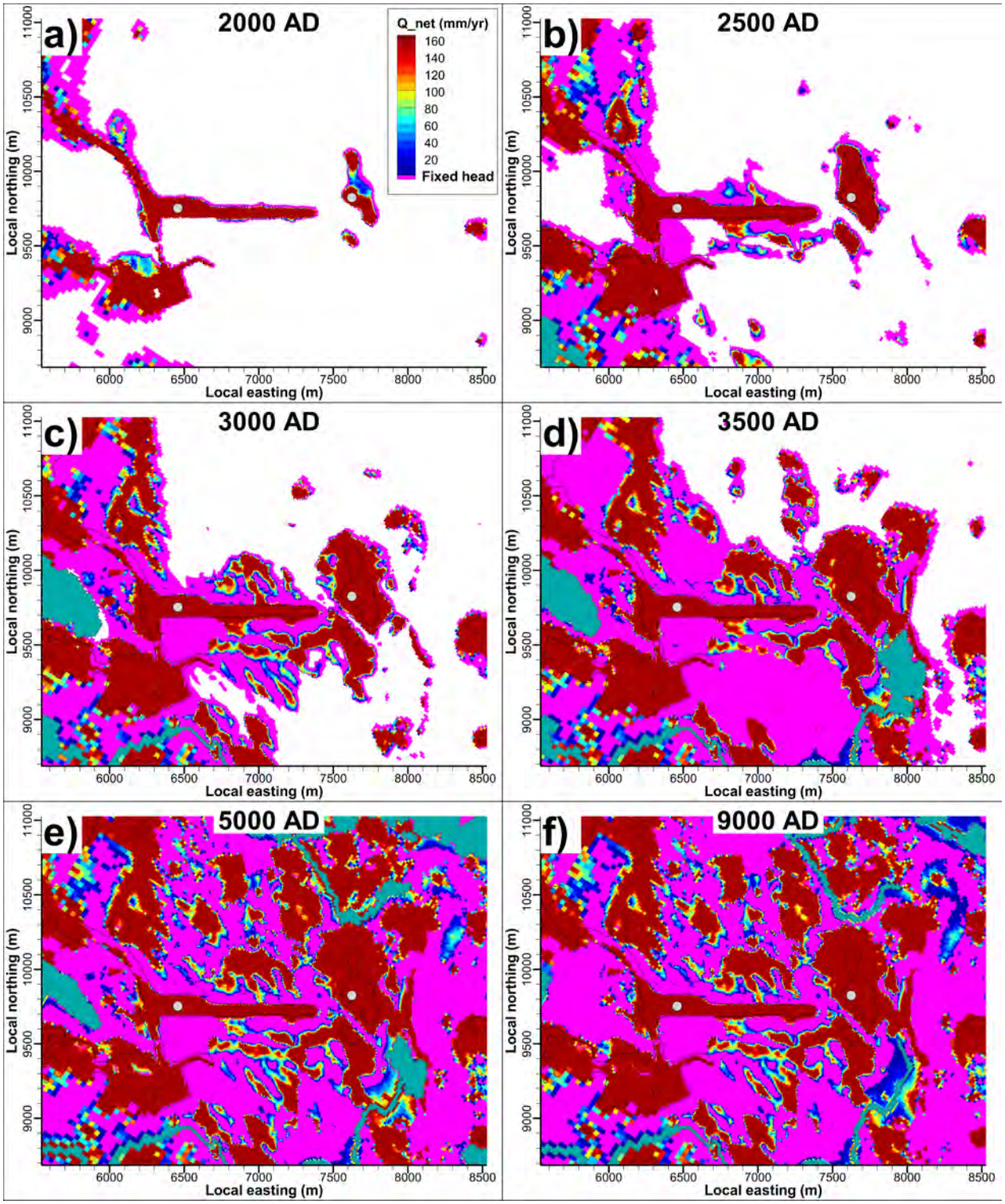

Figure 5-3. *Simulated local recharge for selected time slices in TD08a. Fixed-head cells shown as pink surface. Head monitored below topographical peaks in the pier and in an islet east of the pier (grey points).*

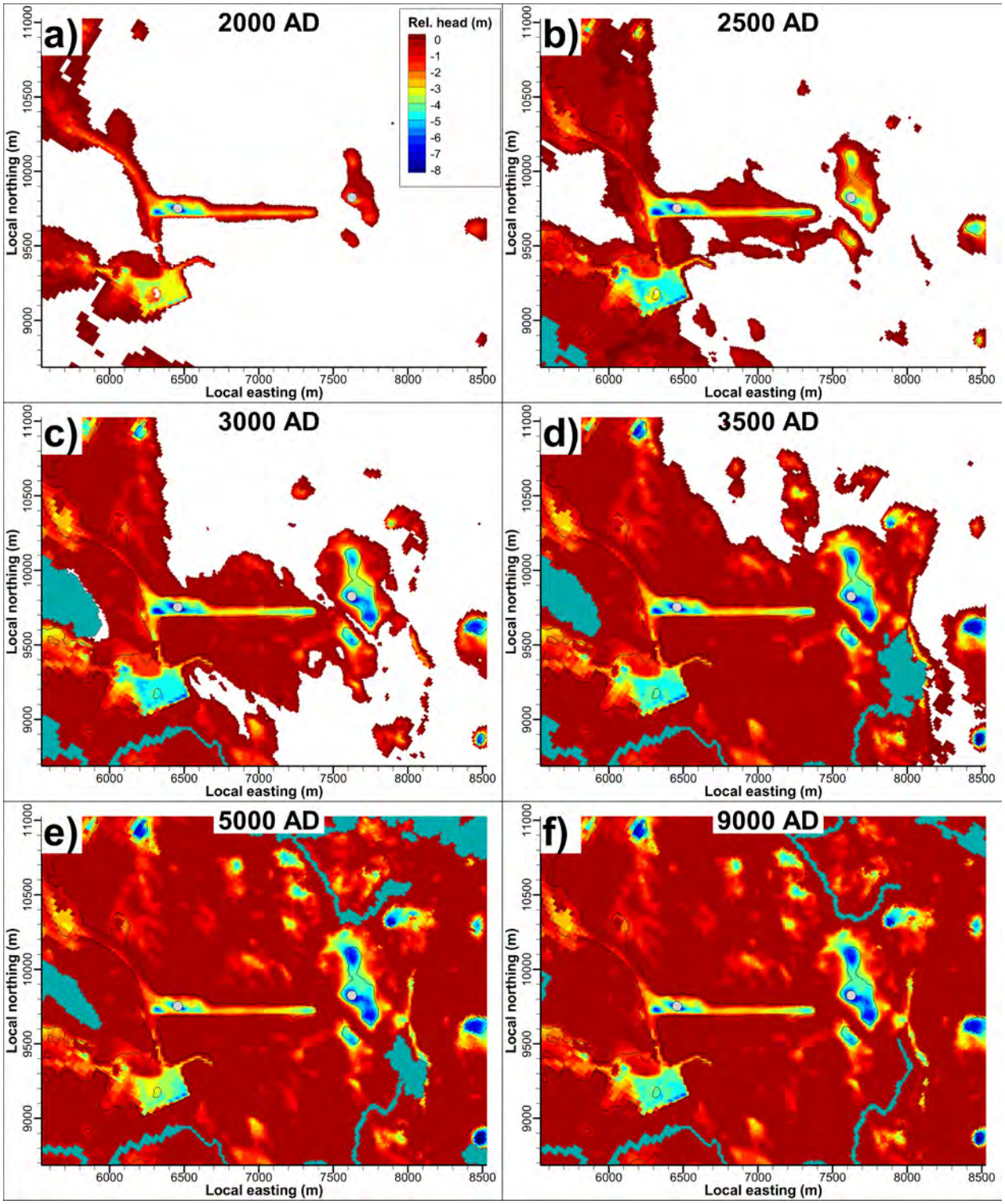

Figure 5-4. *Simulated relative ground-surface head for selected time slices in TD08a. Pre-defined surface water shown as blue-grey surfaces. Head monitored below topographical peaks in the pier and in an islet east of the pier (grey points).*

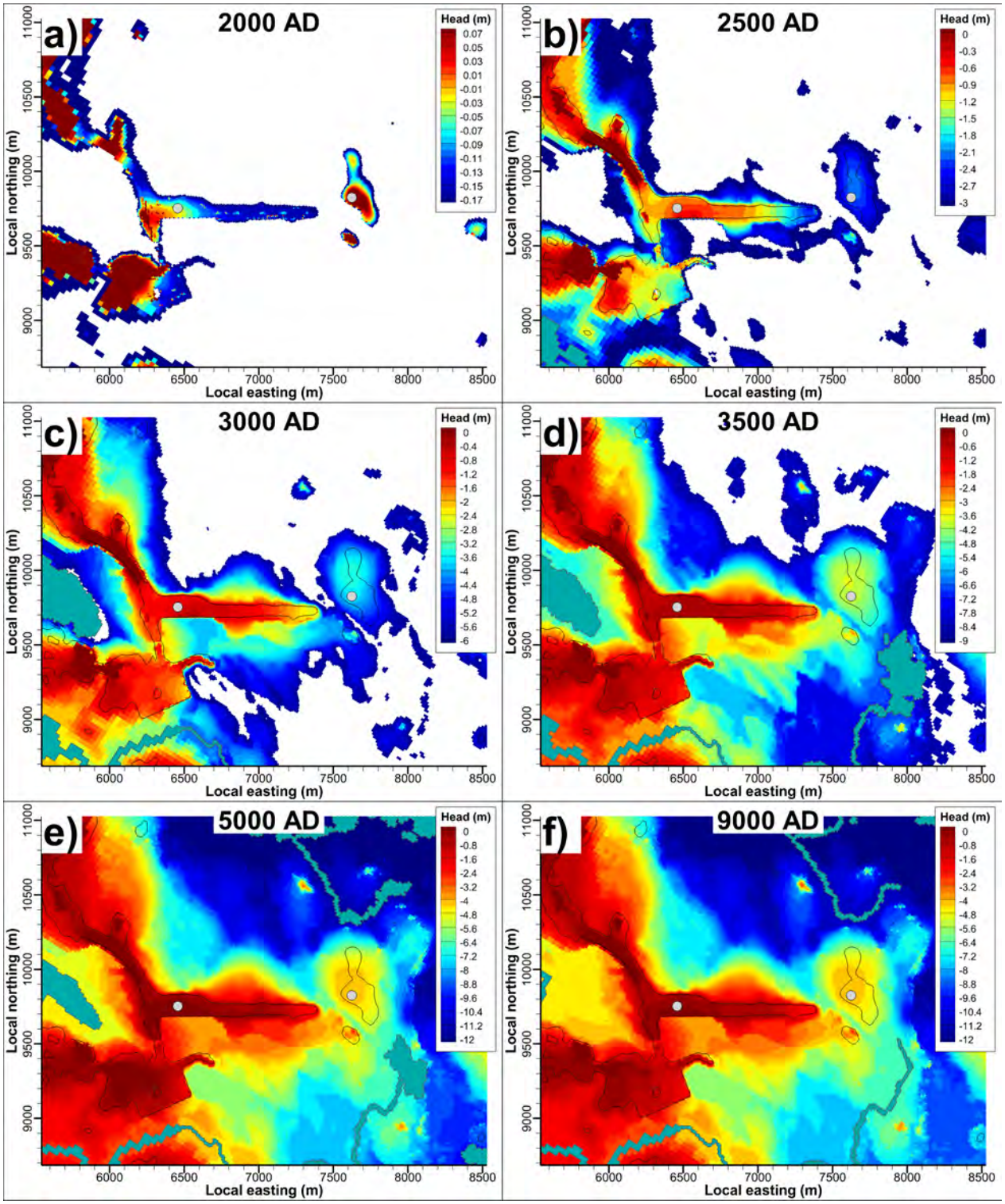

Figure 5-5. *Simulated ground-surface head for selected time slices in TD08a. Head is expressed in the fixed-bedrock reference (Section 2.3.5). Pre-defined surface water shown as blue-grey surfaces. Note the varying contouring scales.*

5.2 Disposal-facility cross flow

5.2.1 Comparison to earlier results (TD08a)

The TD08a total tunnel flow in SFR1 is compared against earlier simulation results (Holmén and Stigsson 2001 and Odén 2009) (Figure 5-6 and Figure 5-7). Important differences among earlier model setups are related to modelling tools, geometric aspects, and available topography data; these are commented in Ch. 4 in Odén 2009. Another important aspect is that the transient behaviour in Holmén and Stigsson 2001 was forced to match early excess-head data that were assumed to reflect transient effects of land lift (causing higher flow at 2000 AD in Figure 5-6). It may be suspected that remnant shut-in pressure from transient land lift is depleted during the SFR-operational time period (i.e., atmospheric pressure conditions apply in the SFR near field), and thus remnant transient effects (i.e., prior to the construction of SFR) should not be propagated to future stages. On the other hand, studying the flow field as steady-state time slices, as done in TD08a, completely neglects transient effects and may exaggerate the rate of changing flow regime.

A few differences between the current TD08 model setup and earlier work should be noted:

1) TD08 is based on updated deformation-zone geometry and hydraulic parameterisation
2) The bedrock in TD08a is represented by a “pessimistic” DFN realisation, R85 (e.g., Figure 5-8), whereas the earlier work represents “average” bedrock characteristics.
3) Technical barriers of the silo are not included in TD08 (Table 3-1; i.e., the silo has a considerably higher conductivity parameterisation in TD08, as compared to earlier work.
4) A new algorithm for determining groundwater level has been applied. Results indicate that this algorithm is not yet mature (Section 5.1) and should be improved in coming SR-PSU simulation Tasks.

Among the three studies, TD08a has the most dramatic rate of change during the period 2000 to 3000 AD, after which the inflow stabilises after c. 3500 to 5000 AD (Figure 5-6). The same stationary appearance occurs at c. 4000 to 5000 AD in Holmén and Stigsson 2001, whereas tunnel flows are still rising at 5000 AD in simulations by Odén 2009.
At 2000 AD, the Holmén and Stigsson 2001 results are at least one order of magnitude higher than TD08a and Odén 2009. This is probably due to the transient effect of shut-in pressure modelled in Holmén and Stigsson 2001, which is not included in the steady-state time-slice approaches of TD08a and Odén 2009.

High flows are simulated in BLA and Silo, both at 3000 AD and 5000 AD (Figure 5-6). As part of TD8b, tunnel inflows are simulated for an ensemble of DFN realisations, which allows placing the TD08a parameterisation in context of the overall range (R85 marked red in Figure 5-8). Note that TD8b addresses 3500 AD, and therefore results are not directly comparable, in terms of magnitude. The R85 inflow is about twice the median flow of the general DFN ensemble R01…R20 (i.e., at least in BLA and the silo). This suggests that the current model is on par with previous models, even for BLA and Silo.

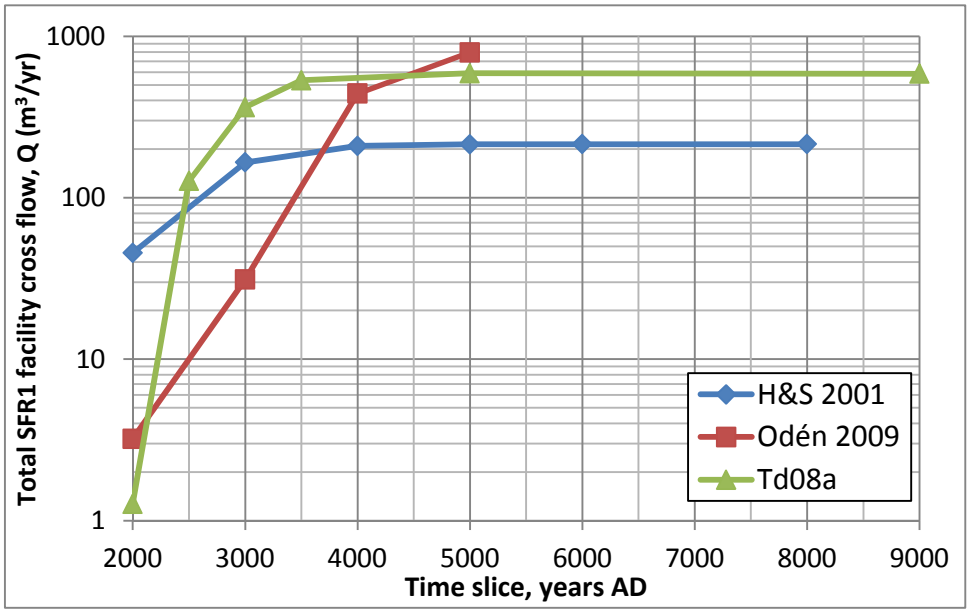

Figure 5-6. *Simulated total cross flow in disposal facilities of SFR1 over time, compared to earlier simulations.*

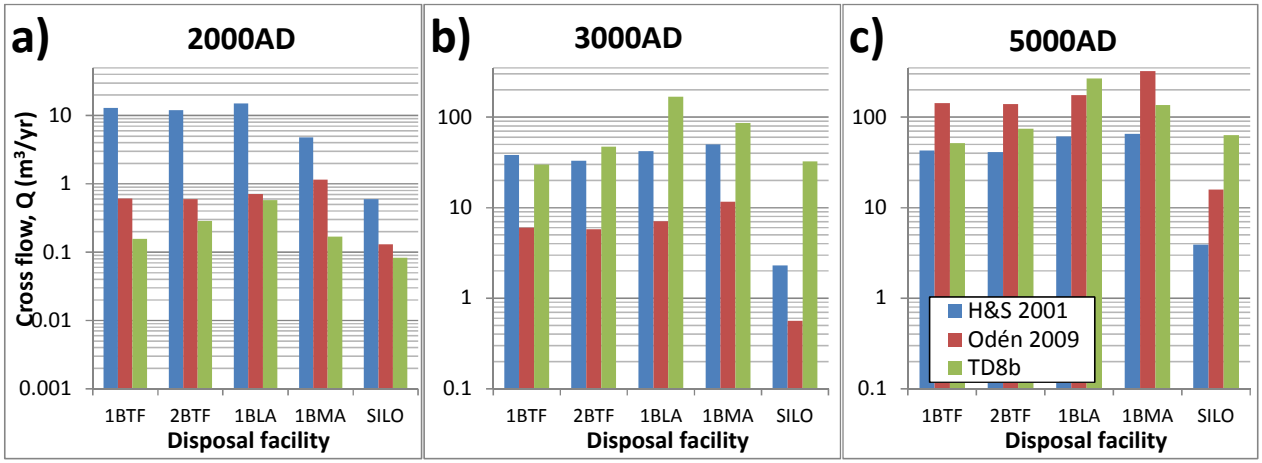

Figure 5-7. *Simulated disposal facility cross flow for three selected time slices, compared to earlier simulations.*

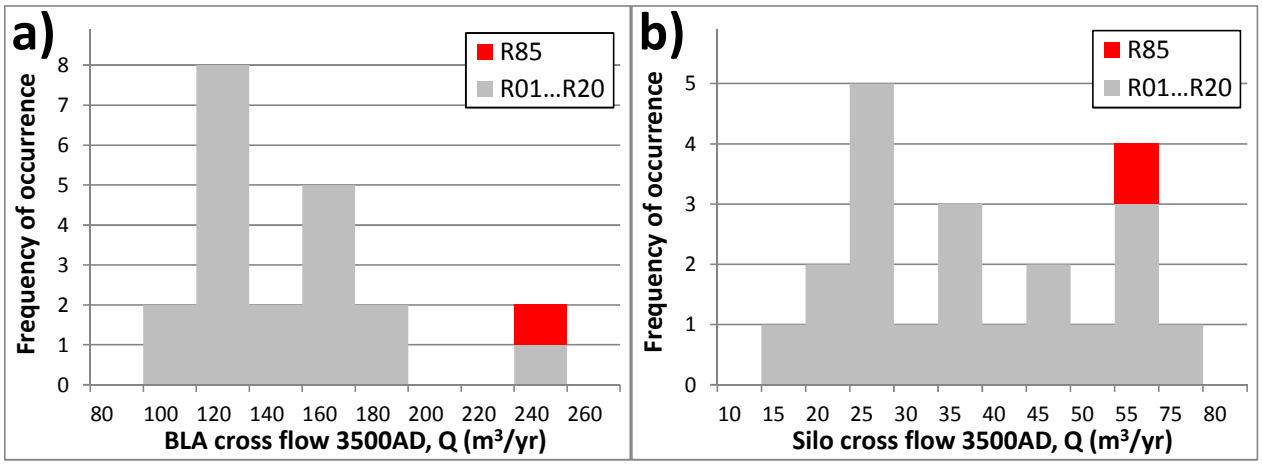

Figure 5-8. *Simulated cross flows in TD08b for HCD base case combined with HRD realisation R85 (red) versus larger ensemble R01…R20 (grey); a) BLA and b) Silo (c.f., Figure 5-15).*

5.2.2 Effect of extension on the existing SFR1 (TD08a)

The effect that the planned extension has the existing SFR1 facility is evaluated by comparing the disposal-facility flow in SFR1 between the case where both facilities co-exist, Q_{L1B}^{SFR1}, and the case where only SFR1 exists, $Q_{No\,L1B}^{SFR1}$ (Table 1-1).

The effect of extension on SFR-1 tunnel flow is expressed as a ratio:

$$Effect = \frac{Q_{L1B}^{SFR1} - Q_{No\,L1B}^{SFR1}}{Q_{No\,L1B}^{SFR1}}. \tag{5-1}$$

The effects on disposal facilities are typically small, c. ± 0 to 5% (Figure 5-9b). The effects are largest by 2000 AD and declines with time. Although the effects are small, they are correlated to distance from the planned extension L1B (i.e., largest in the silo and smallest in 1BMA). The extension *reduces* flow in 1BTF, 2BTF, 1BLA, and 1BMA, but *increases* cross flow in Silo. Again, note that Silo barriers are not implemented. The largest effects are found in the NBT tunnel, which is located right above 1BRT (Figure 2-3). It should also be noted that large sections of UB and IB are modelled as intact bentonite-plugs, which is expected to be insensitive to changing flow patterns.

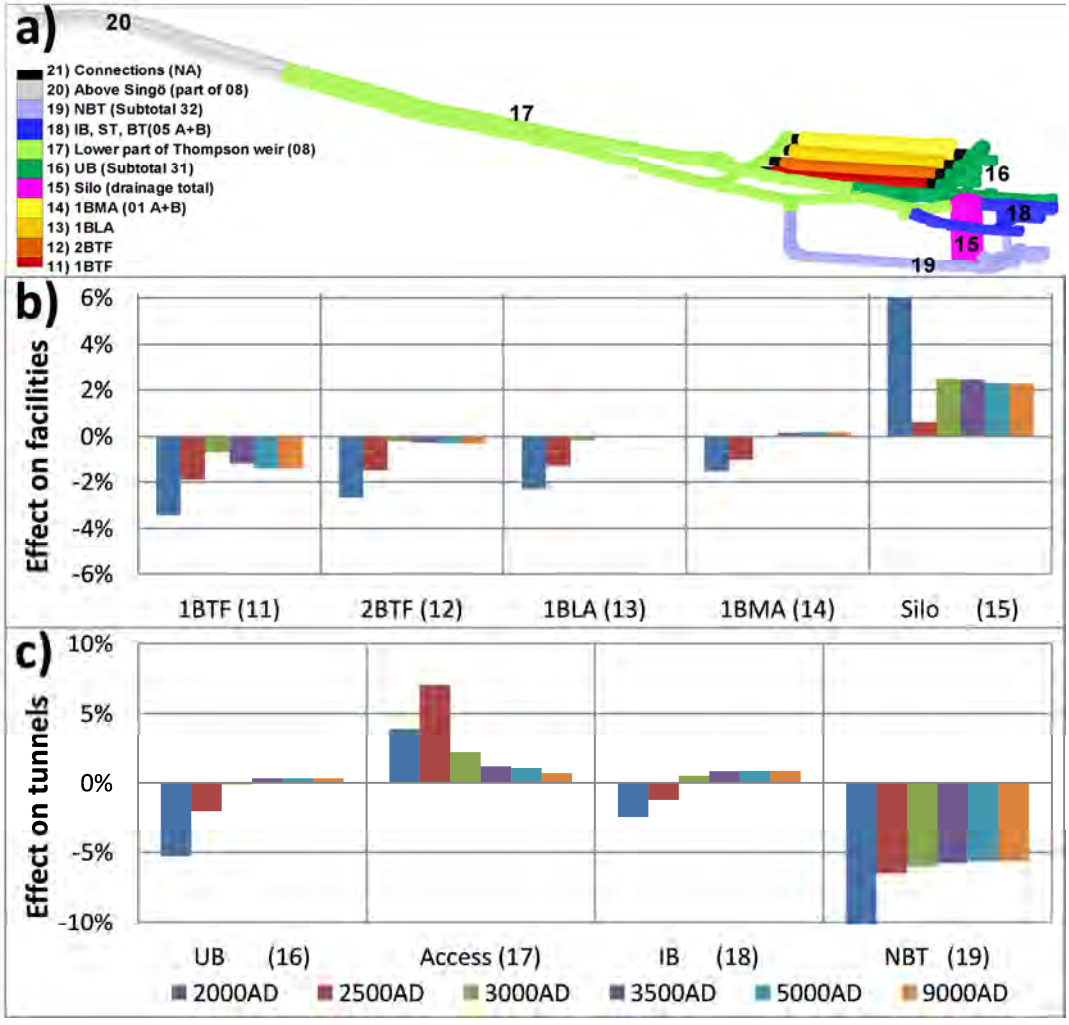

Figure 5-9. *Effects on SFR1 inflow due to construction of planned extension; a) classified tunnel sections in existing SFR, b) effect of disposal-facility flow, c) effect on tunnel flow.*

5.2.3 Dominating structures and heterogeneous parameterisation

The TD08b sensitivity analysis (Section 5.2.4) demonstrates that the disposal-facility cross flow in L1B is sensitive to heterogeneous HCD parameterisation. In retrospect, an error has been identified in the numerical implementation of heterogeneous HCD transmissivity. This section therefore analyses key structures for disposal-facility cross flow and the implication of the identified error.

Key structures in disposal-facility cross flow

As observed in Section 5.2.1, the flow regime changes dramatically during the early time slices. Simulated head and tunnel inflow in TD08a are shown for selected time slices in Figure 5-5 (note: different scales for 2000 AD, and "inflow" defined as directed into the tunnel wall). By 2000 AD, the simulated head-field is clearly related to distance from the SFR pier, with 1BMA being close to sea level (-0.17 m elevation; Table 2-7) and 1BRT almost 0.01 m above sea level. Thus, transversal gradients exist across the tunnel system, from 1BTF towards 1BMA, but also towards 2BMA. During the later time slices, 3500 AD and 9000 AD, the hydraulic gradients are higher, but the transversal component across facilities declines (i.e., in relative terms). As may be expected, the hydraulic gradients are large in bentonite-plugged tunnel sections (c.f., Figure 3-1). Tunnel IB is a notable low-point in simulated head is (i.e., the upper tunnel, just north-east of the silo; Figure 5-9a), which is due to its modelled intersection with ZFMNW0805B (Figure 1-1).

Due to a topographical depression along its ground-surface intercept, ZFMNW0805B is identified as a discharging zone (c.f. Figure 5-19).
The simulated pattern in tunnel inflow is primarily correlated to four deformation zones;

1) ZFMNNW1209 (Zone 6), intersecting 1BTF to 1BMA in the existing SFR
2) ZFMWNW0835, intersecting 3BLA to 2BMA in the planned extension L1B
3) ZFMWNW8042, intersecting all disposal facilities in the planned extension L1B
4) ZFMENE3115, intersecting 1BRT to 3BLA in the planned extension L1B

During the early flow regime, at 2000 AD, both facilities have upward-directed flow (indicated by blue contouring, which corresponds to outward-directed tunnel flow). Notably, ZFMWNW8042, which is located immediately south of the SFR pier, has downward flow. By 2000 AD, the magnitude in tunnel flows are about two orders of magnitude lower than it is at later stages.

During later time slices, 3500 and 9000 AD, L1B is clearly dominated by downward-directed flow (yellow to red contouring, indicating inward-directed tunnel flow). In SFR1, 1BTF and 2BTF have down-ward directed flow, while 1BMA has upward-directed flow via ZFMNNW1209 towards the junction between ZFMNW0805B and ZFMNNE0869 (c.f. Figure 5-19).

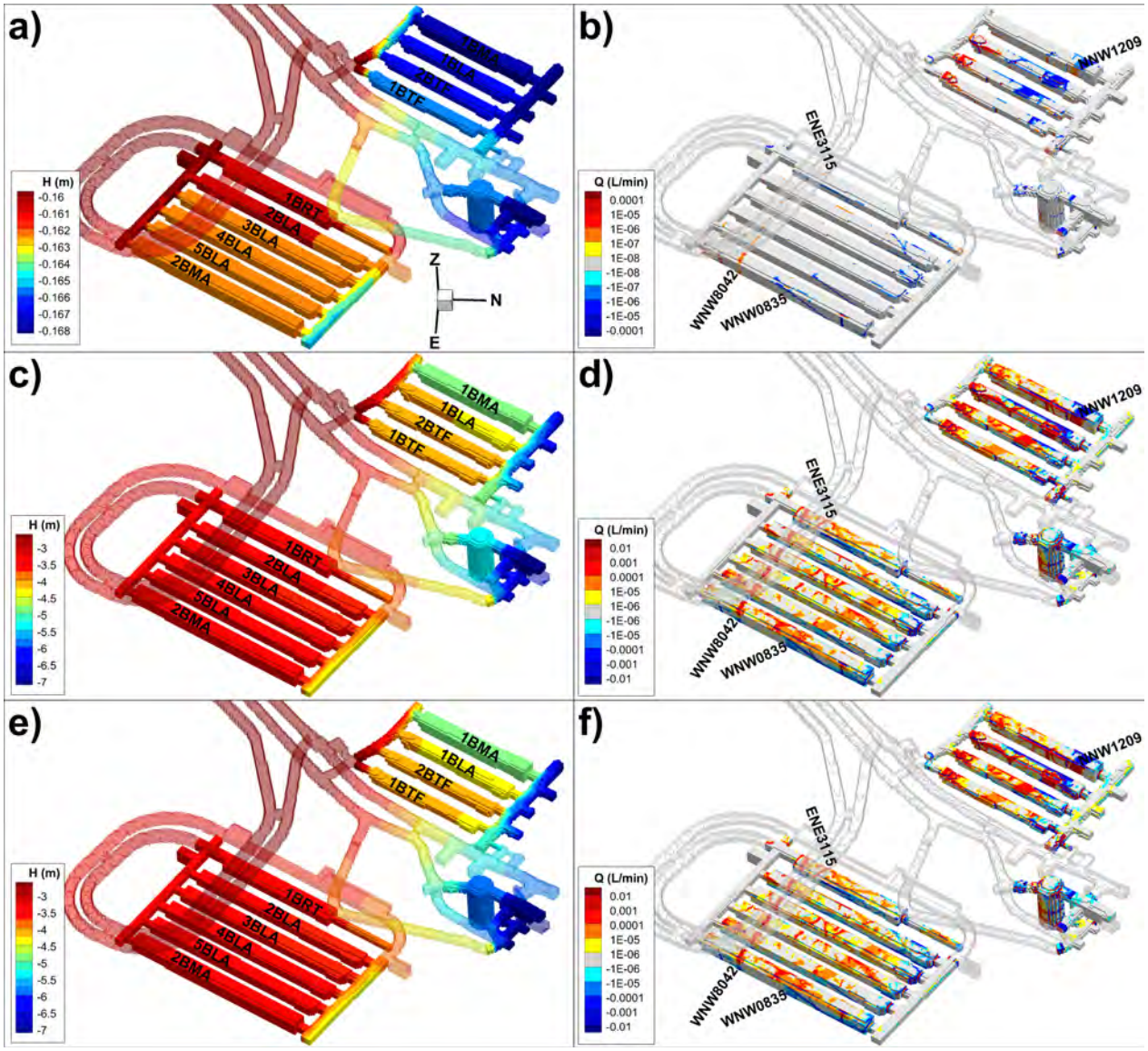

Figure 5-10. *Simulated head and disposal-facility inflow in TD08a [BASE_CASE1_DFN_R85]; a) and b) 2000 AD, c) and d) 3500 AD, e) and f) 9000 AD. Note the different scales in contouring for 2000 AD.*

The largest flows in the TD08b sensitivity analysis are found for HETERO_R03, while intermediate flows are found for HETERO_R10 (Figure 5-11). It is noted that heterogeneous transmissivity parameterisation of ZFMENE3115 and ZFMWNW0835 have considerable higher tunnel inflow, as compared to BASE_CASE1_DFN_R85. The same applies to the ZFMNNW1209 intersection with 1BTF. The corresponding ECPM conductivity for BASE_CASE1_DFN_R85 and the two heterogeneous realisations are shown in a horizontal cross section above the planned extension L1B (Figure 5-12).

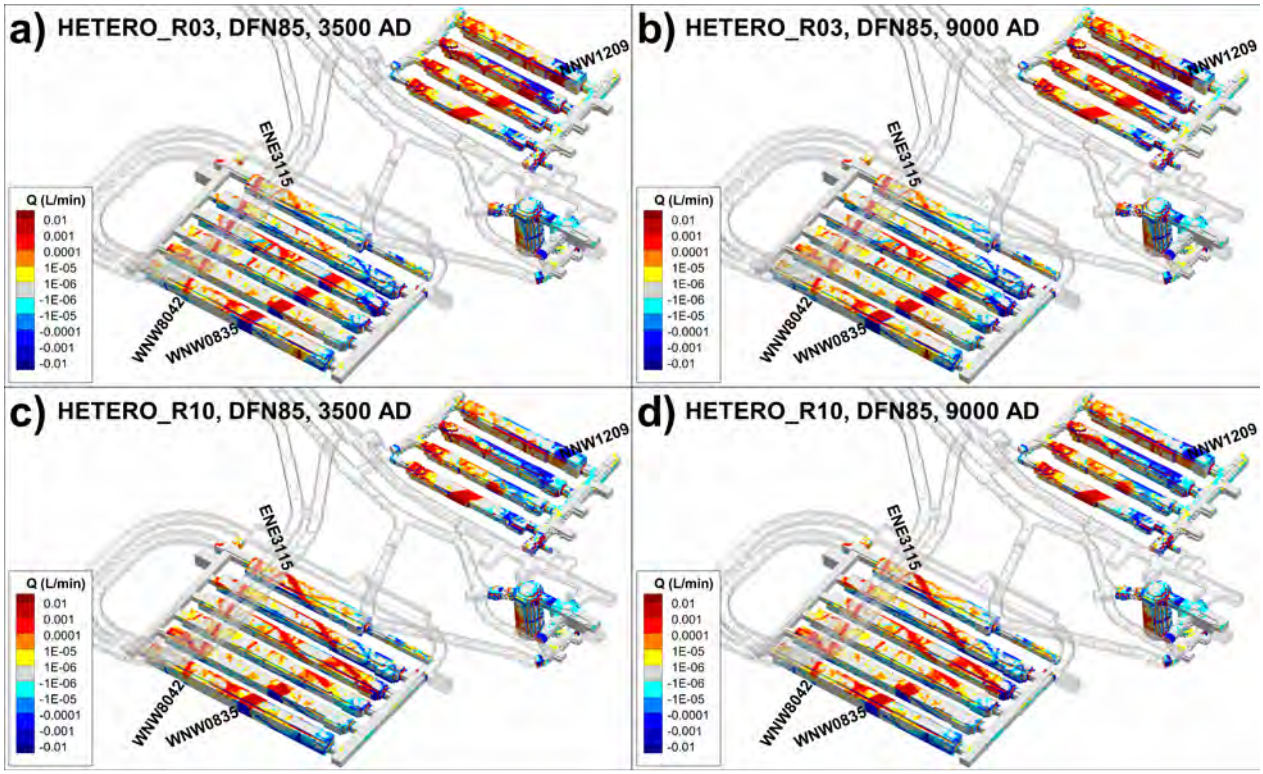

Figure 5-11. *Simulated disposal-facility cross flow in two realisations of heterogeneous HCD parameterisation in TD08b; time slices 3500 and 9000 AD.*

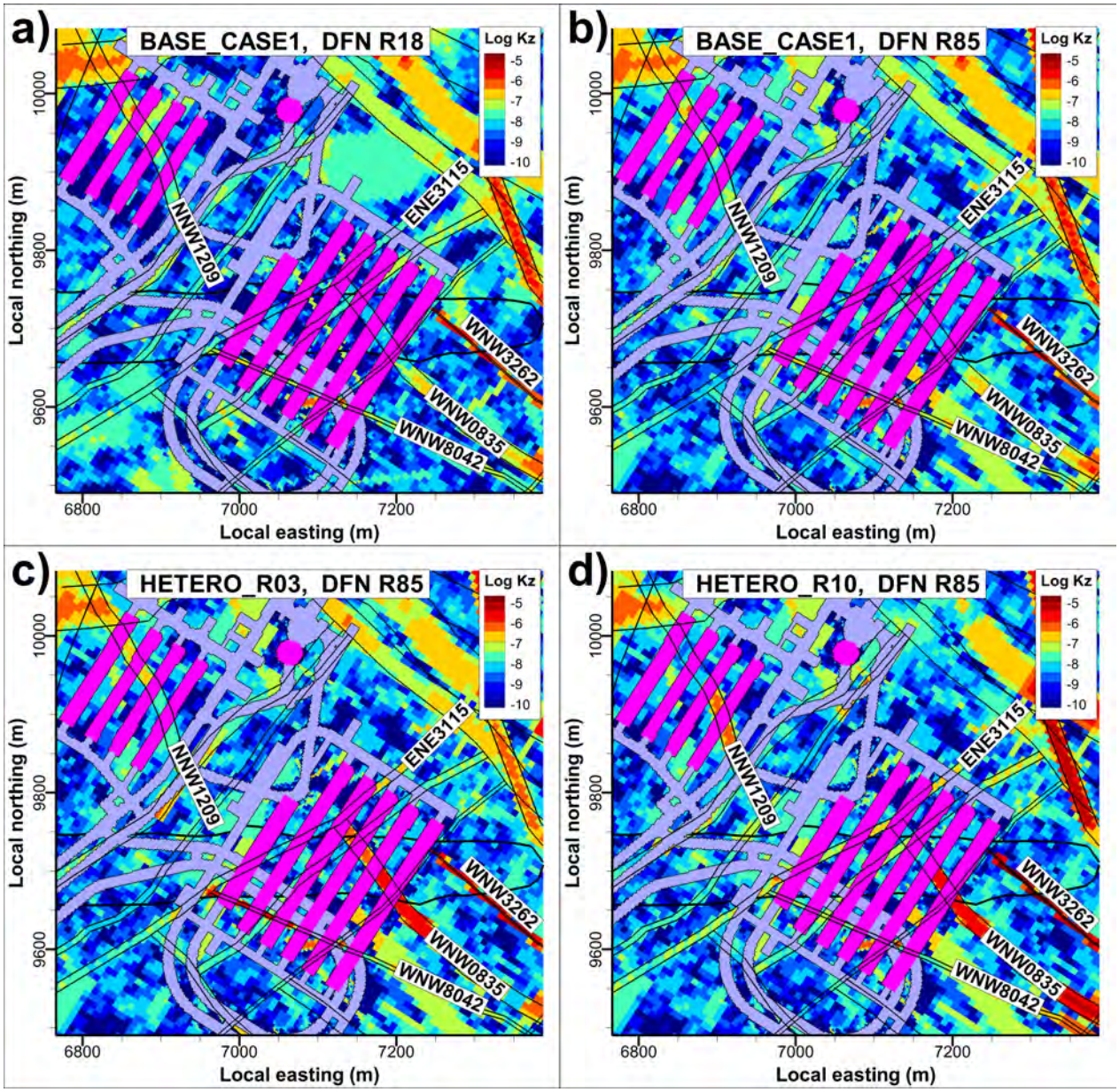

Figure 5-12. *ECPM conductivity of selected bedrock cases in a horizontal cross section above the planned extension L1B (z = -108 m). Disposal facilities pink-shaded, deformation-zone intersections outlined in black.*

Evaluation of the numerical error in heterogeneous transmissivity parameterisation

The error is evaluated by comparing the *applied* HCD transmissivity against the *correct* implementation at tunnel intercepts for the ensemble R01 to R10 (c.f., pink and green box-whisker plots in Figure 5-13). The *significance* of the error is evaluated by comparison against the theoretical input distribution (c.f., brown lines in Figure 5-13), as well as, the transmissivity of intersecting stochastic fractures (i.e., DFN realisations R01 to R20 and R85; grey box-whisker plots in Figure 5-13). The following can be noted:

- The range of variability in applied HCD transmissivity is exaggerated. Fortunately, the exaggerated variability is smaller in two identified key zones for L1B, ZFMWNW0835 and ZFMENE3115, (Figure 3-2).

- Some ensemble variability ranges seem “offset” as compared to the input distribution. For example, of ZFMENE3115 intercepts with 1BRT and 2BLA typically exceed the upper quartile, while its intercepts with 3BLA are more in line with the input distribution (c.f. box-whiskers and brown lines in Figure 5-13d). It is noted that the pattern is repeated in the “corrected” transmissivity parameterisation (c.f. pink and green box-whiskers in Figure 5-13d). The offset is a *geometric artefact* related to the combination of: 1) resolution in HCD-geometry triangulation and 2) binning of the random field. In effect, the 3BLA intersection sample one heterogeneity value, whereas the 1BRT and 2BLA intersections sample more than one heterogeneity values.
- Within the limited sample size, R01 to R10, the range of variability in the applied HCD transmissivity is contained reasonably well within 95% of the input distribution (c.f., brown lines in Figure 5-13). It is noted that the variability in applied transmissivity exceeds the 95% interval for some disposal facilities in ZFMNNW1209 and ZFMWNW8042 (Figure 5-13a and b).
- Errors in parameterisation of ZFMNE3112 and ZFMNE3137 are less critical, as their hydraulic role is clearly subordinate to DFN transmissivity (Figure 5-13e and f).
- For ZFMNE3137, both the applied transmissivity and the “correct” implementation lie outside the input distribution for 2BMA, but not for 5BLA (Figure 5-13f). The reason for this is a combination of coarse HCD geometry triangulation and the depth-interval binning of transmissivity, which can cause an artificial spread in $T_{eff}(z)$ at a given elevation, z (e.g., Figure 3-4c). The implication of this artefact is minor, as the transmissivity of ZFMNE3137 is clearly subordinate to the transmissivity of intersecting stochastic fractures (i.e., grey box-whisker plots in Figure 5-13f).
- The transmissivity is correlated among several deformation-zone/disposal-facility intersections, which related to the resolution of HCD geometry triangulation and HCD heterogeneity binning (i.e., more than one disposal facility may be affected by the same “triangular element” or “heterogeneity bin” of one HCD; Figure 3-4).

The following can be concluded about the error in *applied* heterogeneous HCD parameterisation:

- In general, the implication of the error in transmissivity implementation is subordinate to *geometric artefacts* arising from combinations of: 1) resolution in HCD-geometry triangulation, 2) binned transmissivity depth intervals, and 3) resolution in heterogeneity field (Section 3.2.1).
- In two cases (ZFMNE3112 and ZFMNE3137), the hydraulic significance of HCD parameterisation is clearly subordinate to the transmissivity intersecting stochastic fractures.
- Generally, the *applied* parameterisation is contained within the intended 95% variability interval for tunnel intercepts in the studied realisations (R01 to R10); exceptions are given below:
    - **ZFMNNW1209**: one realisation (R07) has intercept transmissivity outside the 95% interval for 2BTF, 1BLA, and 1BMA.
    - **ZFMWNW8042**: three realisations (R03, R04, and R07) have intercept transmissivity outside the 95% interval for 1BRT, 2BLA, and 3BLA. One additional realisation (R08) is barely outside the interval for 3BLA, 4BLA, 5BLA, and 2BMA.

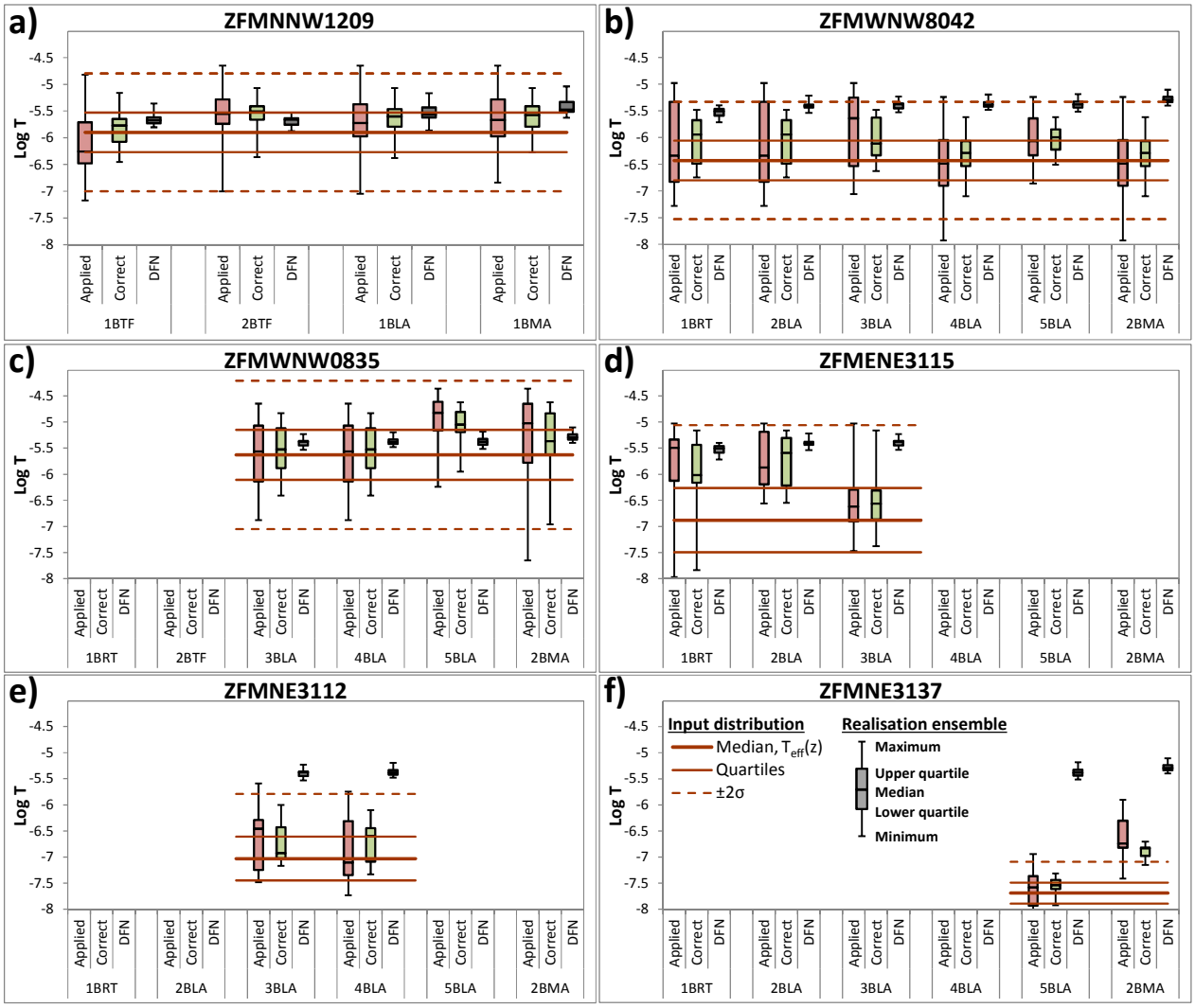

Figure 5-13. *Applied HCD transmissivity at tunnel intersections (pink), compared against correction (green), DFN transmissivity (grey) and theoretical input distribution (brown lines).*

5.2.4 Sensitivity to bedrock parameterisation (TD08b)

As part of TD08b, the model sensitivity to HRD and HCD heterogeneity is evaluated in terms of disposal-facility cross flow. Evaluation is made in terms of "average facility flow", as well as at the level of individual disposal facilities (Figure 5-14 and Figure 5-15, respectively). Expectations are that disposal-facility cross flow is most sensitive to the dominating heterogeneity component, i.e., HCD or HRD, which may vary among the different disposal facilities.

Evaluation of average facility flow

Two "average facility cross flows" can be calculated; over the 5 disposal facilities of SFR1 and over the planned 6 disposal facilities of L1B. The distribution of average facility cross flow are compared for the different model setups (Figure 5-14). The following can be noted:

1) In SFR1, simulated flow for BASE_CASE1 with DFN realisations R18 and R85 (blue and red dashes) compares well with the median in the corresponding heterogeneous HCD cases (black dashes). This suggests that the heterogeneity components of HCD and HRD are additive. In L1B, the median flow for heterogeneous HCD parameterisation is clearly higher than in BASE_CASE1. This difference is due to the local borehole-conditioning in BASE_CASE1 (see Figure 3-2 and discussion in Section 3.2.1).

2) In SFR1, although the simulated flows for DFN R18 and R85 do not cover the full range of HRD variability, it is reasonable to refer to these as "optimistic" and "pessimistic" realisations, respectively (i.e., blue and red dashes in Figure 5-14a). On the other hand, neither of the two realisations represents extreme values for flow in L1B; both are below the median flow (blue and red dashes in Figure 5-14b).
3) The flow increases only moderately between the time slices 3500 and 9000 AD (i.e., c. 10% in SFR1 and 5% in L1B). This increase is rather "constant" among all bedrock cases.
4) Extended geometry of ZFM871 has a surprisingly small impact on disposal-facility cross flow (c.f. grey and orange box-whiskers in Figure 5-14). On average, flow increases by c. 15% in SFR1 and by 4% in L1B.
5) The range of variability for heterogeneous HCD parameterisation is larger in SFR1 than it is in L1B. There are several reasons for this:
    a. Analysis at the level of individual disposal facilities (Figure 5-15), demonstrates that the variability range for heterogeneous HCD parameterisation does not differ dramatically from BASE_CASE1. However, the average flow in SFR1 is dominated by two disposal facilities 1BLA and 1BMA, which have a relatively high contribution to variability. This suggests that the arithmetic averaging of "facility flow" may not be entirely appropriate for discussing variability.
    b. SFR1 has only 4 HCD intersections, related to *one* deformation zone (ZFMNNW1209), and owing to the coarse heterogeneity resolution, 100 m, the individual disposal-facility cross flows are strongly correlated. Thus, "disposal-facility averaging" of flow has comparatively small "smoothening effect" for SFR1.
    c. L1B has 17 HCD intersections, involving *five* HCDs, which implies that tunnel intersections cover a larger sample of HCD heterogeneity. In turn, this implies that the averaging over all disposal facilities has a comparatively larger smoothening effect for L1B.
    d. In retrospect, an error has been found in the numerical implementation of HCD parameterisation which exaggerates the HCD heterogeneity. The effect of this error is higher for ZFMNNW1209 (Section 5.2.3), i.e., particularly affects SFR1. This error has been corrected in the final delivery from TD11.

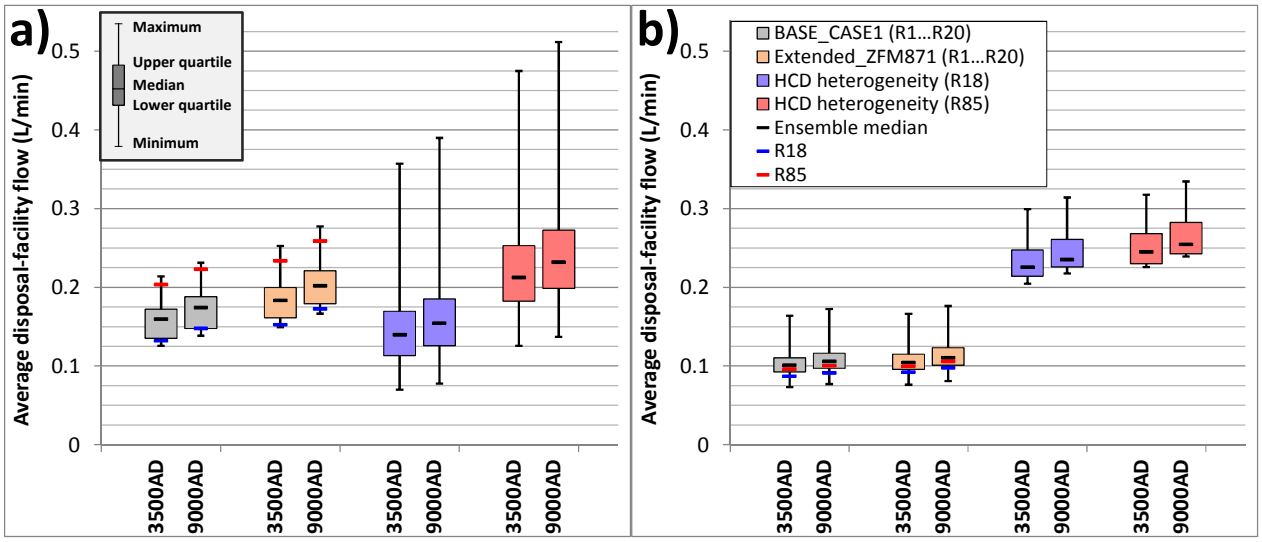

Figure 5-14. *Box-whisker plots of "average facility cross flow", in different model setups; a) existing SFR1, and b) planned extension L1B. Demonstrated at the more detailed level in Figure 5-15.*

The 10 heterogeneous HCD realisations are ranked in terms of total flow through disposal rooms and placed in context of the Base case (Table 5-1). The total flow includes all 11 disposal

rooms of both facilities (SFR1 and SFR3) and is calculated for the time slice 3500 AD, and averaged over the two DFN realisations R18 and R85. The Base case stands out with the lowest total cross flow, owing to its local conditioning of tunnel intercepts for SFR3. The "median total cross flow" occurs for HCD realisation R01, while the highest total cross flow occurs for HCD realisation R07.

Table 5-1. Total flow across all disposal rooms of SFR1 and SFR3[1)]

HCD variant	Total flow, Q (L/min)
BASE_CASE1	1.39
HETERO_R08	1.81
HETERO_R10	2.07
HETERO_R06	2.17
HETERO_R02	2.19
HETERO_R01	2.20
HETERO_R04	2.24
HETERO_R05	2.39
HETERO_R09	2.66
HETERO_R03	2.86
HETERO_R07	3.91

1) Time slice 3500 AD, averaged over DFN realisations R18 and R85

Evaluation of individual disposal-facility flow

The following can be noted in flow at the individual disposal-facility level:

1) In logarithmic scaling, the flow in individual disposal facilities, as organised by different HCD parameterisation groups, exhibit rather similar patterns, with an overall median cross flow of c. 0.1 L/min. A few disposal facilities stand out, e.g., 1BLA, 1BMA, 3BLA, and 2BMA. It should be noted that, in BASE_CASE1, ZFMNNW1209 is locally conditioned with a high transmissivity at the 1BLA intercept.
2) At the level of individual disposal facilities, the variability ranges of the different HCD-parameterisation groups typically have wide overlaps (Figure 5-15). Notably, the overlaps between BASE_CASE1 and heterogeneous HCD parameterisations are smaller in L1B (e.g., 3BLA), which is primarily an effect of the local borehole conditioning in BASE_CASE1 (see Figure 3-2 and discussion in Section 3.2.1). For the silo, it can be noted that the two heterogeneous HCD parameterisations lack overlapping variability ranges; this suggests local dominance of the HRD heterogeneity component, which may be expected as the silo has no HCD intersections.
3) Within each HCD-parameterisation group, the range of variability is relatively low. The ranges in flow are typically below one order of magnitude (on average, the largest flow is four times higher than the lowest flow). A notable exception is 1BLA, where the heterogeneous HCD parameterisation with DFN R18 yields lower flow with high variability (the largest flow is c. 14 times higher than the lowest flow). It is also noteworthy that the silo, which has no HCD intercepts, is rather insensitive to HCD heterogeneity for DFN R85, but less so for DFN R18.
4) DFN R85 is "pessimistic" for BLA and the silo, but *clearly not* for all facilities (c.f. relative position of red dashes in Figure 5-15)

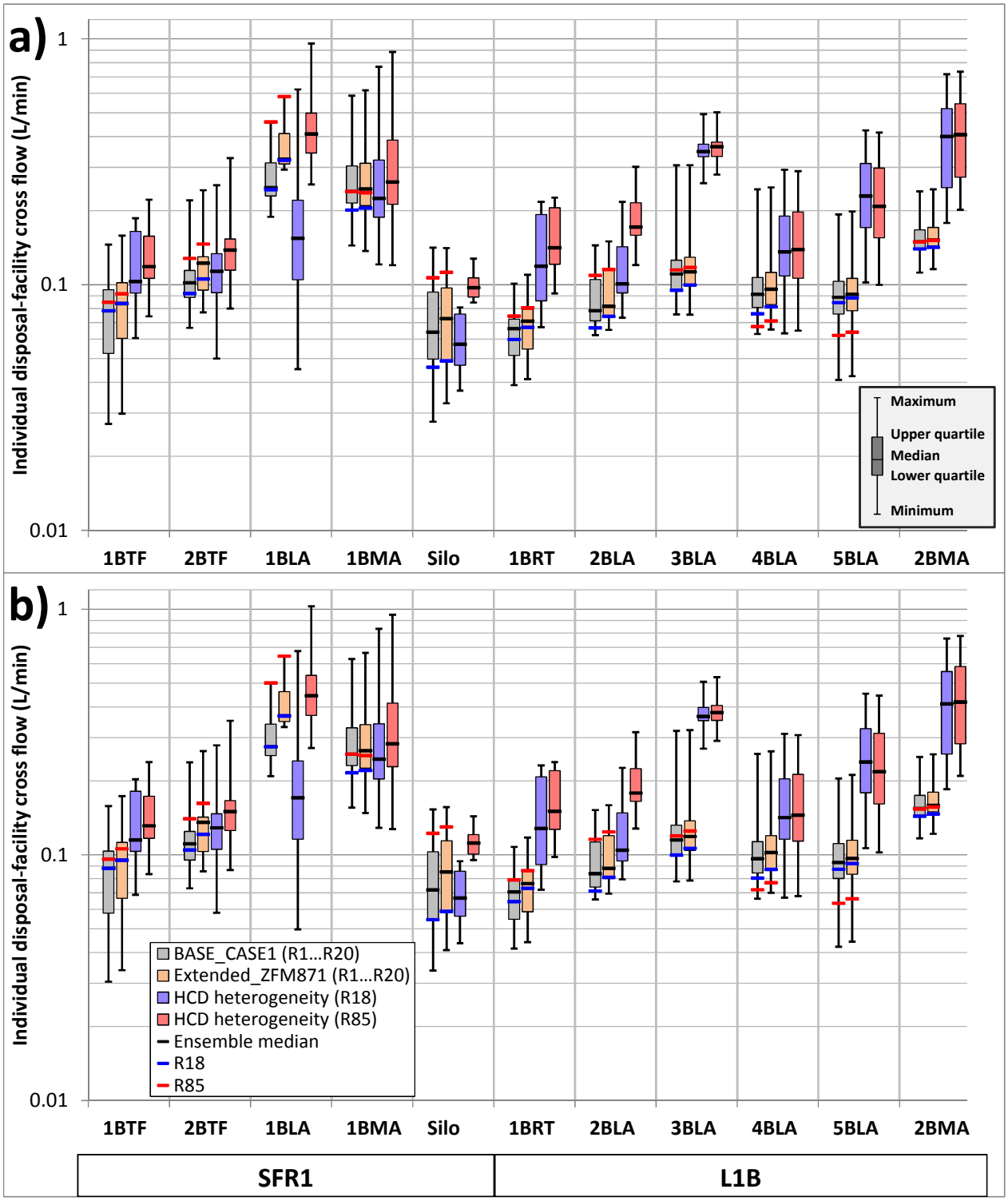

Figure 5-15. *Box-whisker plots of individual disposal-facility cross flow", in different model setups; a) 3500 AD, and b) 9000 AD. Note logarithmic scaling on the y-axis.*

5.3 Particle-trajectory interactions between facilities

Possible interactions between disposal facilities are evaluated by analysing the fraction of particle trajectories that intersect adjacent facilities, referred to as "interactions". The detailed

geometry of interior of disposal facilities is not resolved in the DarcyTools model setup (e.g., containers, concrete walls, pressure-equilibrating drains, etc.). Therefore, trajectories observed crossing disposal facilities in the DarcyTools grid do not necessarily imply chemical interaction with stored waste.

5.3.1 Interactions between L1B and existing SFR1

Only interactions between the planned extension and SFR1 are presented in this section. 100,000 particles are released in each of the 6 disposal facilities of L1B for model setups 7 to 12 in TD08a and model setups 1 to 124 in TD08b (a total of 78 million particles). Analogously, 65 million particles are also released within SFR1 to identify possible interactions in L1B. However, no such interactions are found, indicating that L1B is upstream of SFR1.

In TD08a interactions from L1B to SFR1 are studied for six different time slices (BASE_CASE1, DFN realisation R85). For this bedrock case, the only interactions between the planned extension L1B and SFR1 occur from 1BRT and 2BLA to the silo. It should be noted that no technical barriers of the silo are implemented in TD08, and that it is difficult to speculate how implementation of barriers would affect these interactions. Maximum interaction occurs during the vertical flow regime at 2000 AD. The interactions virtually vanish during the intermediate flow regime at 2500 AD, and stabilises at around 3500 AD (Figure 5-16). During this latter period, 3500 to 9000 AD, the bedrock case BASE_CASE1, DFN realisation R85, can be placed in context of all bedrock cases addressed in the TD08b sensitivity analysis (Figure 5-17). The comparison demonstrates that the TD08a base case has relatively high interactions (typically, around the 75 percentile). Notably, the ZFM871 extension decreases the L1B-SFR1 interactions, in contrast to the heterogeneous HCD parameterisation variants.

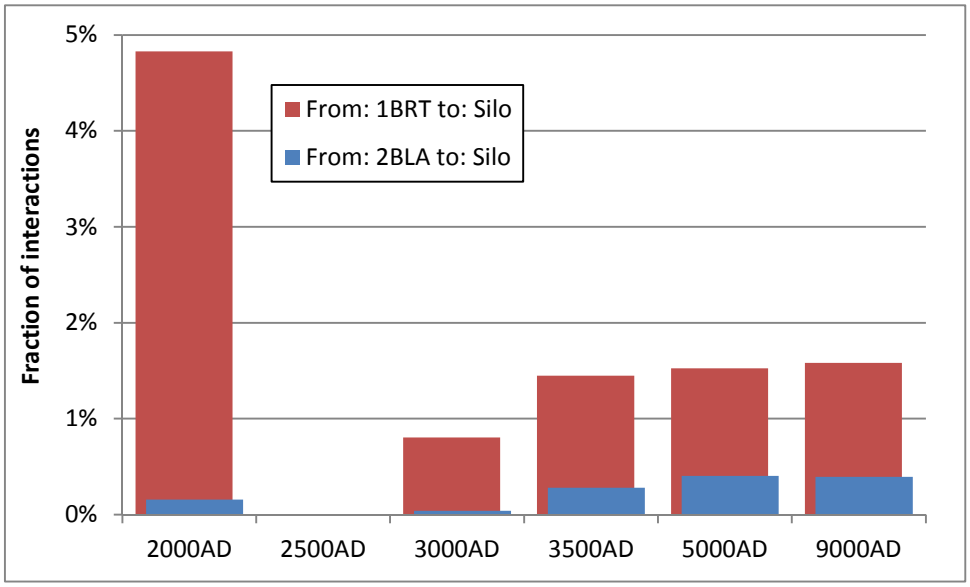

Figure 5-16. *Fraction of interactions from planned extension L1B to existing SFR1 in BASE_CASE1, DFN realisation R85, with changing flow regime (TD08a).*

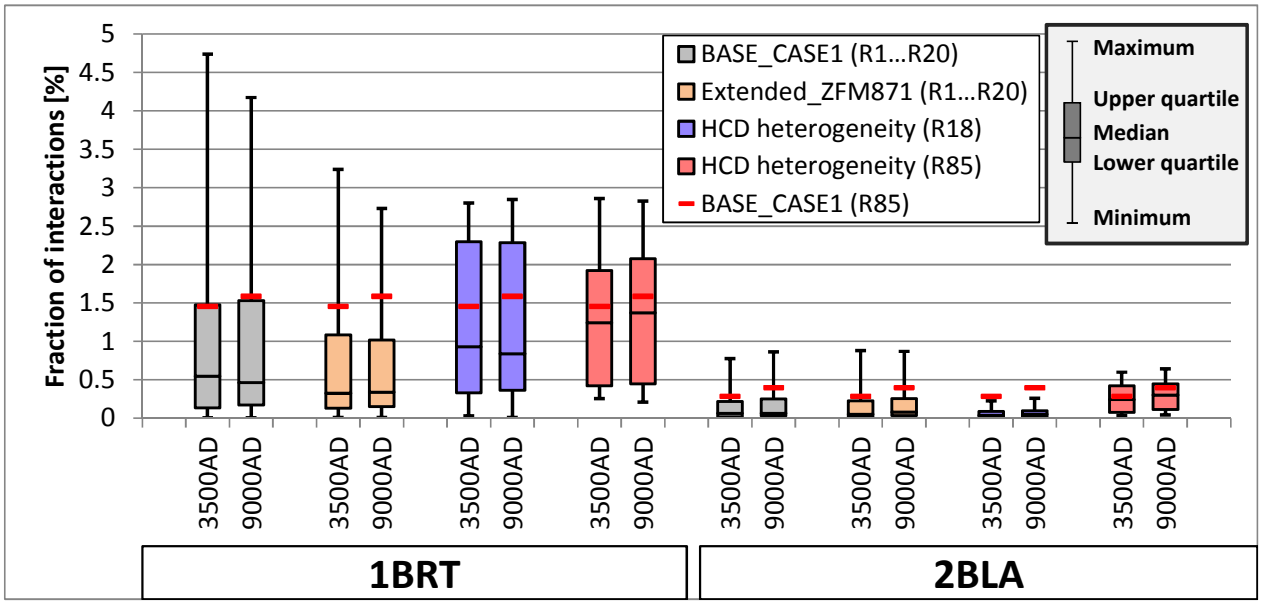

Figure 5-17. *Interactions from planned extension L1B to the existing SFR1 (i.e., the silo) for all bedrock cases in the TD08b sensitivity analysis (Table 1-2). Some bedrock cases also include interactions from 3BLA to the silo. These are very few, and hence they are not shown.*

5.3.2 Interactions within the planned extension, L1B

Evaluation of internal interactions within L1B is performed analogously to the evaluation of L1B-SFR1 interactions (Section 5.3.1). For the TD08a base case (BASE_CASE1, DFN realisation R85), the change in interactions in studied over time (Table 5-2), and during the later time slices, 3500 to 9000 AD, the TD08a base case can be placed in context of all bedrock cases addressed in TD08b (Table 5-3).

Similarly to the L1B-SFR1 interactions, the maximum internal L1B interactions occur at 2000 AD, although the internal L1B interactions are still high by 2500 AD. The differences at later time slices, c. 5000 to 9000 AD, are small. Notably, there are no interactions from 3BLA after 3000 AD, while the interactions from 4BLA are re-directed from 5BLA towards 3BLA. A similar re-direction seems to occur in 5BLA, where part of its interactions is successively re-directed from 2BMA towards 4BLA.

The compiled results from TD08b reinforce the notion of 3BLA as a "downstream facility" (i.e., interactions *to* 3BLA exceed interactions *from* 3BLA). These 3BLA interactions are particularly high in both heterogeneous HCD parameterisation variants. Generally, the extension of ZFM871 has only minor impact on interactions.

Table 5-2. Interactions over time within L1B [%][1)]

From	to	2000AD	2500AD	3000AD	3500AD	5000AD	9000AD
1BRT	2BLA	40	13	9.7	7.2	5.8	5.9
	3BLA	1.9	0.55	0.05	0.003	0.001	0.001
	4BLA	0.01					
2BLA	3BLA	29	21	12	3.4	0.75	0.91
	4BLA	0.31	0.002				
3BLA	4BLA	11	3.2				
	5BLA	0.002	0.14				
	2BMA		0.004				

4BLA	3BLA			0.63	2.3	3.3	3.2
	5BLA	2.1	13				
	2BMA	0.02	0.93				
5BLA	4BLA			0.14	1.9	2.7	2.7
	2BMA	38	33	9.3	4.3	1.6	2.2

1) Fraction of particles released in L1B disposal facilities that cross adjacent facilities within planned extension, expressed as percentage. Results from TD08a, model setups 7 to 12 in Table 1-2.

Table 5-3. Average interactions within L1B [%] in the TD08b sensitivity analysis[1)]

From \ To	1BRT	2BLA	3BLA	4BLA	5BLA	2BMA
BASE_CASE1						
1BRT	-	3.79	0.09			
2BLA	0.17	-	5.07	<0.01		
3BLA		0.14	-	0.28		
4BLA			3.6	-	<0.01	
5BLA			0.44	3.93	-	1.99
2BMA			0.5	1.39	3.61	-
Extended ZFM871						
1BRT	-	3.05	0.07			
2BLA	0.17	-	4.34			
3BLA		0.39	-	0.11		
4BLA			4.1	-		
5BLA			0.31	4.36	-	1.64
2BMA			0.54	1.29	3.66	-
HCD heterogeneity (R18)						
1BRT	-	3.16	1.39	0.27		<0.01
2BLA	<0.01	-	22.99	1.33	0.04	<0.01
3BLA		0.2	-	8.88	0.63	<0.01
4BLA		0.01	11.91	-	2.27	0.05
5BLA			0.71	0.85	-	3.82
2BMA					0.06	-
HCD heterogeneity (R85)						
1BRT	-	6.28	1.42	0.09	0.04	<0.01
2BLA	<0.01	-	23.56	0.92	0.1	0.03
3BLA		0.88	-	6.05	0.95	0.26
4BLA		0.05	10.63	-	3.85	0.91
5BLA			1.14	1.75	-	5.98
2BMA					0.22	-

1) Average fraction of particles released in L1B disposal facilities that cross adjacent facilities within planned extension, expressed as percentage. Average percentage for time slices 3500 and 9000AD in TD08b model setups, 1 to 124 (Table 1-2), coloured by value; high = red, <0.01% = white, none = blank.

5.4 Particle tracking

5.4.1 Recharge locations with shoreline retreat (TD08a)

Recharge locations for SFR1 and L1B are simulated by backward particle tracking. One million particles are released uniformly within the disposal facilities of SFR1 and in L1B, respectively. Particle trajectories are backtracked upstream from the storage facilities, to determine the spatial density in recharge locations at the bedrock surface. Recharge locations are determined for each of the six time slices in TD08a, however, results appear stationary after c. 3000 AD, and hence are not shown (Figure 5-18). Remote recharge locations, associated to local topographical peaks and deformation-zone traces in the Forsmark inland, occur by 2000 AD. From 2500 AD and onwards, the recharge locations are isolated to the SFR pier. It can be noted that, although the SFR1 and L1B recharge locations partially overlap, the densities are correlated to the respective locations of SFR1 and L1B (i.e., the peaks for SFR1 are shifted somewhat west and the peaks of L1B are shifted somewhat east).

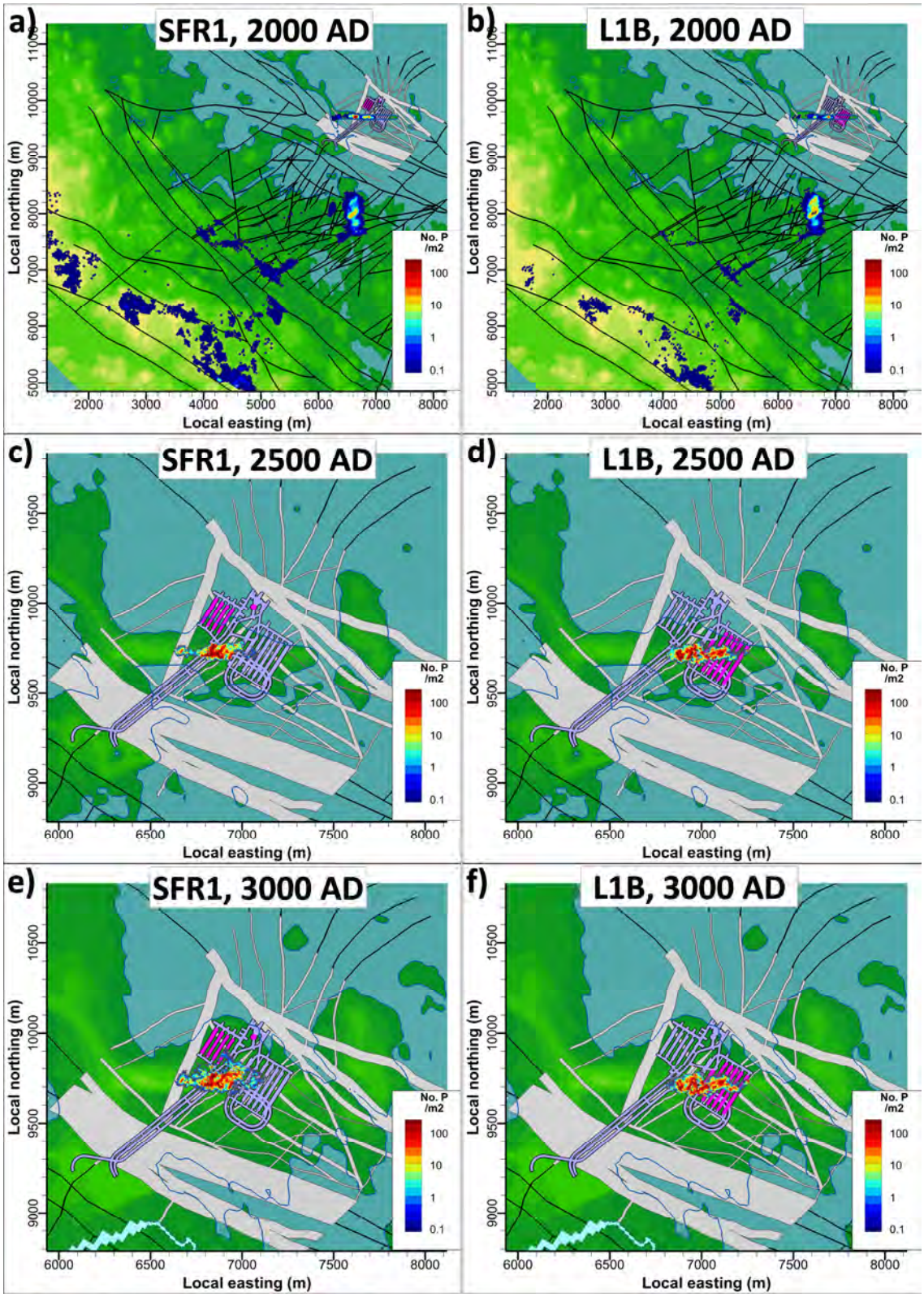

Figure 5-18. *Spatial distribution of recharge locations from SFR1 and L1B.*

5.4.2 Exit locations with shoreline retreat TD08a

Exit locations can be evaluated analogously to the analysis of recharge locations (Section 5.4.1). The spatial distributions of discharge locations (or "exit locations") are evaluated for the TD08a model setups (Figure 5-19 to Figure 5-21). A couple of characteristics can be noted:
During early time slices, 2000 to 3000 AD, the exit locations are intimately concentrated to deformation-zone traces below sea. The changing flow regime with land lift, successively re-directs the exit locations with the retreating shore line (i.e., still concentrated to deformation-zone traces below sea). At later stages of land lift, 5000 to 9000 AD, the exit locations are concentrated along valleys or local topographical depressions.

SFR1 has only exit locations north of the SFR pier. The dominant discharge paths for SFR1 are via ZFMNNW1209 (Zone 6) and ZFMNNE0869 (Zone 3) for 1BTF, 2BTF, 1BLA, and 1BMA, and ZFMNW0805A/B (Zone 8) for the Silo. Inspection of bedrock surface flux (i.e., Figure 5-19d and f) demonstrates how the SFR1 exit locations are "cornered in" towards the junction between the discharging zones ZFMNNE0869 and ZFMNW0805A/B.
In contrast to SFR1, L1B has exit locations both south and north of the SFR pier (Figure 5-20 and Figure 5-21). The peak density occurs along ZFMNW0805A/B, just north-east of L1B. Particles passing through ZFMNW0805A tend to follow ZFMNS3154 towards north. Unlike SFR1, L1B also has minor fractions of remote exit locations in the area around lake object 116 (i.e., Charlie's lake), during later time slices, 5000 to 9000 AD. The fraction of exit locations south of the SFR pier appears to be "cornered in" by discharging ZFMWNW0001 (Singö deformation zone; c.f., Figure 5-19d and f). It can also be noted that fraction of exit locations south of the SFR pier decreases during later time slices and is divided into two areas: 1) Singö deformation zone (at the south-eastern boundary of the SFR Regional domain) and 2) the junction between Singö deformation zone and ZFMNW0805A (outside the SFR Regional domain). It should be noted that the exit locations occurring at the SFR Regional domain boundary may be a model artefact, as it coincides with a discontinuity in HCD parameterisation (Section 3.3).

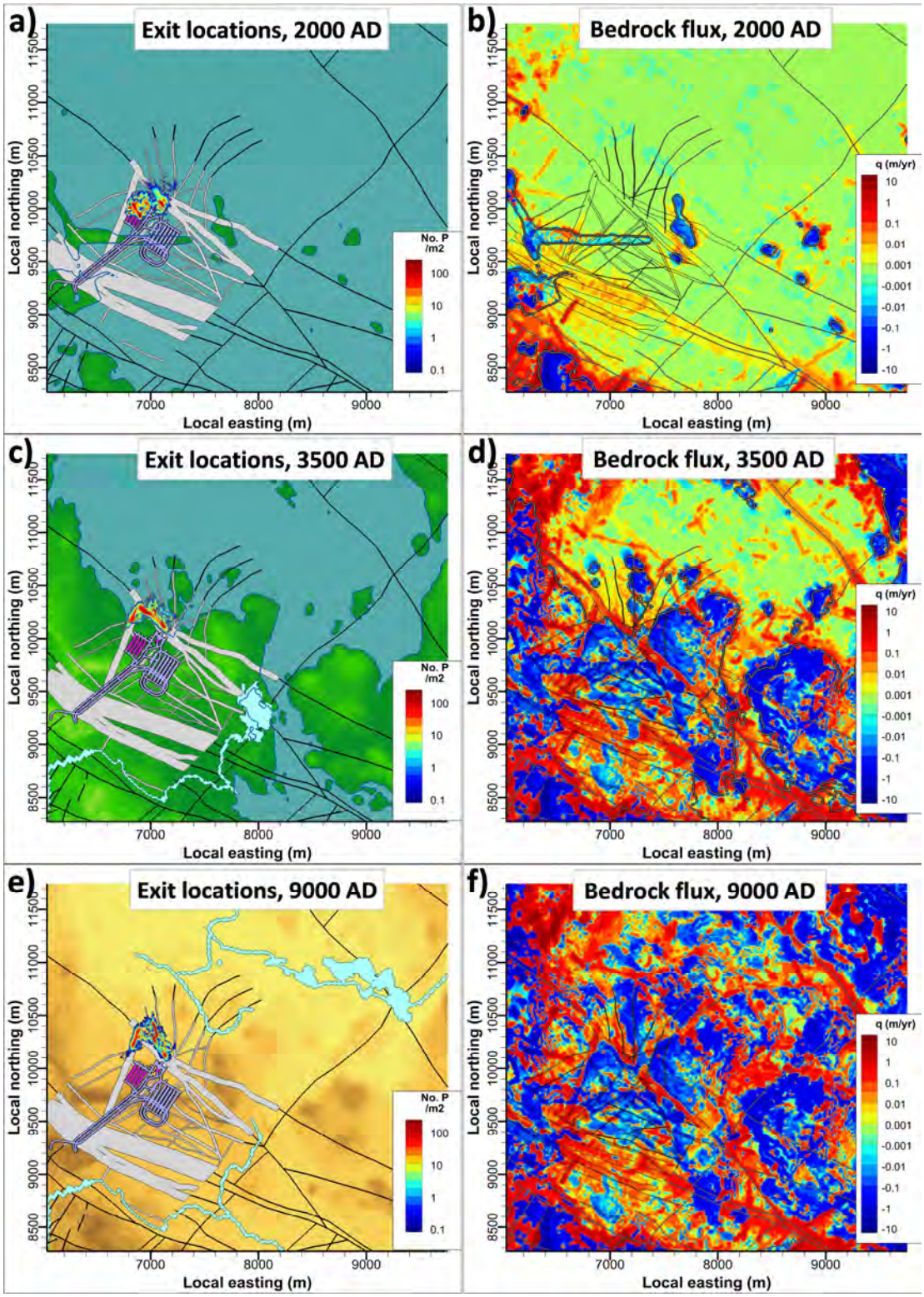

Figure 5-19. *Exit locations from disposal facilities in SFR1 (left; contoured by areal density) and bedrock-surface flux (right), [BASE_CASE1_DFN_R85], selected time slices.*

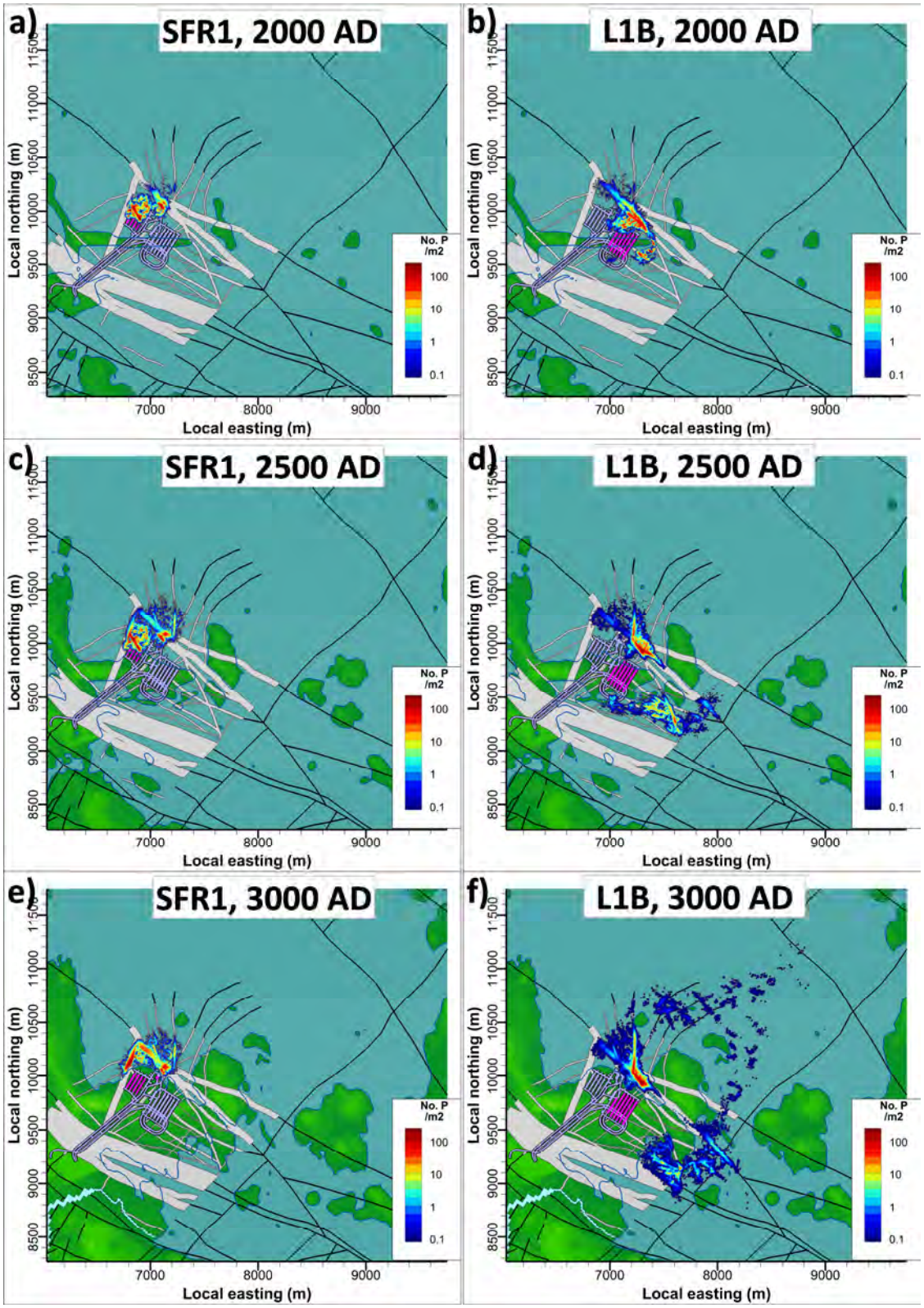

Figure 5-20. *Exit locations (contoured by areal density) from disposal facilities in SFR1 and L1B (release points pink shaded), [BASE_CASE1_DFN_R85], time slices 2000 to 3000 AD.*

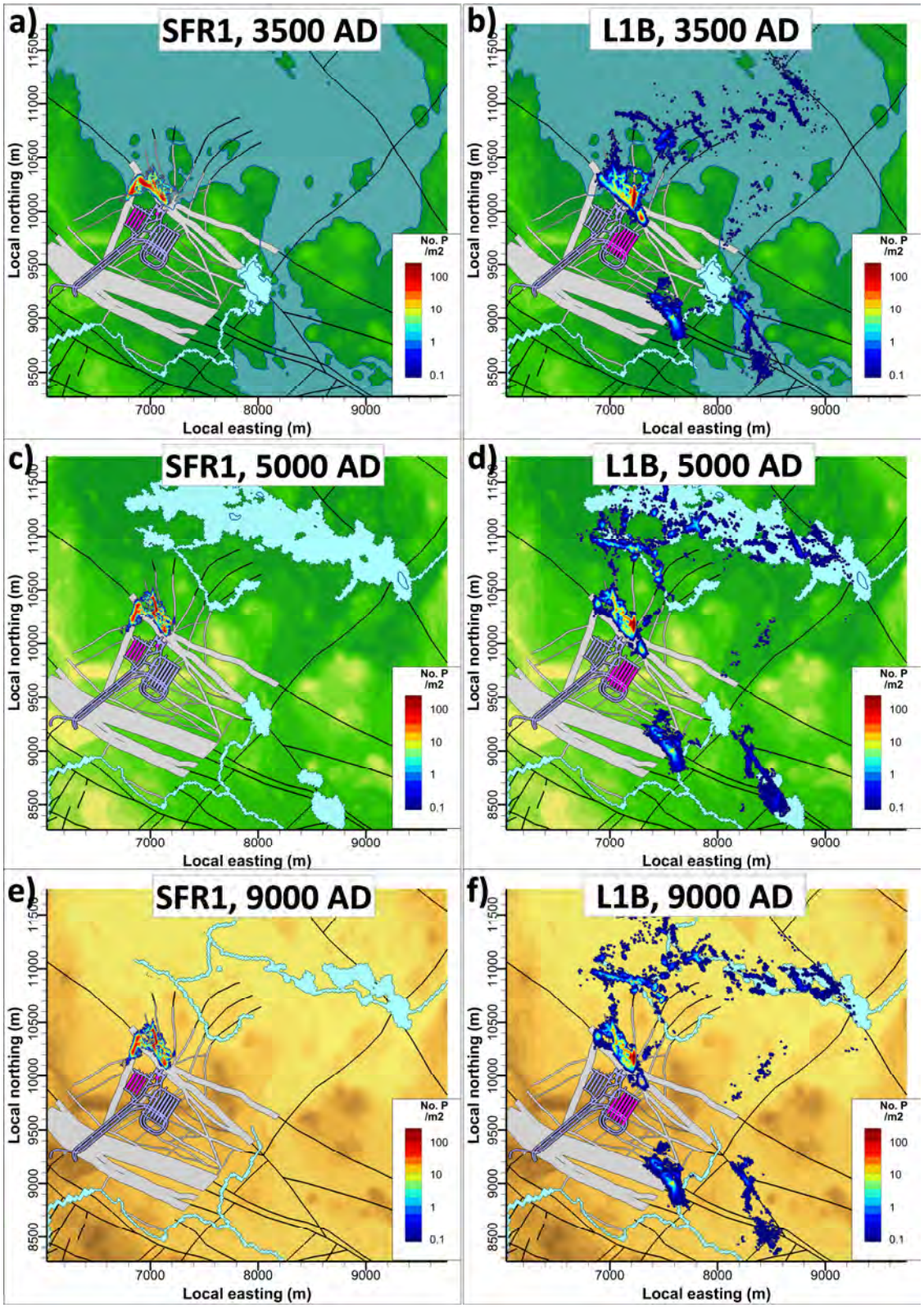

Figure 5-21. *Exit locations (contoured by areal density) from disposal facilities in SFR1 and L1B (release points pink shaded), [BASE_CASE1_DFN_R85], time slices 3500 to 9000 AD.*

5.4.3 Exit locations and sensitivity to bedrock parameterisation (TD08b)

Exit locations and travel time are also studied for individual disposal facilities for all bedrock cases in the TD08b sensitivity analysis. Results are organised per time slice (3500 and 9000 AD) and the following 3 HCD parameterisation groups:

- BASE_CASE1 (DFN realisations R01…R18 + R85)
- EXT_ZFM871 (DFN realisations R01…R18 + R85)
- HCD_HETERO (HCD realisations R01…R10, with DFN realisations R18 and R85)

In total, 134 million particles are released (100,000 particles × 11 facilities × 21 (or 20) realisations × 3 HCD groups × 2 time slices). Detailed results are available in SKBdoc 1395705. In summary, lumped results (Figure 5-22) suggest that:

1) The general pattern is similar to the TD08a results (i.e., exit locations primarily determined by topography, or simulated groundwater level)
2) Addressing a larger ensemble of DFN realisations smears, to some extent, out exit the locations.
3) The ZFM871 extension has minor impact on exit locations (i.e., SFR1 exit locations “cornered in” by discharging zones ZFMNNE0869 and ZFMNW0805A/B).

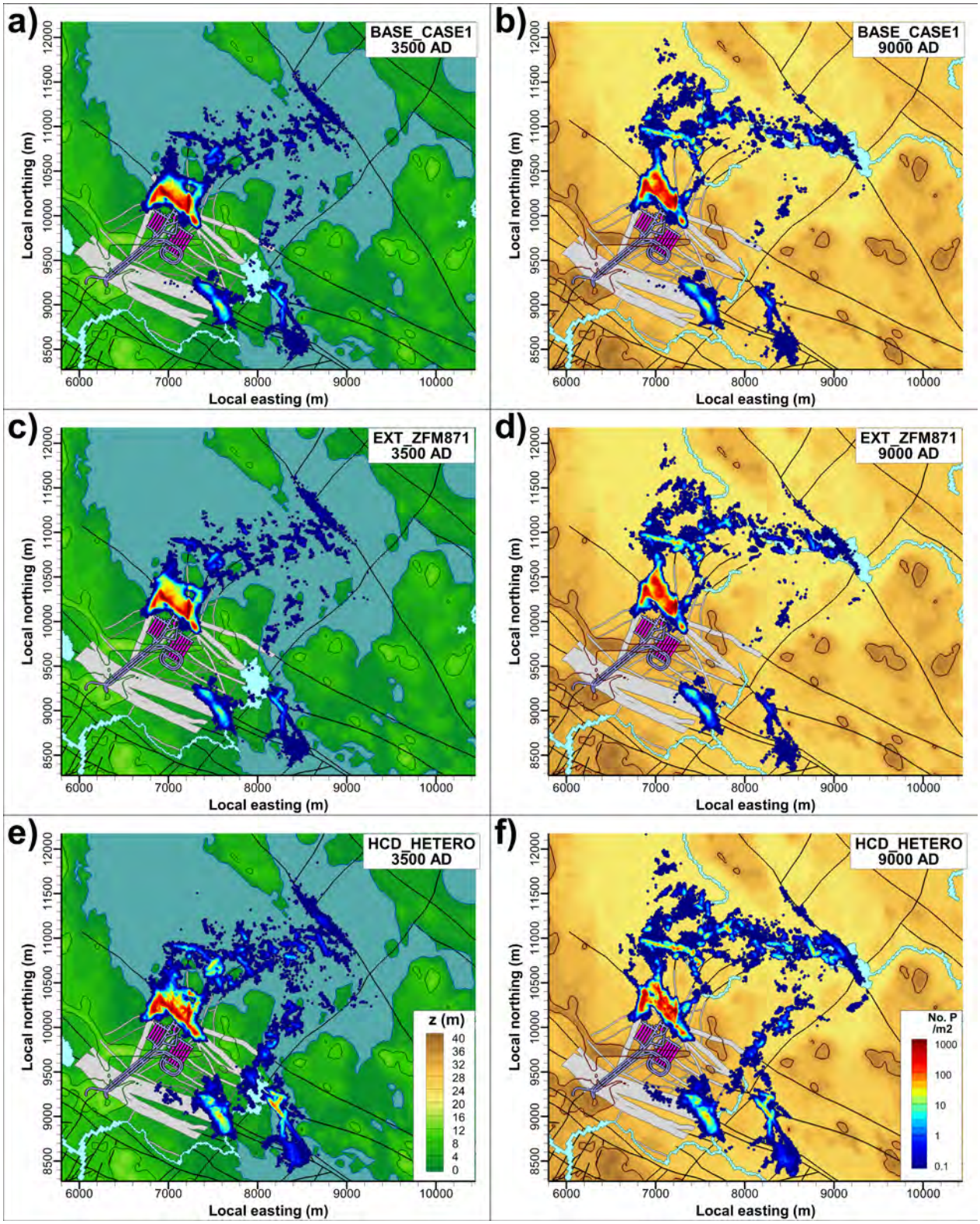

Figure 5-22. *Exit locations (contoured by areal density) by HCD parameterisation group from all disposal facilities in SFR1 and L1B (release points pink shaded), time slices 3500 to 9000 AD.*

5.5 Travel-time

5.5.1 Shoreline retreat (TD08a)

Porosity parameterisation variant 1 (Table 4-2) is applied in particle tracking for six stages of shoreline retreat (i.e., TD08a, BASE_CASE1, DFN R85). 100,000 particles are released uniformly within each disposal facility (i.e., 11 release locations; Table 4-8). The following can be noted (Figure 5-23):

- The upward-directed flow regime during the submerged conditions at 2000 AD renders long travel times.
- As the land lift successively re-directs flow towards a horizontal regime, 2500 to 3000 AD, the travel times are reduced about two orders of magnitude (c.f. tunnel flows in Figure 5-6).
- After c. 3500 AD, the travel times stabilise, with medians of a few years, or less (Figure 5-24)
- Travel time distributions of SFR1 and L1B have wide overlaps (marked as "common" in Figure 5-23), although the travel times for L1B are consistently longer, and its response to the changing flow regime is somewhat delayed, as compared to SFR1.

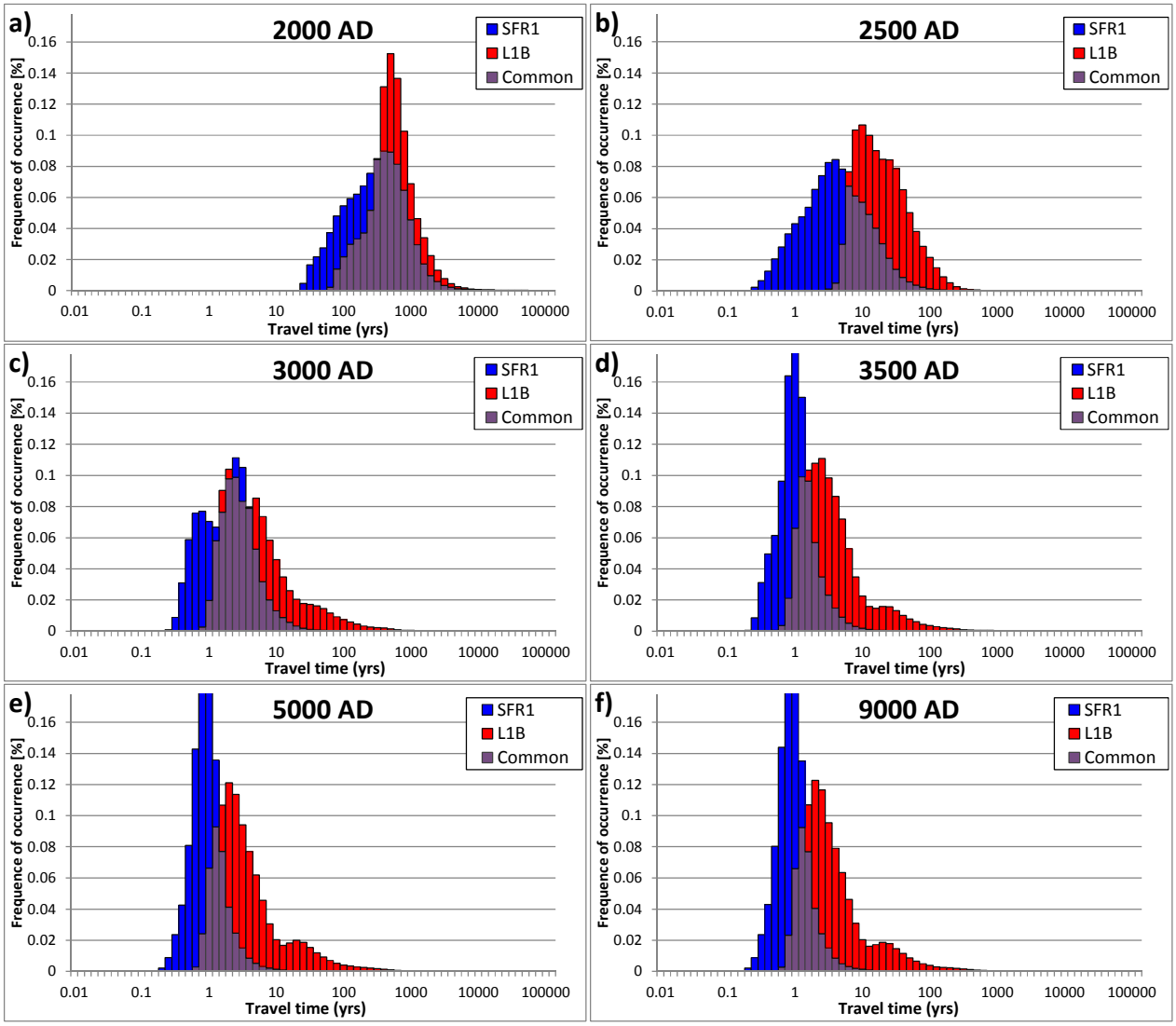

Figure 5-23. *Travel-time distribution with shoreline retreat.*

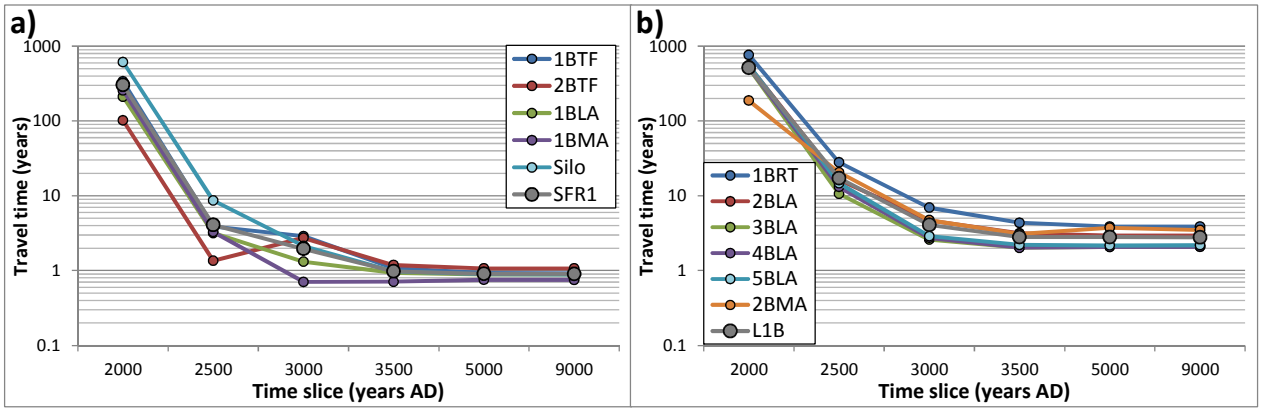

Figure 5-24. *Median travel-time with shoreline retreat; a) SFR1 and b) L1B.*

5.5.2 Sensitivity to porosity parameterisation (TD08b)

The four porosity parameterisation variants (Table 4-2) are tested in particle tracking of TD08b results. Altogether, 545 million particle trajectories are studied (100,000 particles released × 11 disposal facilities × 62 bedrock cases × 2 time slices × 4 porosity variants). The following is noted:

- **Variant 1:** has the shortest median travel time and relatively narrow spread in distributions.
- **Variant 2:** has about one order of magnitude longer travel times, and somewhat larger spread in distributions, as compared to variant 1. This is expected, as the equivalent porosity in the empirical relation of (Hjerne et al., 2010) is slightly more than one order of magnitude higher than in (Dershowitz et al. 2003) (**Error! Reference source not found.**).
- **Variant 3:** the SFR1 mode is similar to that in variant 1, although the distributions are skewed towards longer travel times, which primarily affects L1B (i.e., reducing the overlap of SFR1 and L1b, marked as “common”). This demonstrates that the upscaled porosity for SFR1 is typically 10^{-4} (as expected from Figure 4-1), while it is typically lower for L1B.
- **Variant 4:** as compared to variant 3, travel-time distributions are identical but displaced by a factor of 50. This confirms the concept adopted by (Holmén and Stigsson 2001), that travel time scales linearly to porosity, such that the uncertainty in porosity can be handled separately in the safety analysis.

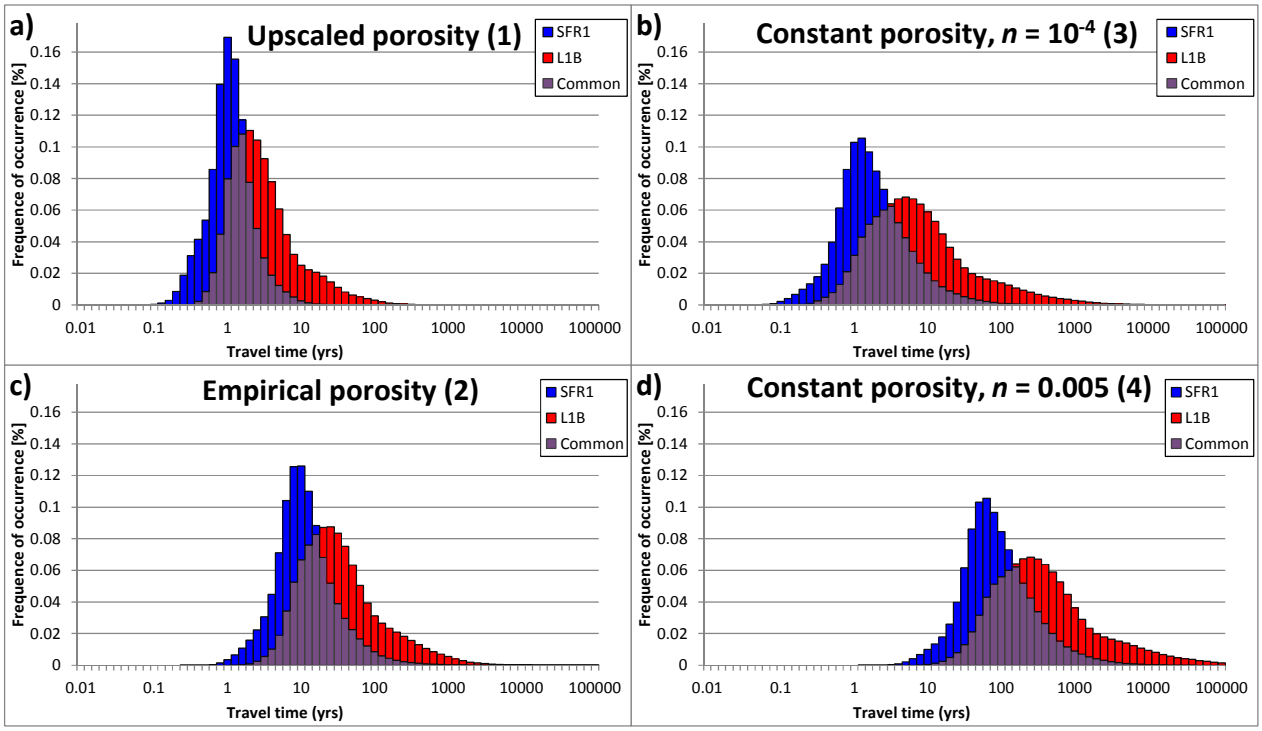

Figure 5-25. *Comparison of travel-time distributions for the four tested porosity parameterisation variants (Table 4-2). Travel time refers only to bedrock retention properties (i.e., trajectories from tunnel wall to bedrock surface). Only time slice 3500 AD for the 62 bedrock cases of TD08b (Table 1-2).*

5.5.3 Sensitivity to bedrock parameterisation (TD08b)

Porosity parameterisation variant 1 (Table 4-2) is selected in further particle tracking of TD08b results. In one particle-tracking execution, 100,000 particles are released uniformly within a single disposal facility (i.e., one out of the possible 11 release locations; Table 4-8). This particle-tracking execution is repeated 1,364 times, to address the entire sequence of TD08b mode setups (11 disposal facilities × 62 bedrock cases × 2 time slices. Altogether, 68 million particle trajectories are studied. From each particle-tracking execution, the following travel-time percentiles are identified (presented in Figure 5-28 to Figure 5-33):

- Minimum travel time (i.e., the 0.001 percentile)
- The 10 percentile
- The median (i.e., 50 percentile)
- The 90 percentile
- Maximum travel time (i.e., the 99.999 percentile)

These percentiles are used to overview the travel-time sensitivity to bedrock parameterisation. The TD08b model setups are organised into four groups:

- BASE: (BASE_CASE1, with DFN realisations R01…R18 + R85)
- EXT: (EXT_ZFM871, with DFN realisations R01…R18 + R85)
- HET(18): (heterogeneous HCD realisations R01…R10, with DFN realisation R18)
- HET(85): (heterogeneous HCD realisations R01…R10, with DFN realisation R85)

The variability in travel-time percentiles, within these groups, is presented for 3500 AD (Figure 5-26) and 9000 AD (Figure 5-27). The average percentiles for a group (90 percentile, median, and 10 percentile) are shown by diamond markers, while their corresponding minimum and maximum for each group is shown by error bars. The following can be noted:

- As may be expected, travel time is inversely correlated to disposal-facility cross flow (c.f., Figure 5-15), where L1B generally has longer travel times. This is probably related to its deeper location.
- Travel time is not very sensitive to extension of ZFM871. In the case with extended ZFM871, the silo has somewhat longer travel times, while 1BRT has shorter travel times.
- Travel time is sensitive to heterogeneous HCD parameterisation, which is manifested by wide spans in travel-time percentiles within a group (i.e., long error bars). In L1B, heterogeneous HCD parameterisation typically delays the median and the 90 percentile. For HET (R85), a few realisations render 10 percentiles with very short travel times in 1BTF, 1BLA and 1BMA.

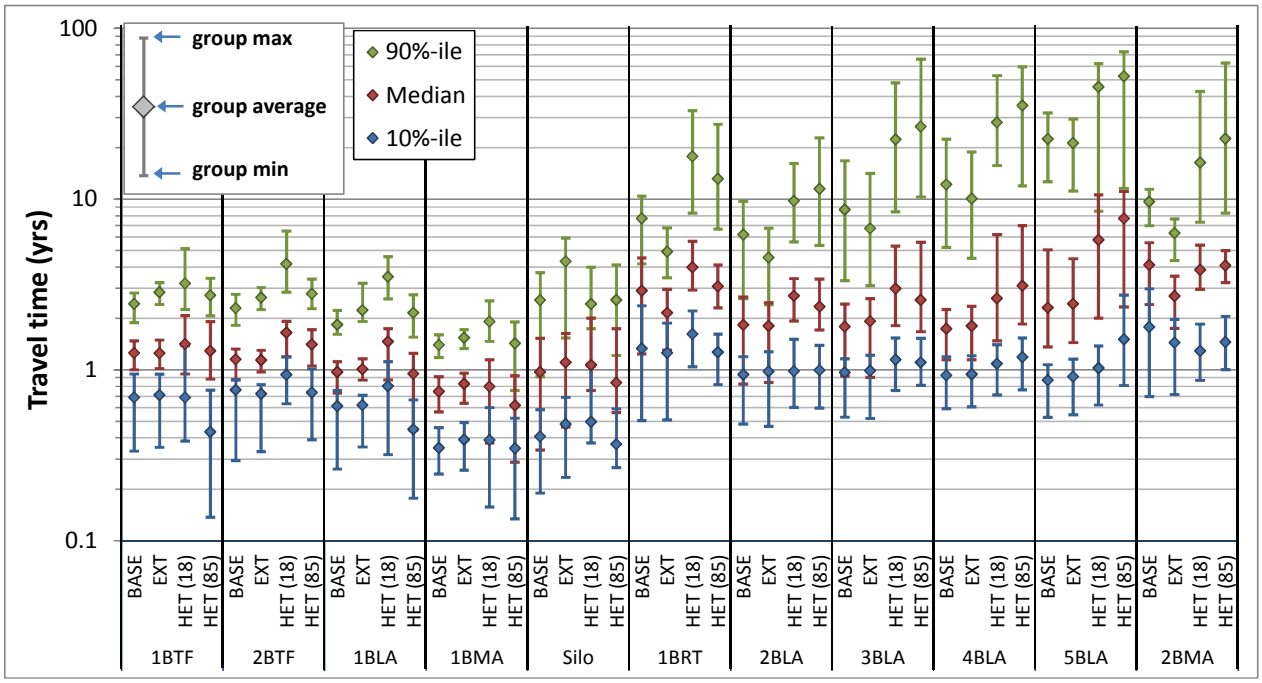

Figure 5-26. *Variability in travel-time percentiles related to bedrock parameterisation. TD08b bedrock cases organised by groups. Individual disposal facilities, time slice 3500 AD.*

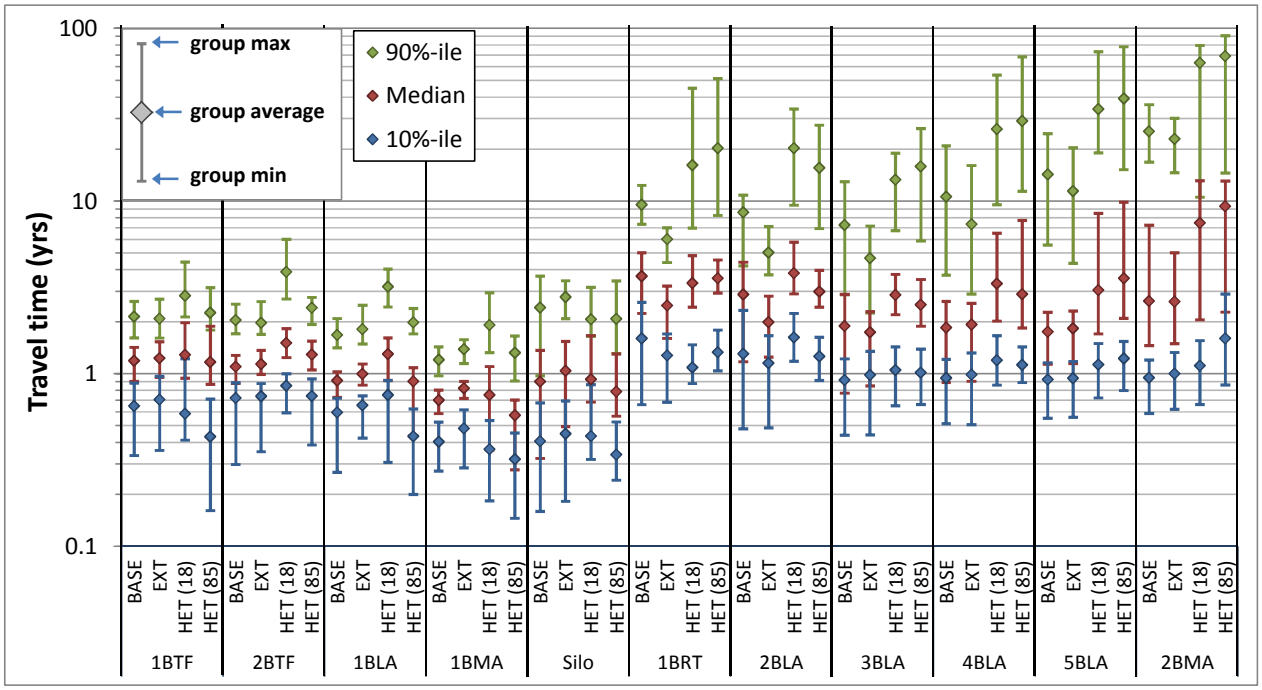

Figure 5-27. *Variability in travel-time percentiles related to bedrock parameterisation. TD08b bedrock cases organised by groups. Individual disposal facilities, time slice 9000 AD.*

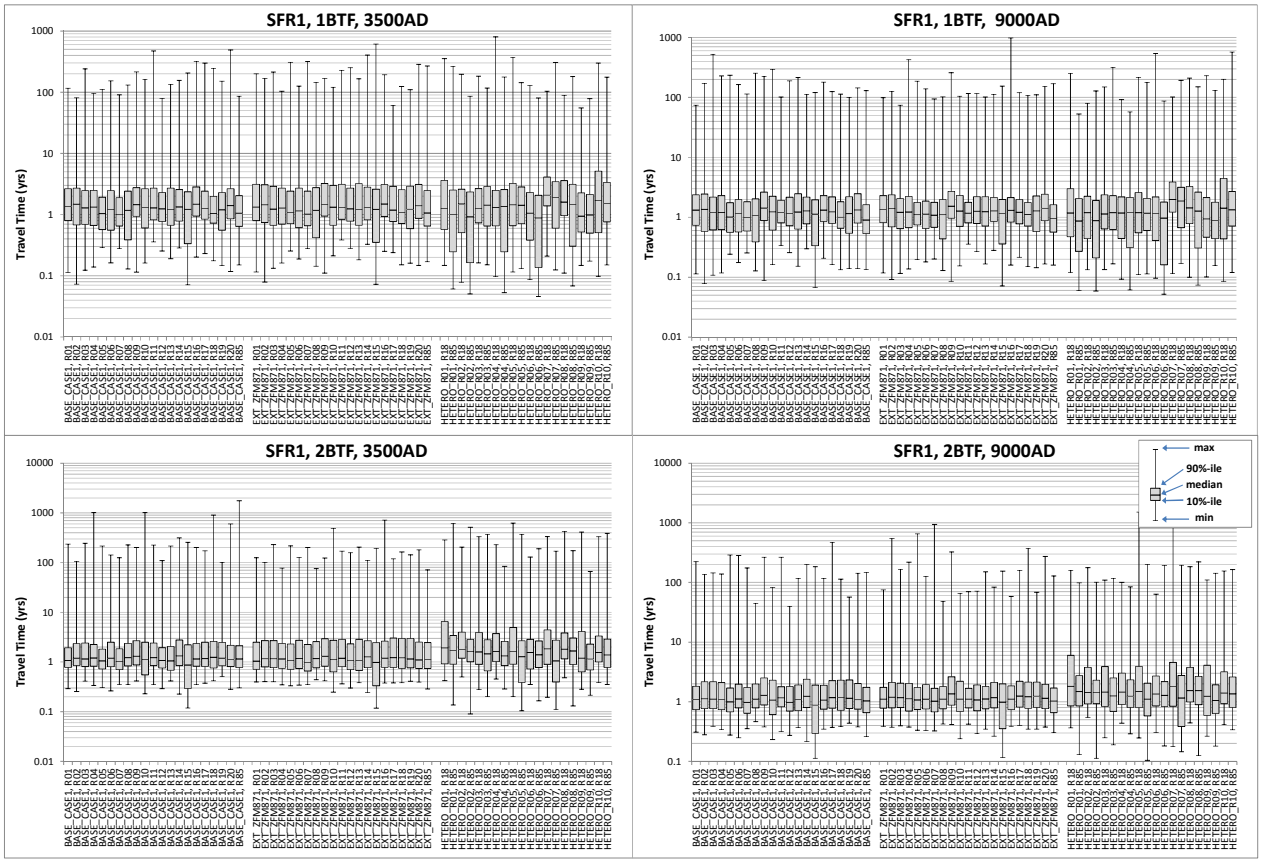

Figure 5-28. *1BTF and 2BTF travel-time percentiles for TD08b bedrock cases, 3500 and 9000 AD.*

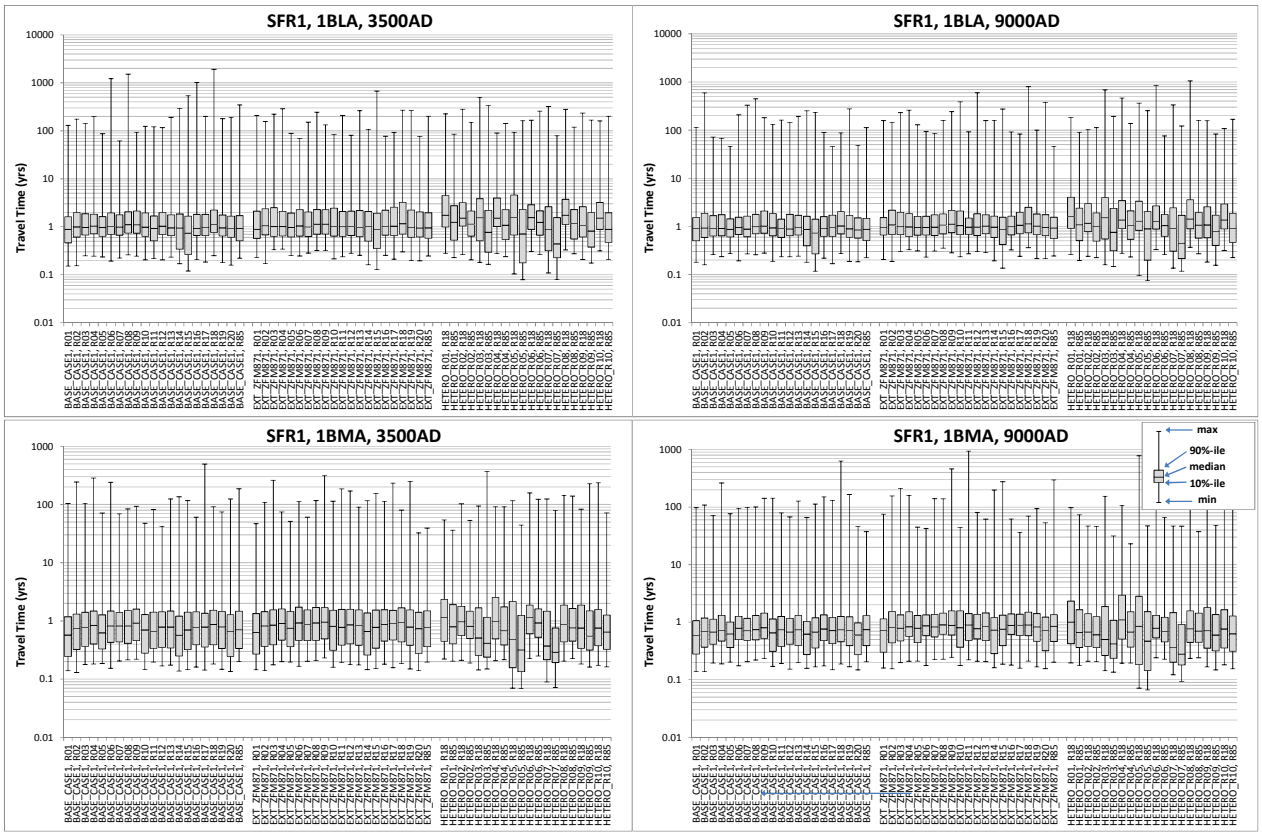

Figure 5-29. *1BLA and 1BMA travel-time percentiles for TD08b bedrock cases, 3500 and 9000 AD.*

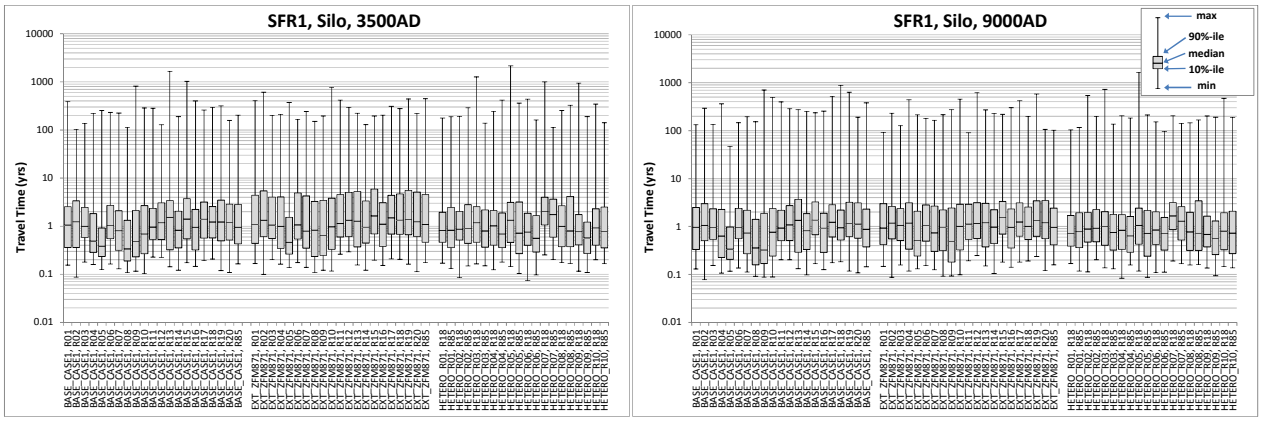

Figure 5-30. *Silo travel-time percentiles for TD08b bedrock cases, 3500 and 9000 AD.*

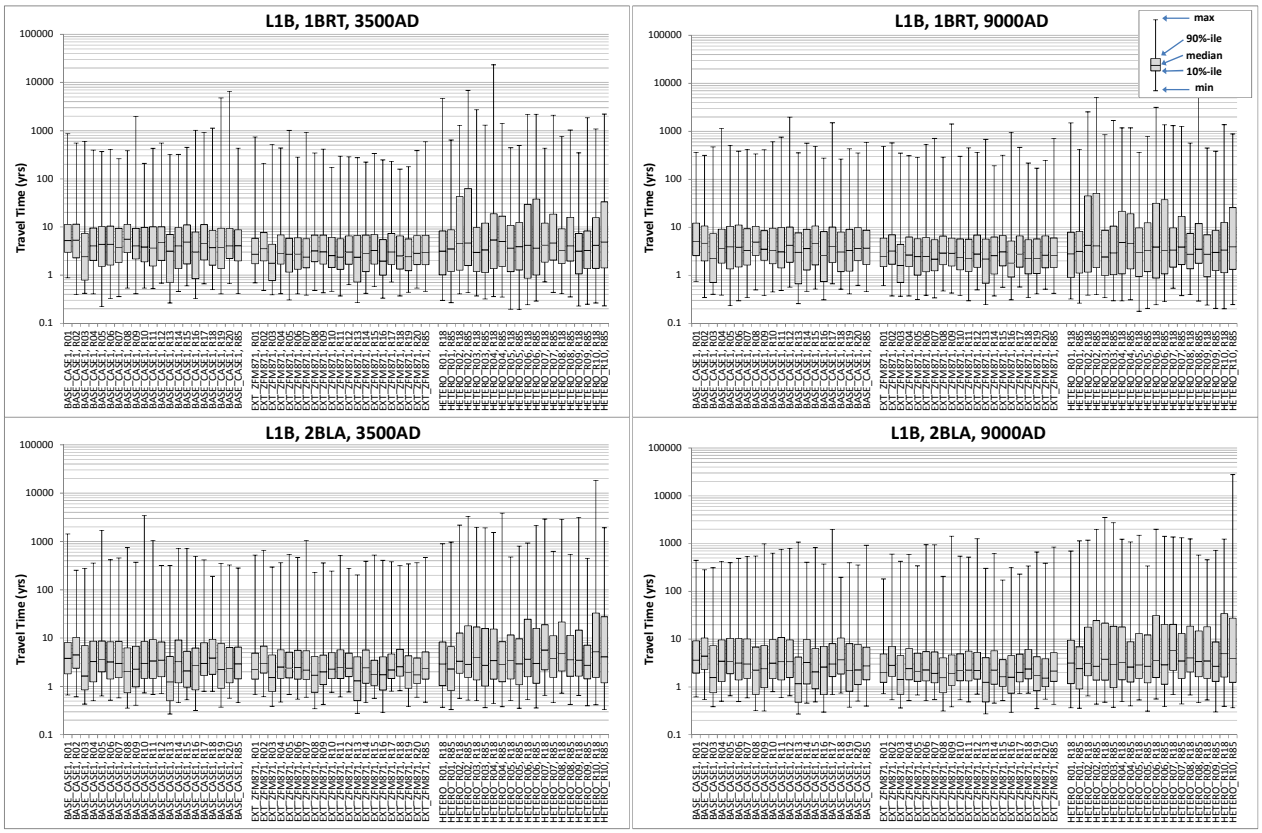

Figure 5-31. *1BRT and 2BLA travel-time percentiles for TD08b bedrock cases, 3500 and 9000 AD.*

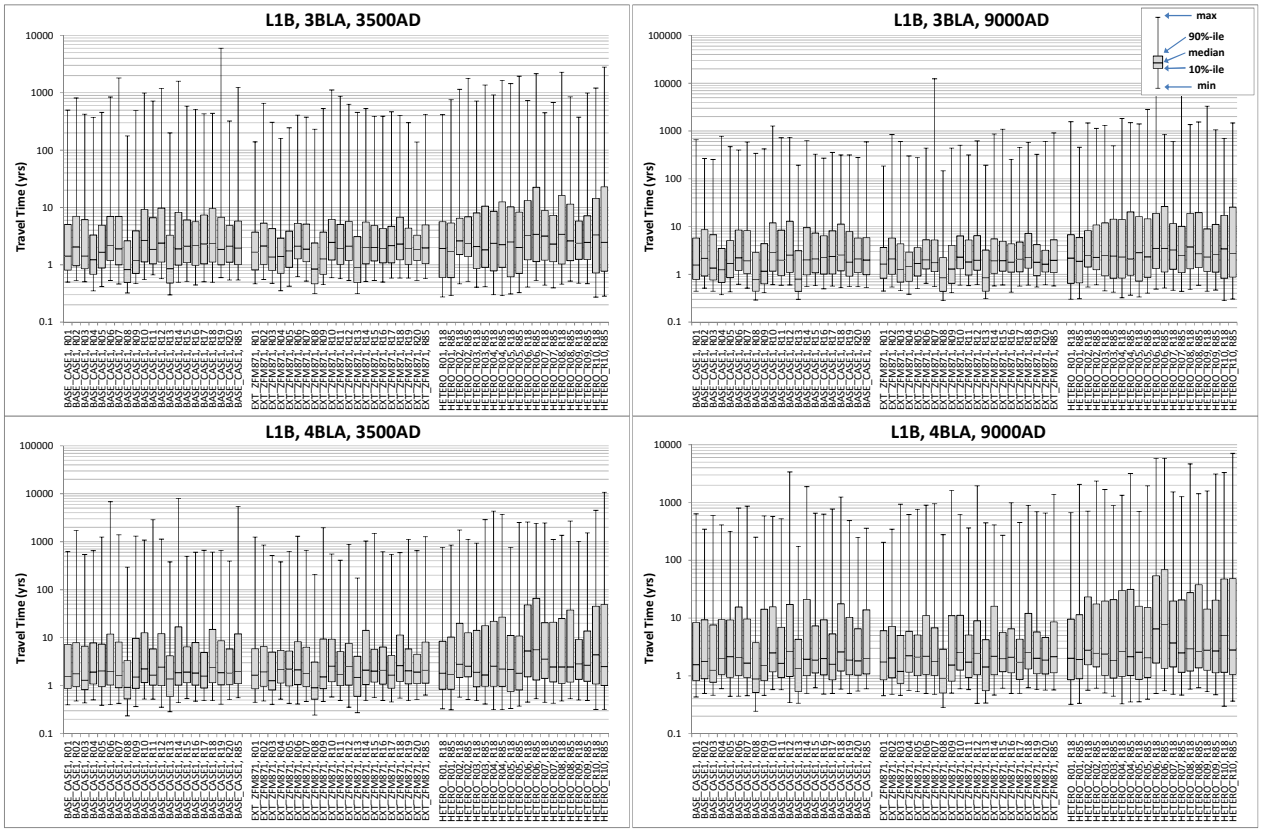

Figure 5-32. *3BLA and 4BLA travel-time percentiles for TD08b bedrock cases, 3500 and 9000 AD.*

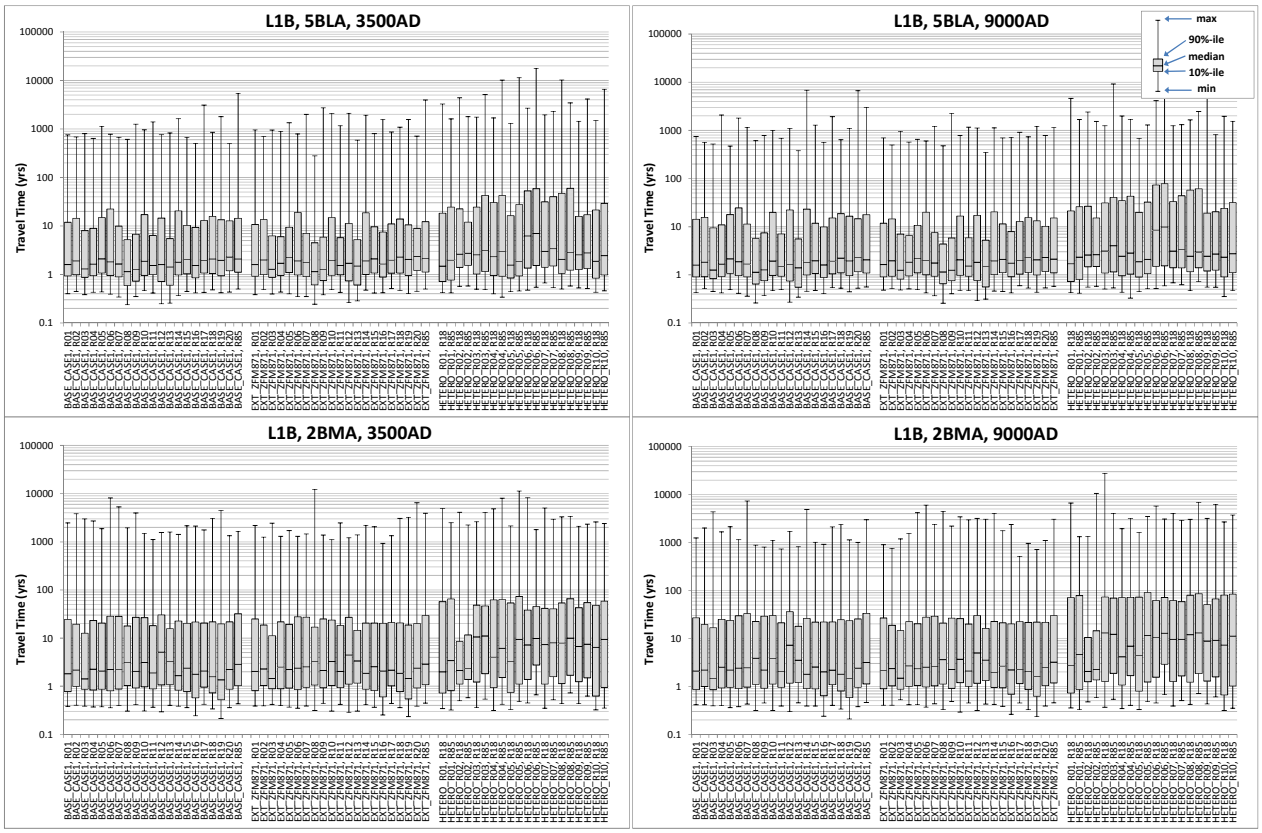

Figure 5-33. *5BLA and 2BMA travel-time percentiles for TD08b bedrock cases, 3500 and 9000 AD.*

6 Conclusions

The following observations have been made in the TD08b sensitivity analysis:

- Methods to automatize the execution of flow simulations have been presented (including DFN generation, ECPM conversion, solving the steady-state phase, and particle tracking). This automatisation reduces the risk of manual errors. Instead, automatisation allows efficient and consistent handling of large number of model setups, where traceability is provided via systematic name conventions in all input/output data files. However, the execution procedure should be developed further in subsequent SR-PSU Tasks. For example, unmotivated differences in file name conventions should be avoided, e.g., different conventions in TD08a and TD08b (Table 4-7) complicate the post-processing of data files.
- A method to solve groundwater level in a "recharge phase" has been presented (or, more precisely, head in the ground-surface layer of the computational grid; Section 4.3.2). In principle, the results are promising, but indicate that the approach is not fully mature and can be improved in several aspects (Section 5.1).
    - It is suspected that stricter convergence criteria will provide more gradual patterns in simulated local recharge, which in turn, will reduce the areas of required fixed-head.
    - It is recommended that particular emphasis is given to details of the constructed pier above SFR.
    - In TD08, the recharge phase is simulated for all six time slices in TD08a (i.e., <**Bedrock case**> = BASE_CASE1_DFN_R85). The ground-surface head solution is then *assumed* to be a valid boundary condition for all bedrock cases in TD08b. In subsequent SR-PSU Tasks, it is recommended that the recharge phase is performed for all bedrock cases.
- Different porosity parameterisation variants (Table 4-2) have been tested for relating Darcy flux and path length to travel time (Section 4.4.2). Based on consideration of results, a project decision was taken that variant 1, Upscaled ECPM porosity, with a minimum value of 10^{-5}, will be used in formal deliveries for SR-PSU.
- During the execution of TD08, no geometric data were available for differentiating the technical barriers of the silo. Therefore, the technical barriers of the silo are not resolved in TD08, and instead the silo is assigned a homogeneous conductivity of 10^{-6} m/s. Hence, no results evaluated for the silo in TD08 are representative of an intact plug state (i.e., primarily cross flow and interactions).
- The TD08a performance measures demonstrate that the largest changes in flow regime occur before 3500AD (i.e., disposal-facility flow, interactions, recharge, and exit locations)
- The extension, L1B, has minor impact of SFR-1 cross flow (Section 5.2.2) and has few interactions with the silo, even without technical barriers (Section 5.3.1).
- The extended geometry of ZFM871 has minor impact on simulated disposal-facility flow, interactions and exit locations. A probably reason for this is that particle trajectories from SFR1 are "cornered in" by the junction of the discharging zones ZFMNNE0869 and ZFMNW0805A/B (Figure 5-19).
- Disposal-facility cross flow in the planned extension, L1B, is subject to conceptual uncertainty in the parameterisation of ZFMWNW0835 and ZFMENE3115. This uncertainty concerns the interpretation of large transmissivity contrasts between deep and shallow data (Figure 3-2a). For these zones, the borehole conditioning (in BASE_CASE1) implies a significant transmissivity reduction in at L1B intercepts, as

compared to their effective parameterisation (Figure 3-2b). The model sensitivity to this conditioning is manifested in terms of disposal facility cross flow (Figure 5-15). Thus, borehole-conditioning implies a risk of underestimating the uncertainty related to deformation-zone parameterisation (i.e., providing *non-conservative/optimistic* results). It is recommended that this conceptual uncertainty is studied further in subsequent SR-PSU Tasks.

- In BASE_CASE1, the disposal-facility cross flow in SFR1, is subject to local conditioning of ZFMNNW1209, which is based on scoping estimations of mapped early tunnel inflow and grouting requirements (Table A-2 in /R-11-10/).
- The DFN realisations R18 and R85 do not cover the full range of HRD variability for SFR1, but can be referred to as "optimistic" and "pessimistic" realisations. It should be noted that:
    - Neither of the realisations represent extreme values for *all* disposal facilities of SFR1
    - Neither of the realisations are representative of the HRD variability range for L1B.

7 References

Bosson E, Sassner M, Sabel U, Gustafsson L-G, 2010. Modelling present and future hydrology and solute transport at Forsmark. SR-Site Biosphere. SKB R-10-02, Svensk Kärnbränslehantering AB.

Curtis P, Markström I, Petersson J, Triumf C-A, Isaksson H, Mattsson H, 2011. Site investigation SFR. Bedrock geology. SKB R-10-49, Svensk Kärnbränslehantering AB.

Dershowitz W, Winberg A, Hermanson J, Byegård J, Tullborg E-L, Andersson P, Mazurek M, 2003. Äspö Hard Rock Laboratory. Äspö Task Force on modelling of groundwater flow and transport of solutes. Task 6c. A semi-synthetic model of block scale conductive structures at the Äspö HRL. SKB IPR-03-13, Svensk Kärnbränslehantering AB.

Follin S, 2008. Bedrock hydrogeology Forsmark. Site descriptive modelling, SDM-Site Forsmark. SKB R-08-95, Svensk Kärnbränslehantering AB.

Hjerne C, Nordqvist R, Harrström J, 2010. Compilation and analyses of results from cross-hole tracer tests with conservative tracers. SKB R-09-28, Svensk Kärnbränslehantering AB.

Holmén J G, Stigsson M, 2001. Modelling of future hydrogeological conditions at SFR. SKB R-01-02, Svensk Kärnbränslehantering AB.

Odén M, 2009. Site investigation SFR. Hydrogeological modelling at SFR using DarcyTools. Site description SFR version 0.0. SKB P-08-94, Svensk Kärnbränslehantering AB.

SKB, 2008. Geovetenskapligt undersökningsprogram för utbyggnad av SFR. SKB R-08-67, Svensk Kärnbränslehantering AB. (In Swedish.)

SKB, 2013. Site description of the SFR area at Forsmark at completion of the site investigation phase, SDM-PSU Forsmark. SKB TR-11-04, Svensk Kärnbränslehantering AB.

Svensson U, Ferry M, Kuylenstierna H-O, 2010. DarcyTools version 3.4 – Concepts, methods and equations. SKB R-07-34, Svensk Kärnbränslehantering AB.

Öhman J, 2010. Site investigation SFR. Hydrogeologic modelling of SFR v 0.1. Influence of the ridge on the flow fields for different target volumes. SKB R-09-43, Svensk Kärnbränslehantering AB.

Öhman J, Bockgård N, Follin S, 2012. Site investigation SFR. Bedrock hydrogeology. SKB R-11-03, Svensk Kärnbränslehantering AB.

Öhman J, Follin S, Odén M, 2013. Site investigation SFR. Bedrock hydrogeology – Groundwater flow modelling. SKB R-11-10, Svensk Kärnbränslehantering AB.

Unpublished documents

SKBdoc id, version	Title	Issuer, year
1395705 ver 1.0	Results_TD8_Summary_of_Exitlocations	SKb,2013